

Oda Alstad Førli

NTNU
Norwegian University of
Science and Technology
Faculty of Engineering
Department of Civil and Environmental Engineering

Oda Alstad Førli

2D numerical modeling of Mannåselva to ensure flood protection

June 2019



Norwegian University of
Science and Technology

2D numerical modeling of Manndalselva to ensure flood protection

Oda Alstad Førli

Bygg- og miljøteknikk

Submission date: June 2019

Supervisor: Nils Rüther

Co-supervisor: Per Ludvig Bjerke

Norwegian University of Science and Technology
Department of Civil and Environmental Engineering

M.Sc. THESIS IN HYDRAULIC ENGINEERING

Candidate: Ms. Oda Alstad Førli

Title: 2D numerical modeling of Manndalselva to ensure flood protection.

1. Background

The area of the Center for Northern Peoples in Manndalen in Kåfjord municipality is often exposed to floods. The NVE plans to set up a flood protection measure in this area and needs to know the water levels of the re-occurring flood levels. The usual procedure at NVE is to run a 1D model to obtain the flood levels. Unfortunately, this method is biased by some uncertainties that are mainly caused by the simple hydraulic model and by few available topographic input data.

Recent development in data acquisition, storage, and processing make high-density terrain data easily available for numerical modelers. Use of this data could improve the accuracy of 1D models but also opens for the possibility to use more advanced numerical models.

NVE is interested in whether using a 2D numerical model with the input of the data available will improve the results in comparison to a 1D model.

In addition, more advanced methods are available for the measurement of bathymetry and topography close to the river. Within this work, the use of UAV to measure bathymetry data of shallow water bodies will be investigated.

The candidate will set up a 2D numerical model with additional bathymetry data and evaluate the height of given flood scenarios, in addition, to test a new method for bathymetry data measurements. The thesis will include a discussion on the use of 1D and 2D numerical models with regards to accuracy, and a discussion on the use of UAV based photogrammetry to measure bathymetry.

2. Work description

The thesis shall cover, though not necessarily be limited to the main tasks listed below.

Based on the available documentation, the following shall be carried out:

1. Literature review on 2D numerical modeling of floods.
2. Taking bathymetry data at Manndalselva
3. 2D numerical simulation of Manndalselva, including parameter sensitivity and verification test.
4. Discussion of the results with regards to numerical modeling and UAV measurements
5. Conclusions

6. Proposals for future work
7. Presentation

The literature review should outline the previous contributions in a condensed manner and result in the motivation for the current study.

3. Supervision

Associate Prof. Nils R  ther will be the main supervisor and Per Ludvig Bjerke at NVE will be the co-supervisor. The supervisors shall assist the candidate and make relevant information, documents, and data available.

Discussion with and input from other research or engineering staff at NTNU or other institutions are recommended. Significant inputs from others shall be referenced in a convenient manner.

The research and engineering work carried out by the candidate in connection with this thesis shall remain within an educational context. The candidate and the supervisors are free to introduce assumptions and limitations, which may be considered unrealistic or inappropriate in contract research or a professional/commercial context.

Trondheim, 14. January 2019



Nils R  ther

Associate Professor

Department of Civil and Environmental Engineering

NTNU

Abstract

The area around the Manndalen River has throughout the ages been exposed to floods. To ensure flood protection, it is desirable with a simulation of the water surface elevation performed by 2-dimensional numerical modeling. In the thesis, a 2D model in HEC-RAS 5.0.6/5.0.7 will be set up. Measurements for the bathymetry have been completed and interpolated with existing terrain data. The model has been calibrated against water surface elevation measurement and water flow from the gauging station in Manndalen. A sensitivity analysis has been conducted, and the model is validated against a situation with higher flow than normal conditions. A flood simulation for a 200-year flood was performed, and a comparison between raw LiDAR data and the interpolated terrain was made. The data used for calibration was prone to human errors, and the calibration cannot be trusted entirely. The model showed to be sensitive to specific parameters, especially the grid size and computation equation used for the simulation. The validation showed a different water surface elevation for the real-time event and the simulated situation. The reason for the differences are the terrain used in HEC-RAS. During the flood scenario simulation, the kindergarten and Center of Northern Peoples, located close by the river, were not affected by the flood, but protection measures should be considered as erosion of the terrain is a threat. The Riddu Riddu festival area is flooded, but an existing flood embankment showed to be effective against the water in the simulation. A longer and higher embankment should therefore be considered, as well as raising the road between the Center of Northern People and the river.

Sammendrag

Området rundt Manddalselva har gjennom tidene vært utsatt for flom. For å kunne sikre best mulig mot ødeleggelse på grunn av flom, er det ønskelig med en to-dimensjonal vannlinjeberegning utført ved hjelp av numerisk modellering. I masteroppgaven som presenteres vil en 2D modell settes opp i HEC-RAS 5.0.6/5.0.7. Innmålinger for elvetrauet er gjennomført, og disse er interpolert sammen med eksisterende terrengdata. Modellen er kalibrert mot innhentede målinger av vannlinje og vannføringsdata fra målestasjonen i Manddalselva. En sensitivitetanalyse er gjennomført, og modellen er validert opp mot en situasjon med høyere vannføring enn normalsituasjonen. En flomsimulering for en 200-års flom er fullført, og en sammenligning mellom simulering med LIDAR-data og det behandlet terreng er gjennomført. Målingene brukt til å kalibrere modellen er utsatt for menneskelige feil, som fører til at modellen kan være kalibrert mot unøyaktige målinger. Modellen viste seg å være sensitiv mot flere parametere, og spesielt cellestørrelse og hvilke type ligning som ble brukt i simuleringene. Valideringen av modellen viste at det er forholdsvis store forskjeller mellom virkeligheten og resultatet fra simuleringen, og at en av årsakene til dette kan være terrengdataen brukt som underlag. Flomsimuleringen viser at Senter for nordlige folk og barnehagen på sletta ved elva ikke er påvirket i stor grad av flommen, men at sikringstiltak bør vurderes med tanke på erosjon. Riddu Riddu sletta oversvømmes, men en eksisterende flomvoll på sletta viser seg å være en effektiv avleder mot vannet i simuleringen. En lengre og høyere flomvoll bør derfor vurderes, samt heving av veggen på nedsiden av Senter for Nordlige folk.

Preface

This report is the final product of the course "*TVM4910 Hydraulic Engineering, Master thesis*" at the Norwegian University of Science and Technology (NTNU), Department of Civil and Environmental Engineering. I would like to thank my supervisors Nils R  ther and Per Ludvig Bjerke, for guidance and advice throughout the process of writing my thesis. I would also like to thank NVE Region Nord, and especially Knut H  seth, for the possibility to work with hydraulic modeling and allowing me to start of the preliminary studies and fieldwork during my summer job at NVE. In addition, a special thanks to Anders Bjordal in NVE, who drove all the way from Alta to Manndalen to help me with the study, and who took the measurements used for the validation.

As several hours have been spent on YouTube watching videos of tips and tricks in HEC-RAS, I would like to send my gratitude to all the engineers and professors making tutorial videos.

I would also like to thank Kasper Eriksen and Arne F  rlie for proofreading the thesis.

Finally, I would like to thank all of the people at Verkstedloftet, who made my final year so great.

Table of Contents

1.	Background	I
2.	Work description	I
3.	Supervision	II
	List of Figures	X
	List of Abbreviations (or Symbols)	XI
1	Introduction	1
2	Background and theory.....	2
2.1	Study area	2
2.2	Historical flood situations	3
2.3	Previous studies	5
2.3.1	Spezialisation project.....	6
2.4	Literature review on flood modeling.....	6
2.5	HEC-RAS 5.0.6/5.0.7	7
2.5.1	Theoretical background HEC-RAS 2D	8
2.6	Computer specifications	12
3	Method and material	13
3.1	Terrain.....	13
3.1.1	Terrain preparation	13
3.1.2	Photogrammetry	14
3.2	HEC-RAS.....	15
3.2.1	Operations in HEC-RAS	15
3.3	Calibration.....	18
3.4	Parameter sensitivity	20
3.4.1	Grid size	21
3.4.2	Theta.....	22
3.4.3	Full momentum vs. Diffusion wave	22
3.4.4	Fixed Time Step	22
3.4.5	Eddy viscosity.....	22
3.4.6	Initial Conditions Rampup Fraction Time and Initial Conditions Time	23

3.4.7	Friction Slope	23
3.5	Flood Simulation	24
3.6	Validation of Model	25
4	Results	27
4.1	Calibration.....	27
4.2	Sensitivity analysis	31
4.2.1	Grid size	31
4.2.2	Theta.....	35
4.2.3	Full momentum vs. Diffusion wave	36
4.2.4	Fixed Time Step	40
4.2.5	Eddy Viscosity	43
4.2.6	Initial Conditions Rampup Fraction Time	45
4.2.7	Friction Slope	46
4.3	Flood Simulation	47
4.4	Terrain.....	52
4.4.1	The water flow of 6.33 m ³ /s	52
4.4.2	200-year flood	54
4.5	Validation of Model	56
5	Discussion.....	58
5.1	Calibration.....	58
5.2	Sensitivity analysis	59
5.2.1	Cell size	61
5.2.2	Theta.....	61
5.2.3	Diffusion wave	62
5.2.4	Fixed Time Step	62
5.2.5	Eddy Viscosity	63
5.2.6	Initial Conditions Ramp up Fraction time	63
5.2.7	Friction Slope	63
5.3	Flood Simulation	64
5.4	Terrain.....	65

5.5	Validation of model.....	66
6	Conclusion	68
7	References	70
	Appendices	73

List of Figures

Figure 1: Area of Manndalen	2
Figure 2: Water flow measurements by gauging station 206.3.0 in Manndalen	4
Figure 3: Map of the landslide masses. Notice Fossen furthest north in the figure (Fossen is just south of the Center of Northern People)	5
Figure 4: Computer specifications	12
Figure 5: Integrated bathymetry to terrain	14
Figure 6: Computation mesh with breaklines (red lines).	15
Figure 7: Manning’s regions for Manndalen. A bigger map is found in Appendix 10.	18
Figure 8: Location for measurements used in the calibration	20
Figure 9: The catchment for Manndalen River	24
Figure 10: Flow hydrograph used for flood simulation	25
Figure 11: a) The depth and b) velocities for the calibration simulation.	30
Figure 12: The difference in WSE between grid size 3 m and a) 1 m and b) 0.5 m.	32
Figure 13: Difference in WSE between 3 m and a) 2 m and b) 5 m	33
Figure 14: Difference in WSE between 3 m and 10 m	34
Figure 15: The difference in WSE between theta 0.6 and a) 1 and b) 0.8.	35
Figure 16: Differences in WSE for full momentum and diffusion with cell size a) 3 m b) and 1 m.	37
Figure 17: Difference in WSE for full momentum and diffusion wave with cell size a) 5 m and b) 10 meters.	38
Figure 18: Difference in WSE for full momentum and diffusion wave for grid 0.5	39
Figure 19: The difference in WSE for Courant conditions and time step a) 0.1 second and b) 1 second	41
Figure 20: Difference in WSE for Courant Condition and a) 3 seconds and b) 1 second	42
Figure 21: Difference in WSE for Eddy coefficient value of a) 0 and 0.2 and b) 0 and 0.3.	43
Figure 22: Difference in WSE for eddy coefficient of 0 and 5	44
Figure 23: Differences in WSE between an increasing flow hydrograph and a rampup time	45
Figure 24: Difference in WSE for a friction slope of a) 0.01 and 0.05 and b) 0.01 and 0.5.	46
Figure 25: Center of Northern People and the kindergarten in a flooded situation	47
Figure 26: Flood simulation with an overview of cross-sections further investigated.	48
Figure 27: Cross-section A flood simulation.	48
Figure 28: Cross-section B flood simulation.	49
Figure 29: Cross-section C flood simulation.	49
Figure 30: Cross-section E flood situation.	50
Figure 31: Cross-section H flood situation.	50
Figure 32: Velocity in flood simulation.	51
Figure 33: Cross-section A for original LiDAR terrain and interpolated terrain. $Q = 6.33 \text{ m}^3/\text{s}$	52
Figure 34: Cross-section C for original LiDAR terrain and interpolated terrain. $Q=6.33 \text{ m}^3/\text{s}$	53
Figure 35: Cross-section G for original LiDAR terrain and interpolated terrain. $Q = 6.33 \text{ m}^3/\text{s}$	53
Figure 36: Cross-section A for original LiDAR terrain and interpolated terrain - $Q=190 \text{ m}^3/\text{s}$	54
Figure 37: Cross-section G for original and interpolated terrain. $Q = 190 \text{ m}^3/\text{s}$	55
Figure 38: Cross-section C for original and interpolated terrain. $Q = 190 \text{ m}^3/\text{s}$	55
Figure 39: Measured and modeled WSE, $Q=14.7 \text{ m}^3/\text{s}$	56
Figure 40: Measured and modeled WSE, $Q=24.2 \text{ m}^3/\text{s}$	57
Figure 41: Terrain in problematic areas (a bigger picture is found in appendix X)	59
Figure 42: a) Depth and b) velocities with a flow= $6.33 \text{ m}^3/\text{s}$ and settings from the calibration.	60
Figure 43: Flow patterns for flood simulation.	64
Figure 44: Comparison of original LiDAR terrain and interpolated terrain	65
Figure 45: Difference between aerial photo (Kartverket) and integrated terrain for Manndalselva	66

List of Abbreviations (or Symbols)

NVE	Norges vassdrags- og energidirektorat (The Norwegian Water Resources and Energy Directorate)
NTNU	The Norwegian University of Science and Technology
WSE	Water surface elevation
ArcGIS	A GIS for working with maps and geometric information developed by ESRI
ArcMap	An ArcGIS applications
GIS	Geographical Information System
GPS	Global positioning system
HEC-RAS	The Hydrologic Engineering Center – River Analysis system
LIDAR	Light Detection and Ranging
USACE	US Army Corps of Engineers
UAV	Unmanned Aerial Vehicle

1 Introduction

In Norway, both the intensity and frequency of precipitation is expected to increase due to climate change. People have traditionally lived and worked close to rivers, as the surrounding land is usually flat and fertile. As a consequence, river floods often cause death, homes, and businesses that are located in the flood plains of the river. The area around the Center of Northern People in Manndalen has throughout ages been exposed to flooding. The Norwegian Water Resources and Energy Directorate (NVE) are planning flood protection measures in the area to protect from further damages. It is necessary to find height of the water level during a flood situation in order to find the best protection measurements.

There are several numerical models available for flood modeling, and HEC-RAS (Hydrologic Center's River Analysis System) 5.0.6/7 will be used to calculate the WSE. The thesis intends to set up a two-dimensional model in HEC-RAS.

Manndalen is exposed to additional natural hazards. Not only is it exposed to floods due to precipitation and snowmelt, but the area is also exposed to floods as a result of rockfalls from the mountain Gámmanjuni. Gámmanjuni is one of Norway's most unstable mountain areas and is under constant surveillance. NVE has executed computation for dam break waves from a landslide generated dam after rockfalls.

In the thesis, a setup of an HEC-RAS 2-dimensional model will be carried out, as well as a calibration of the model, a sensitivity test and a flood simulation. Note that all maps in the thesis points north.

2 Background and theory

2.1 Study area

Manndalen is a small village in Kåfjord municipality in Troms County. The river Manndalselva goes through Manndalen and is a preserved river by the NVE. The river has been protected since 1973 (NVE, 2018). The area has a unique landscape, with steep mountains surrounding a wide and flat midsection. The landscape is the reason for the river being protected.

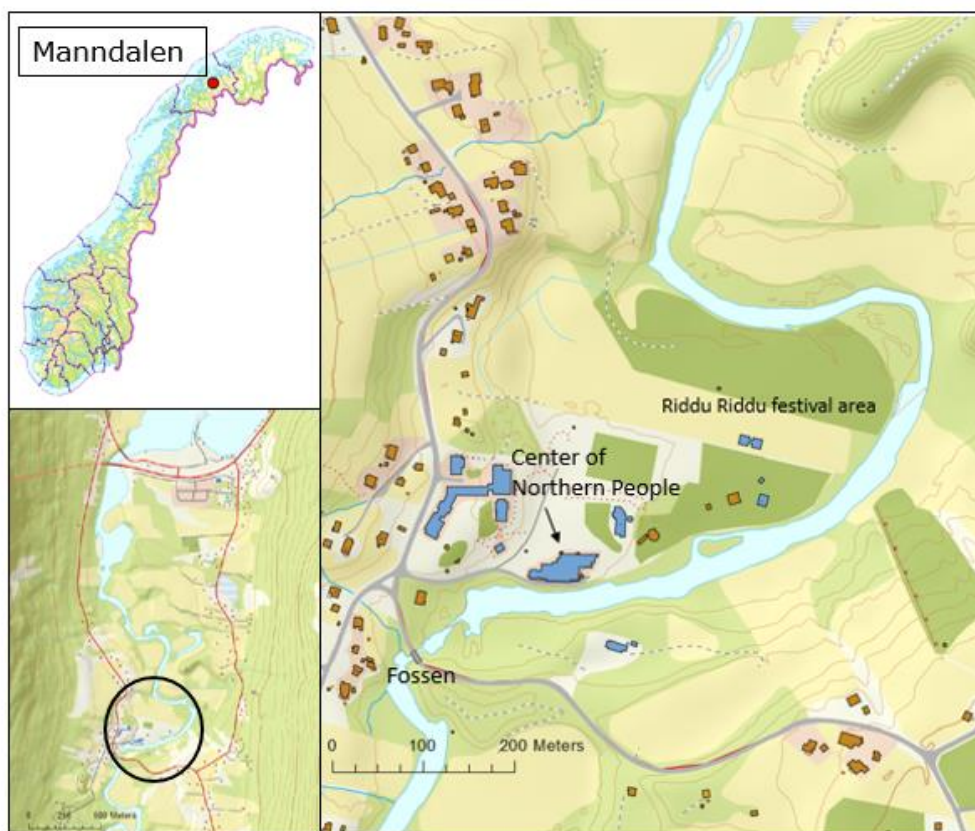


Figure 1: Area of Manndalen

The river Manndalselva has a catchment area of 207 km², and the elevation difference in Manndalen is 1319-0 meters above sea-level. The river's source is as far in as the valley goes, and the history of the river is visible in the landscape. Down the course of the river, several oxbow lakes and stream terraces are a result of the post-glacial rebound. The flow pattern of the river has been changed in recent years by flood protection measurements done by the NVE (NVE, 2018). The lower parts of the river go through a cultural landscape with agriculture on both sides of the river. These agricultural areas were earlier exposed to significant flooding events. Part of the river has a channel-like appearance today, after several inventions due to flood security measurements and agriculture. Changes to the river have been done since the early 1900s, and not up to the standards of today's needs and environmental standards. The NVE has done several

interventions in the later years to bring the river back to a natural state. (NVE, 2003). The area around the river bank is used for recreation, and there are several spots for fishing alongside the river.

Figure 1 shows the central area of interest. In this area, the Center of Northern people is located, which is a Sámi cultural center. The area also contains a kindergarten and a school. The thesis aims to propose flood security measures for this area, and the HEC-RAS modeling will concentrate on the area in figure 1. The Riddu Riddu culture festival is held each year at the plains close to the river, as shown in figure 1.

To the north of Manndalen, the mountain Gámanjunni is located, which has several unsteady mountainside. Gámanjunni 3 has the most unsteady sections and was classified as a high-risk area in 2016 by the NVE. Rockfall from this section could lead to retention of the river, and if the retention dam breaks, the result will be a flooding event downstream. The rockfall can also reach the settlement in Manndalen (NVE, 2018).

2.2 Historical flood situations

Significant rainfall events and snowmelt have several times led to landslide and flooding events. 10th of June 2011 a 10-year flood was registered by gauging station 206.3.0 in Manndalen. The water flow was 106 m³/s (Pettersson, 2011). The gauging station is placed above the waterfall *Fossen*.

Table 1: Flooding situations in Manndalen

Flooding situation	Flow [m³/s]
Mean annual flood	68.8
Five-year flood	83.3
10-year flood	94.8
50-year flood	119.2

Table 1 presents the flood values made from data dating from 1972 to 2017 (NVE, 2019). *Sildre.nve.no* presents the real-time flow values for the gauging station (NVE, 2019). Figure 2 shows the water flow [m³/s] for the period 1.-15 June .2011, when the 10-year flood was registered. Appendix A shows the water flow for period 1. June 2018-1. June 2019.

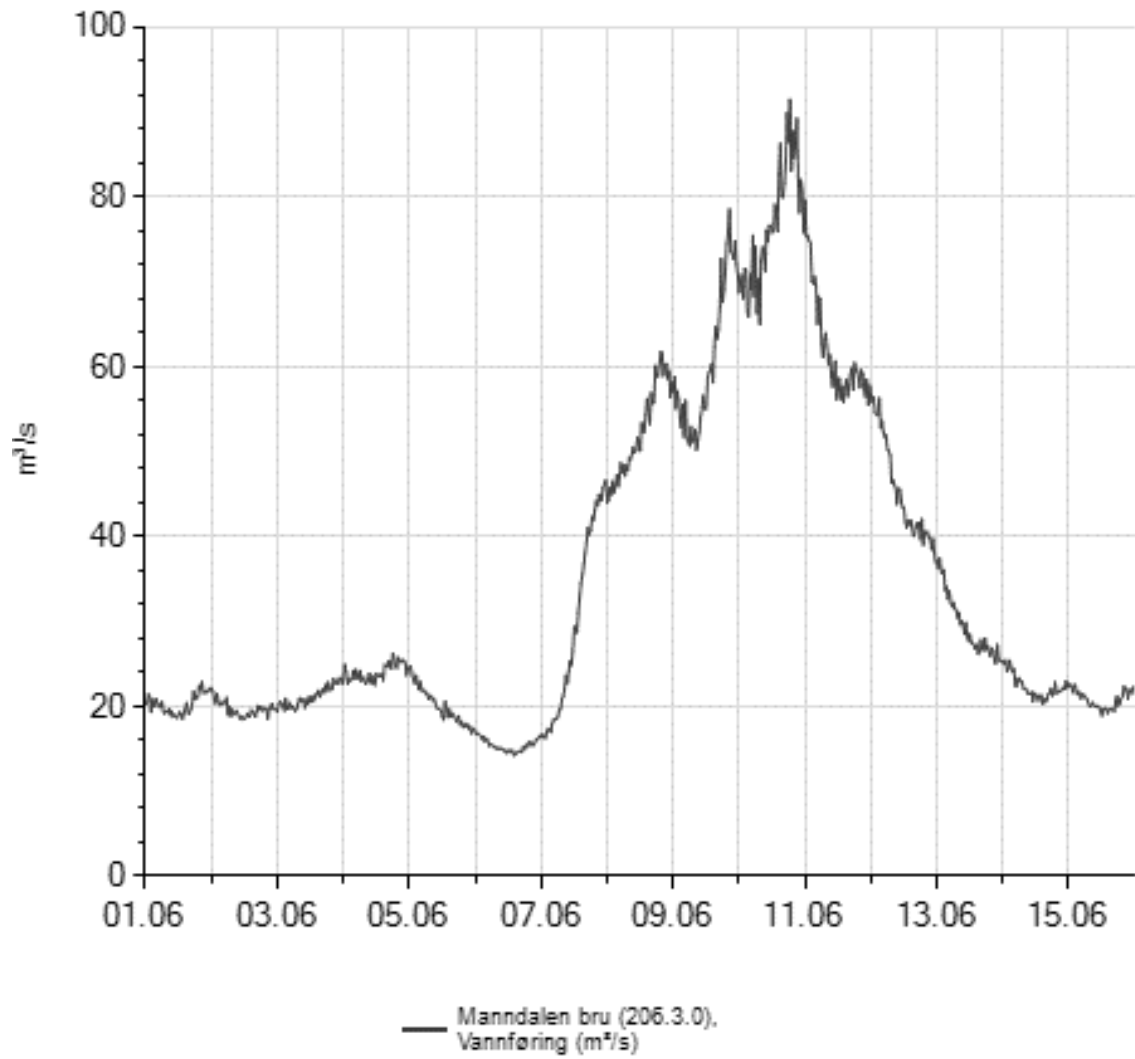


Figure 2: Water flow measurements by gauging station 206.3.0 in Manddalen

2.3 Previous studies

The NVE has conducted a dam break wave computation for a dam generated by a landslide from the mountain Gámanjunni 3 in Manndalen. Rockslides can reach the river, and cause damming of Manddalselva. For further reading, see *Dambruddsanalyse – skredgenerert dam i Manddalselva* (Bjerke, Majala, & Forsgren, 2017). The terrain used in this thesis is from work on the dam break computations done by Per Ludvig Bjerke.

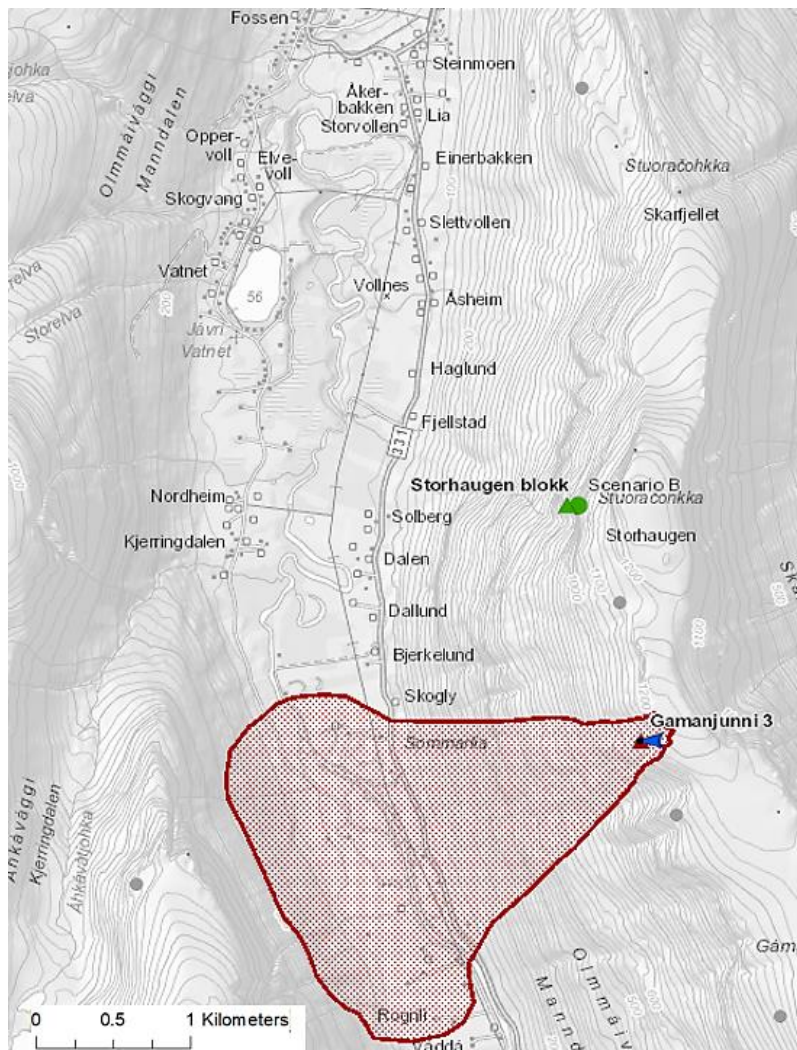


Figure 3: Map of the landslide masses. Notice Fossen furthest north in the figure (Fossen is just south of the Center of Northern People)

Figure 3 shows the reach of the rockslide. NGU reports that the landslides masses can be up to 26 millions m^3 . The possibility for this happening is bigger than 1/100. (Böhme, et al., 2016).

2.3.1 Specialisation project

During the fall of 2018, a specialization project was conducted, where a 1D model of Manndalselva was set up in HEC-RAS. The model used the same terrain as the 2D model built in this thesis. The conclusion for the project was that a new interpolation of the terrain should be done. The 1D model was not calibrated, and it was therefore concluded that the model does not represent the real flow situation.

2.4 Literature review on flood modeling

Several softwares for modeling flood hydraulics exist today. The best known 2D modeling programs are HEC-RAS, TELEMAC-2D, SRH-2D, and FST2DH. HEC-RAS also allows the modeler to do 1D and 1D-2D models. A quick overview of 1D modeling and 2D modeling will be given in this chapter. In 1D models, the cross-sections describe the topography of the river and the river banks. The water level is calculated using the 1-dimensional form of the Saint Venant equation. As the 1D model only needs topographical data in the cross-sections, the pre-work of the model is less time-consuming. This is an advantage when access to topographic data is limited. When the flow is restricted to the channel banks, a 1D model performs well. Which means it is not very well suited when the extent of a flood is of interest. Gharbi et al. recommend using 1D modeling for longer rivers, or for rapid studies that do not require too much precision. The 2D models are more accurate, but take a longer time to set up and run. For rivers being modeled, the 2D option can be used for the more critical parts of the river, while the rest is 1D (Gharbi, Soualmia, Dartus, & Masbernat, 2016).

2D modeling requires a mesh that represents the underlying terrain. The topography has to be continuous in order for the 2D modeling to run. The topography must also cover the whole area of interest. For HEC-RAS the simulation crashes if the topography is missing. In Norway, *Høydedata* offers high-resolution topographic data free of charge, which can be used for 2D flood modeling. The topography is from airborne LiDAR, and LiDAR is not able to penetrate the water surface. This leads to poor bathymetry data, as the area of the river is displayed as flat. The bathymetry must be interpolated from cross-section data, as done in this thesis.

A good 2D modeling requires a great deal of editing, and a good knowledge of the program is a requirement. Many choices have to be done by the modeler, for example concerning grid size, time step, grid size, and Manning's number. To achieve a physically realistic model, many parameters have to be adjusted. This leads to a time-consuming process. A simplified 2D model can be set up only using the raw LiDAR data if the data is good enough (Deal, Parr, & Young, 2017). If the available LiDAR data is good enough, will be investigated in this thesis.

Deal found in his study that HEC-RAS 2D Full momentum predicted the overall highest depth for any given site he tested. In his study, he compared HEC-RAS 2D, SRH-2D, and HEC-RAS 1D. He used HEC-RAS 4.1, 5.0, 5.0.1, 5.02, and 5.03 and SRH-2D version 3.0. SRH-2D, Sedimentation and River Hydraulics, solves the 2D dynamic wave equation and is developed by the Bureau of Reclamation. The SRH-2D tended to return higher depth than the 1D model, but still below the HEC-RAS 2D. In his study, he also found that HEC-RAS 2D was the fastest model. Similar mesh size and timesteps were used, but HEC-RAS performed simulation up against 28 times faster than SRH-2D. SRH-2D requires more excessive pre- and post-processing than HEC-RAS and HEC-RAS interfaced more easily with ArcGIS. Both software are free of charge.

In thesis *2D River Flood Modelling Using HEC-RAS 5.0* J.F. Palau found that HEC-RAS 5.0 2D modeling is comparable to the main hydrodynamic models in use at the time of the study (2016). The models were Delft3D, IBER, SOBEK, and 3Di. For river flooding, he performed simulations with HEC-RAS and IBER and compared the results. J.F. Palau found that HEC-RAS performed realistic river floods when compared to simulations done by experts with IBER (Palau, 2016). GEAMA and Institut of Flumen develop IBER. HEC-RAS 2D modeling was released the same year as this study was conducted, and developments have been made to HEC-RAS in later years

Another option for flood modeling is 1D-2D modeling in HEC-RAS. The river is modeled by 1D, while the floodplains are in 2D. Alexander Betsholtz and Beatrice Nordlöf found in their master thesis *Potentials and limitations of 1D, 2D and coupled 1D-2D flood modeling in HEC-RAS* that 1D-2D and 2D modeling have similar computation time and that 1D-2D models require a less complicated mesh than 2D. The minimum cell size can be bigger than for 2D, but 1D-2D requires smaller time steps to remain stable. The 2D model in his study ran stable at a timestep of 5 seconds, whereas the 1D-2D required a timestep of 1 second. He also found that the 1D-2D model had the largest stability problems, and the model was sensitive to all kinds of parameter changes. In the study, it was concluded that 1D and 2D would be the preferable choice, while 1D-2D was not suitable because of uncertainties.

The former HEC-RAS Development Team member Chris Goodell recommends that if the flood patterns around buildings are important, 2D modeling is necessary. 2D modeling should also be used if the spreading of the flood in multiple directions is of interest.

HEC-RAS 5.0 introduced pure 2D modeling in 2016, and there is a lack of literature investigating the differences to HEC-RAS to other software. Based on the experience from 1D modeling in HEC-RAS from the Specialization project, it was chosen to do the 2D numerical modeling in HEC-RAS

2.5 HEC-RAS 5.0.6/5.0.7

The hydraulic modeling was done by using the two latest versions of HEC-RAS; HEC-RAS 5.0.7 and 5.0.6. HEC-RAS is a software by the U.S. Army Corps of Engineers. The model was built in HEC-RAS 5.0.6, but as the modeling was started a new version came in March 2019. The main difference between the two versions is the fixing of bugs in the previous version. The most critical bug fixed regards to the work of this thesis, was the repair of Manning's Regions Override bugs (U.S. Army Corps of Engineers, 2019).

In this chapter, the basics of modeling in HEC-RAS is introduced, and further knowledge about the software can be found in the HEC-RAS Hydraulic Reference Manual and the 2D modeling Manual.

HEC-RAS 5.0 allows simulating with 2D mesh, which is done in this simulation. Earlier the simulation had to be done by creating cross-sections. The reason for choosing this option is the simplicity in the set-up. CivilGEO recommends HEC-RAS 2D flow modeling for a variety of situations, one of them being detailed 2D channel and floodplain modeling (CivilGEO, 2019).

2.5.1 Theoretical background HEC-RAS 2D

The following chapters are based on chapter 2 *Theoretical Basis for One-Dimensional and Two Dimensional Hydrodynamic Calculations* in the HEC-RAS Reference Manual.

2.5.1.1 Geometric data

For 2D modeling, 2D flow areas are drawn in the geometric data. 2D flow area is used for detailed 2D channel and floodplain modeling. The feature uses a finite volume solution algorithm, which can handle subcritical, supercritical, and mixed flow regime (Brunner, HEC-RAS Reference Manual, 2016). 2D modeling in HEC-RAS requires that a user-defined flow area is created. In this flow area, HEC-RAS divides this area into non-overlapping polygons forming a grid based on input on cell size. The grid does not have to be structured or rectangular, but orthogonality can improve the computational speed. HEC-RAS has a limit on eight sides for the polygonal cells, and the grid cells must be convex. For each cell, the relationships between elevation and profile, and wetter perimeter and Manning's number are computed.

2.5.1.2 Boundary conditions

Boundary conditions are necessary for executing the calculations. For unsteady flow simulations, upstream and downstream boundary conditions are needed. For accurate simulation, sufficient boundary conditions for the inlet and outlet of the area of interest are needed. This is often hard to achieve, as is the case in this thesis.

2.5.1.3 Manning's roughness coefficient regions

By default, the Manning's roughness coefficient is equal in the 2D flow area. RAS Mapper allows the user to change this by adding Manning's value layers. The value layer can be drawn directly in RAS Mapper, or by importing shape-files.

2.5.1.4 Computational background

HEC-RAS 5.0 lets the modeler choose the equation used for the simulation. The choice is between the Diffusion Wave equation and the Saint Venant equation. The Saint Venant equation is often referred to as the shallow water equation and is called Full Momentum in HEC-RAS. Full momentum will be used as a designation in this thesis. For the diffusion wave, gravitation and friction are the driving forces. Unsteady, advection, turbulence, and Coriolis terms of the momentum equation can be disregarded. The time steps can be longer in the diffusive wave equations than with the Saint Venant equation, and still get stable and accurate solutions (Brunner & CEIWR-HEC, 2016, s. 111).

Mass conservation:

$$\frac{\partial H}{\partial t} + \frac{\partial(hu)}{\partial x} + \frac{\partial(hv)}{\partial y} + q = 0 \quad (1)$$

Where H = Water Surface elevation [m.a.s.l]

$$H = H(x, y, t) = z(x, y) + h(x, y, t) \quad (2)$$

h = water depth [m]

$z(x, y)$ = the level of the terrain [m. a. s. l]

$h(x, y, t)$ = water surface elevation [m]

t = time [s]

u,v = velocity components in the x- and y direction respectively [m/s]

q = source/sink flux [m]

2.5.1.4.1 Full momentum (2D Shallow water equation)

Full momentum requires incompressible flow, uniform density, and hydrostatic pressure. It is assumed that the equations are Reynolds averaged so that turbulence motion is approximated using eddy viscosity (Brunner, 2016).

The shallow water equation are:

$$\frac{\partial u}{\partial t} + \frac{\partial u}{\partial x} + v \frac{\partial u}{\partial y} = -g \frac{\partial H}{\partial x} + \nu_t \left(\frac{\partial^2 u}{\partial x^2} + \frac{\partial^2 u}{\partial y^2} \right) - c_f u + f v \quad (3)$$

$$\frac{\partial v}{\partial t} + \frac{\partial v}{\partial x} + v \frac{\partial v}{\partial y} = -g \frac{\partial H}{\partial y} + \nu_t \left(\frac{\partial^2 v}{\partial x^2} + \frac{\partial^2 v}{\partial y^2} \right) - c_f v + f u \quad (4)$$

Where: H = Water Surface elevation [m.a.s.l]

h = water depth [m]

g = gravitational acceleration [m/s²]

ν_t = Eddy viscosity coefficient [m²/s]. See equation (5)

c_f = bottom friction coefficient [s⁻¹]. See equation (6)

f = Coriolis parameter [s⁻¹]

The left side of the equation contains the acceleration terms, while the right hand side are the internal or external forces acting on the fluid.

Eddy viscosity coefficient:

$$\nu_t = D h u_* \quad (5)$$

Where : D= non-dimensional empirical constant

h = water depth [m]

u_* = shear velocity [m/s]

D varies with geometry and bottom surface. The reference manual provides some values for D, as found in table 2.

Table 2: Values for the non-dimensional empirical constant in Eddy Viscosity

D	Mixing Intensity	Geometry and Surface
0.11-0.26	Low	Straight channels, smooth surface
0.3 – 0.77	Moderate	Gentle meanders, moderate surface irregularities
2 - 5	High	Strong meanders, rough surface

Bottom friction coefficient:

$$c_f = \frac{n^2 g |V|}{R^{\frac{4}{3}}} \quad (6)$$

Where: n = Manning's roughness coefficient [$m^{1/3}/s$]. (also called Manning's n, or Manning's number. Units are often omitted).

g = gravitational acceleration [m/s^2]

|V| = magnitude of the velocity vector [m/s]

R = hydraulic radius [m]

Note that the bottom friction can also be expressed by the Chézy formula.

Coriolis parameter accounts for the fact that the frame of reference of the equation is attached to the earth. The parameter will not be used in this thesis, and will therefore not be further explained. See the Hydraulic Reference Manual for additional information.

2.5.1.4.2 Diffusion wave (Diffusive wave approximation of the Shallow water)

When the gravitational- and friction are the driving forces, the diffusion wave equation can be used. The Eddy viscosity, the Coriolis parameter, and the unsteady and advection term can be disregarded. The equations used for full momentum can be simplified to a one equation model:

$$c_f = -g \frac{\partial H}{\partial x} \quad (7)$$

Where: u,v = velocity components in the x- and y-direction respectively

g = gravitational acceleration [m/s^2]

c_f = bottom friction coefficient [s^{-1}].

Bottom friction coefficient:

$$c_f v = -g \frac{\partial H}{\partial y} \quad (8)$$

Where: H = Water Surface elevation [m]

g = gravitational acceleration [m/s^2]

2.5.1.5 Time Step

The Courant Number is used in HEC-RAS to predict if the model can archive correct and stable results, without convergence problems. Grid size and computational time step are essential components to getting accurate answers in 2D flow modeling.

To find the Time step, the user can solve equation (9) or (10) (depending on the chosen method) or use the variable Time Step option in HEC-RAS 5.0.7. The variable time steps

are based on monitoring the Courant number, so that does not exceed the set maximum Courant Number, or go below the minimum courant number. This option can improve model stability, as well as reduce computational time.

Saint Venant Equation (Full momentum):

$$C = \frac{V\Delta T}{\Delta X} \leq 1 \text{ (with a } C_{max} = 3.0) \text{ (9)}$$

Diffusion Wave equation:

$$C = \frac{V\Delta T}{\Delta X} \leq 2 \text{ (with a } C_{max} = 3) \text{ (10)}$$

Where: C= Courant Number

V = Velocity [m/s]

ΔT = Computational time step [s]

ΔX = Average cell size [m]

The Courant number is the number of grid sizes per computations, that is, the number of grid cells the water will travel between computations. If C=1, there is one grid cell per computation. Higher than one means the modeler is skipping grid cells with the computations. For the Full Momentum equation, the Courant number can be as high as 3 and still achieve an accurate result. The variable time step option speeds up the computations when there are not much flow changes in the model. It selects larger time steps. When changes appear, there is a reduction in the time step. For the Diffusion Wave equation, the Courant number can be 5 (Brunner & CEIWR-HEC, 2016, ss. 4-6).

2.5.1.6 Choice of equation

A general approach is to use Diffusion wave when developing the model, and then switch to full momentum when all the problems are worked out. Full momentum requires a smaller computation interval than the diffusion wave to run stable. The two computational equations should be compared, and if there are significant differences, the user should assume that Full momentum is more accurate than Diffusion wave (Brunner & CEIWR-HEC, HEC-RAS 2D Modeling User's Manual, CPD-68A, 2016).

2.5.1.7 Assumptions

In HEC-RAS 2D modeling, some assumptions are made ((Brunner, HEC-RAS Reference Manual, 2016):

- The vertical fluid is negligible
- Velocity is vertically averaged at the cell center
- Energy head is computed at the cell center
- Manning's roughness assigned on cell face using roughness value at the cell face center
- Manning's roughness assumed constant across each cell face

2.6 Computer specifications

Table 4 shows the computer used for the simulation specifications.

Figure 4: Computer specifications

Component	Information
OS	Windows 10 Education. 64-bit operating system, x64-based processor
Processor	Hyper Treading on, 8 x Intel(R) Core(TM) i7-7700 CPU @ 3.60 GHz 3.60 GHz
RAM	32.0 GB

3 Method and material

The method used for the collection of data and the preparation of the model will be explained here.

3.1 Terrain

Airborne LiDAR data of the area of Manndalen was provided by the NVE and originated from *Høydedata*. It dates back from 2015 (Statens Kartverk, 2019)

One of the main disadvantages of LiDAR is that it is not able to penetrate water. It may be able to penetrate a couple of centimeters, but not to the bottom of the river. Because of this, the bathymetry of the Manndalen River was measured by handheld GPS during the summer of 2018. By traversing the river at points of interest, sections of the river were mapped out. Where the river was shallow, the river was crossed by foot, and a boat was used for the deeper parts. The number of measurements varies from 20-40 points for each cross section. The cross-sections measured are as shown in Appendix B..

3.1.1 Terrain preparation

During the work on the specialization project done in advance of the master thesis, the interpolation of the measured bathymetry and terrain was done in ArcMap. ArcMap is an application used in ArcGIS, a geographic information system. The result of the interpolation was not at an acceptable level; thus, a new method was used for this thesis. The problem with the first interpolation was that there were missing areas in the terrain. As 1D modeling only needs terrain data in the cross-sections, 2D modeling crashes if the terrain data is missing. The goal was to replace the measured level of the bottom by the LiDAR with the measured point. A shapefile of the river was created, and an interpolation of the shapefile and the river was done in ArcMap. Inverse distance weighted (IDW) technique was used to interpolate a raster surface from points. The LiDAR river was cut out of the terrain, and the new river replaced the now empty space by the feature *Mosaic to new raster* in ArcMap. Different cell sizes and pixel depths, as well as different interpolation techniques, were tested before an acceptable result was achieved. In the LiDAR data, the houses are removed, so these had to be added again. GeoNorge provided the shapefiles of the houses, and Raster Calculator in ArcMap was used to create height to the buildings. The height was set to 3 meters, as the water level is not expected to go beyond this height. A conversion from raster to TIF was done by "*Raster to other format*" in ArcMap, which in turn can be converted into terrain in RAS mapper.

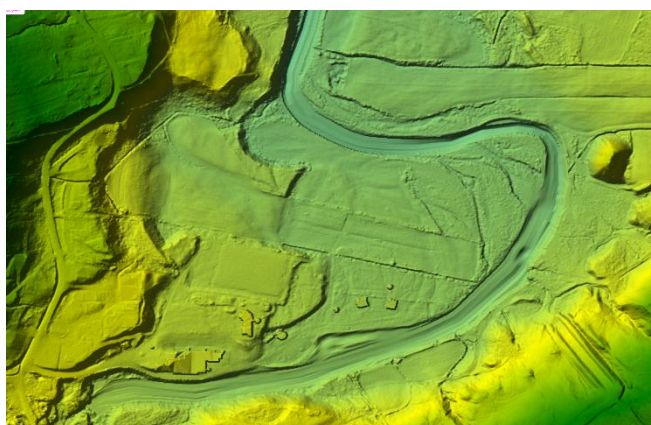


Figure 5: Integrated bathymetry to terrain

A couple of test-simulations were executed to see how the water behaved in the new riverbed. In some areas, the river behaved abnormally. To change the behavior of the river, it is possible to create cross-sections and edit these in the geometric data. The edits were done by comparing the water behavior with pictures of the river and the measured cross-section to get the most accurate results. *Norgebilder* contains aerial photos from several years and is a good source for achieving knowledge about the behavior of the river (Kartverket)

For the sections of the river where there are islands the interpolation done in ArcMap were inadequate, and these areas were specially altered to get the best possible result. The result from the interpolation can be found in Appendix C. Note that the white areas are not missing terrain in appendix C.1, and are of no consequence. The white areas disappear when zooming in, as seen in Appendix C.2.

To compare the interpolated river, simulations with the original terrain were run for a water flow of $6.33 \text{ m}^3/\text{s}$ and the 200-year flood. The sizes of flow will be explained further in chapter 3.3 and 3.5. A grid size of 3 meters was used to save computation time. The settings for the calibration and flood simulation was used for the remaining parameters. At *Høydedata*, the date for the LiDAR scanning is available. The scanning was done the 14th of September 2015, and at *Sildre* the flow that day is found. The gauging station in Mandalen measured an average flow of $3.32 \text{ m}^3/\text{s}$ (appendix K). Since the flow was low, the surface of the river scanned by the laser might not be too far off the actual riverbed. The terrain from *Høydedata* is found in Appendix D.

3.1.2 Photogrammetry

A camera mounted to a drone was used to create maps from aerial photogrammetry. The camera is vertically pointed to the ground. The drone is flown in circular movements, to ensure that all of the landscape below is captured. The drone used for this photogrammetry was a Phantom 4, and the software used to process the raw data was Agisoft PhotoScan. Kordula Valeria Anne Schwarzwälder at NTNU handled the processing of the material. The footages were captured 13.-14. Mai 2019. It has been preferable to do this work earlier this year, but because of large amounts of snow, it was not possible.

3.2 HEC-RAS

3.2.1 Operations in HEC-RAS

The choices and operation chosen in HEC-RAS will be presented in the following chapter.

3.2.1.1 Geometric data

In geometric data, the 2D flow areas, boundary conditions lines, and breaklines are drawn. The user defines a grid resolution, and HEC-RAS builds the computational mesh. After the mesh is built, breaklines can be added, and the mesh can be edited.



Figure 6: Computation mesh with breaklines (red lines).

Figure 6 shows the 2D mesh with a grid size 3 x 3 meters with breaklines. Breaklines represent significant boundaries to flow. The breaklines in figure 6 represent levees, natural embankments, and sudden changes in the landscape. The choice of cell size,

orientation, and geometrical characteristics of the grid plays a significant part in the stability and accuracy of the model (Brunner, HEC-RAS Reference Manual, 2016).

The grid in the flow area must be fine enough to involve all the details in the crucial areas, like flow features and geometric features. The accuracy of the simulations increases with an increasing number of cells, but this also affects the run-time. An increasing number of cells demands a longer run-time for the simulations, and therefore compromises in grid size has to be done (Casey & Wintergerste, 2000). Chris Goodell, a former HEC-RAS Development Team member, advised having a minimum of 5-7 cells across the river. The reason for the minimum limit is that the velocities are computed as averages over a cell face. If there were only one cell face across a river, then the result would be no better than for 1D-modeling – one velocity will be as an average over the width of the river. This smooths the velocity profile and typically yields a higher water surface elevation at that location. Using 5 cells across a river gives a much better velocity distribution across the river and a resulting more accurate water surface elevation. If it is troublesome to get 5 cells across, Goodell recommends getting at the very least 3 cells across.

Note grid size and cell sizes mean the same thing, and both expressions will be used. Mesh is the whole 2D flow area, built by grids. A grid/cell size referred to as 3 meters, means it has a size of 3 x 3 meters. 3 meters is used as a simplification.

3.2.1.2 Boundary conditions

The boundary conditions used for modeling Manndalselva was a flow hydrograph for the upstream boundary and normal depth at the downstream boundary. Normal depth is based on Manning's equation, where the user enters a friction slope. The friction slope should be based on the land slope of the area. The boundary conditions are computed on a per cell basis. (Brunner & CEIWR-HEC, 2016). The upstream boundary, the flow hydrograph, is used to bring water into the flow area. The energy slope is also necessary, and after conversations with professionals it was chosen to use an energy slope of 0.01. This was used for all simulations.

In the modeling of Manndalselva, a simplification of assuming that the downstream area will not affect the result in the area of interest is used.

3.2.1.3 Mannings' roughness coefficient

The Manning's roughness condition was set as default to 0.06 for the 2D flow area. During the calibration, Manning's regions were drawn in RASmapper. The regions were decided by observing maps and pictures of the area, as well as observations were done during fieldwork.

3.2.1.3.1 Performing the Computations

To run a model, the user has to make a plan in the *Unsteady Flow Analysis* window. The procedure is further explained in the 2D Modeling Manual. In the plan, the user has to decide which programs to run, Simulation Time Window, Computation Settings and Calculation Options and Tolerances.

Simulation time defines the starting and end of the simulation period. The time and date are not crucial in this simulation, and the most crucial factor is that the time window is

long enough for stable running. The chosen simulation time window varies with different operations done and is further explained later.

3.2.1.4 Time step

The computation interval is the time step in the simulation, and the modeler can choose between fixed time step, Courant conditions, and time step based on a time series of divisors. The variable time step based on monitoring the Courant number is a new feature in HEC-RAS 5.0.4. This time step options can be used to improve model stability and reduce computational time. By opening the Unsteady Computational Options and Tolerance in the Unsteady flow analysis window, and then chose the options Adjust time step based on courant in the Advanced Time Step Control tab. The user has to specify the maximum Courant, minimum courant, the number of steps below minimum before doubling, and the maximum number of doubling base time steps A Courant Condition with a base time step of 10 seconds was used for simulations done in Mandalselva. A Courant number of minimum of 0.5 and maximum two is chosen for Diffusion Wave and Full Momentum. The number of steps below minimum before doubling were set to 4, and the maximum number of doubling and halving base time step were set to 4. This indicates a maximum time step of 160 seconds and a minimum of 0.63 seconds.

3.3 Calibration

The model must be calibrated to achieve the most accurate flood simulations. To calibrate the model simulated WSE was adjusted to fit the observed WSE measurements from field work. The adjustments were made by changing Manning's n in the river. Figure 7 shows the different Manning's regions in the river and the area around. The flow used for the calibration was the flow registered by the gauging station for Manndalen River. As the measurements were done at different times during the same day, the average flow was used. The maximum flow during the period of measurements was $6.63 \text{ m}^3/\text{s}$, and the minimum was $6.11 \text{ m}^3/\text{s}$. The average was $6.33 \text{ m}^3/\text{s}$.

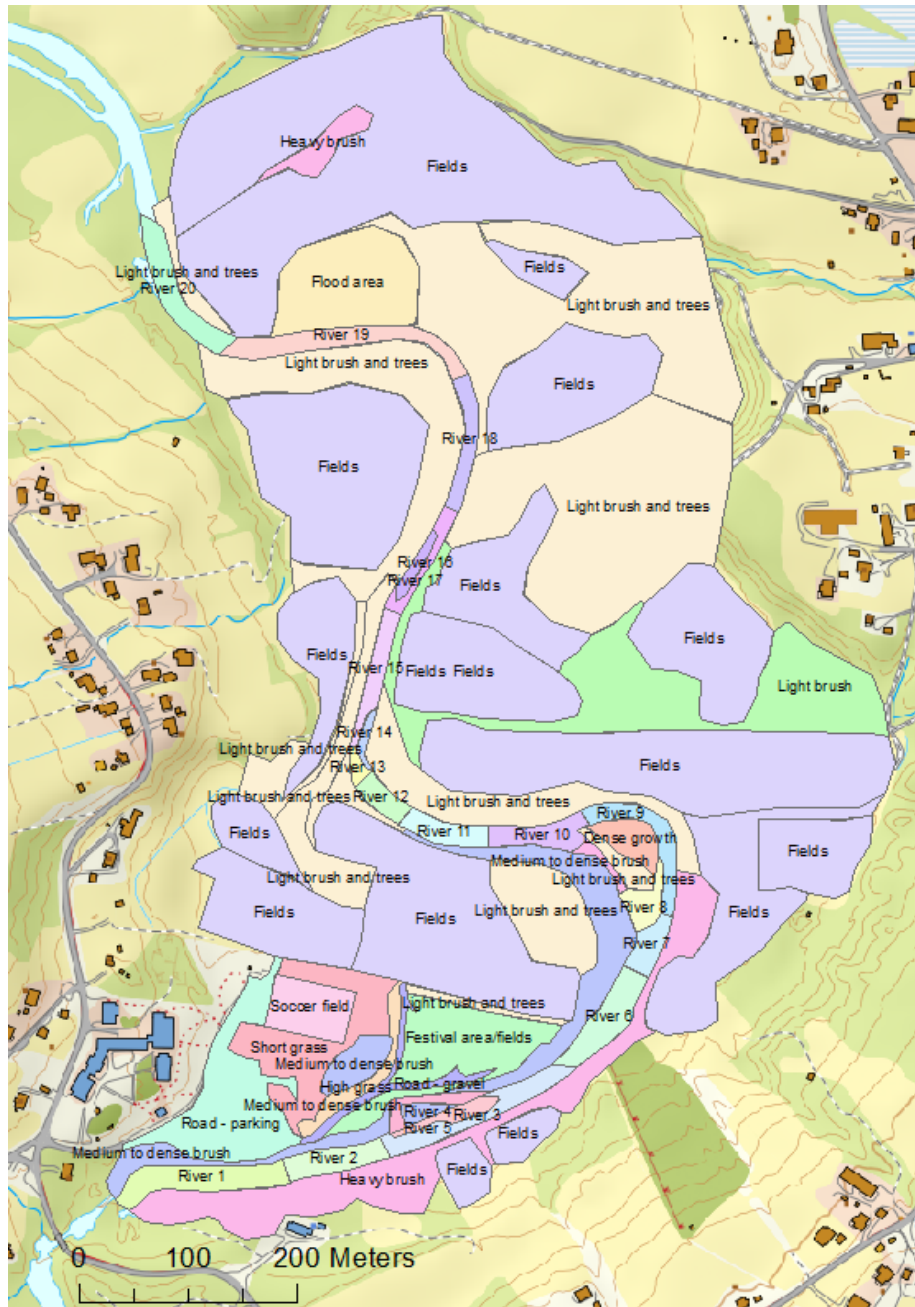


Figure 7: Manning's regions for Manndalen. A bigger map is found in Appendix 10.

The regions have been divided based on observations done at fieldwork and pictures of the area. To select appropriate Manning's n *Vassdragshåndboka* by NVE (NVE, 2017) and *Guide for selection Manning's roughness coefficients for natural channel and flood plain* by the US. Department of Transport (Arcement & Schneider, 1984) was used.

Full momentum was used as the computation equation, as explained in Chapter 2.5. As the model runs stable, the HEC-RAS Reference Manual recommends using theta of 0.6 (Brunner, HEC-RAS Reference Manual, 2016, ss. 8-75).

The first calibrations were done by using a grid size of 10 meters. The Manning's n were adjusted after the simulations were done. The procedure was repeated until the changes were negligible. The Manning's layer that gave the best result was transferred to simulation with grid size 5 x 5 meters, and then 3 x 3 meters. The final calibration was done with cell size 2 x 2 meters. A finer mesh would most likely give a more accurate result but because the calibration data was not accurate, it was decided that the calibration done with 2 meters was at an acceptable level. The simulations with a mesh of 1 meter and 0.5 meters were considered to be too time-consuming, as a simulation could take up to 15 hours.

The difference between the observed WSE was calculated for each simulation for each cross section. Table 3 presents the observed WSE, while figure 8 is the location for the observations.

Table 3: Data used for calibration of the model.

Cross-section	Date of measurement	Time of day	Observed WSE [m]	Flow [m³/s]
1	16.07.2018	17:06	8.414	6.55
2	16.07.2018	17:20	7.963	6.57
3	16.01.2018	18:21	7.08	6.61
4	16.01.2018	18:51	5.844	6.63
5	16.01.2018	19:13	5.465	6.63
6	17.07.2018	11:40	5.24	6.13
7	17.07.2018	12:00	4.828	6.13
8	17.07.2018	12:10	4.622	6.13
9	17.07.2018	13:20	4.187	6.13
10	17.07.2018	14:09	3.491	6.13
11	17.07.2018	15:04	1.845	6.17
12	17.07.2018	15:20	1.705	6.24



Figure 8: Location for measurements used in the calibration

The measurement done for the actual WSE was done by handheld GPS. This is prone to human mistakes, and accurate calibration is not expected. The GPS points were collected by placing the GPS at the waterfront of the river and note down the time of day the measurement was taken. As the GPS points of the waterfront were collected simultaneously as the cross-section was measured, human mistakes could lead to the wrong point being set as the waterfront, or the GPS could have been placed on rocks, etc.

3.4 Parameter sensitivity

A variety of uncertainties can occur in numerical modeling. The European Research Community on Flow, Turbulence, and Combustion (ERCOFTAC) has presented the most critical uncertainties in computational fluid dynamics. These uncertainties are modeling errors, errors in the numerical approximation, errors due to convergence did not compete, round-off errors, uncertainty in input data and boundary conditions, user mistakes, or bugs in the software. These uncertainties are further explained in *ERCOFTAC*

Best Practice Guidelines on Numerical modeling and Hydraulics by Nils Reidar B. Olsen (Casey & Wintersgerste, 2000) (Olsen, 2017).

The uncertainties and errors mentioned above must be considered when looking into the accuracy of the results. Parameter sensitivity testing is a much-used method for this. The testing is done by changing one parameter while keeping the other parameters constant and running the simulation. The result with different values of one of the parameters are then compared, and an evaluation of the deviation is done. Small deviation implies that the parameter has a small impact on the result, and vice versa.

After the computations are done, the modeler must check if the results are stabilized. If not, the simulation time window must be changed. To check if the computation is stable, the time series for WSE is plotted in RAS-Mapper.

For upper boundary conditions, a flow hydrograph with a maximum of 6.33 m³/s is used. Since the model is computed with empty cells, the flow hydrograph used has an increasing flow for the first hour, to fill the cells with water. If this is not done, HEC-RAS will assume a wave is coming, and it fills cells outside of the river. Since HEC-RAS does not adjust for infiltration to the ground, these pools stay there throughout the computations. For downstream boundary conditions, the same conditions as for the calibration was used (friction slope=0.01). The Manning's values used is the values decided by the calibration process. The simulation time window is 6 hours to ensure stable running. The Courant condition is also used. The base grid size is 3 x 3 meters, and the geometric used is as in figure 6. If nothing else is mentioned, the reader can assume the mentioned conditions are valid.

Every parameter that can apply uncertainties should be tested, and values tested should be in a reasonable range. For this model, the parameters tested will be cell size, theta, diffusion wave versus full momentum, fixed time step versus Courant conditions, Eddy Viscosity, and friction slope. A simulation with initial condition ramp-up time will also be conducted, to see if it is adequate to use an increasing flow hydrograph for the flood simulation. The calibration process shows the effect of Manning's number, and how it can affect the results.

After the simulations were done, the result was converted into a raster file by HEC-RAS. This is done in RASmapper under *Result Map Parameter*. The modeler can specify to save *Raster based on Terrain* under *Map Output Mode*, which creates a raster that can later be used in ArcMap. This was done for all the simulations run. The rasters were treated in ArcMap by the function *Minus*. This function subtracts the value of the second input raster from the value of the first input raster on a cell-by-cell basis and gives the difference in the water surface elevation for the simulation area. For the first input, a reference raster was used. The raster used as reference varied by the different parameters tested.

3.4.1 Grid size

To see how sensitive the model is to different cell sizes, a range of cell sizes were tested. The biggest size tested was 10 meters. 5 meter, 3 meters, 2 meters, 1 meter, and 0.5 meters were also tested. The testing were done by comparing the result with different cell sizes to a reference simulation. The simulation used as reference was 3 meters, as the simulation time were short and the running were stable. The computation time was

also interesting, as the result from this testing will have effect on cell sizes used later in the thesis. The boundary conditions and computation settings were the same as for the calibration. The only varying parameter was the cell size. The geometry for the different grid sizes can be found in appendix F.

3.4.2 Theta

During the simulation, a weighting between the current solution timeline and the previously computed timeline is done. The Theta factor does this weighting. A Theta of 1 is set as default in HEC-RAS and implies that only the current solved timeline is used for the spatial derivation. According to HEC-RAS User Manual, this provides for the most stable solution but could lead to a less accurate method (Brunner & CEIWR-HEC, 2016, ss. 4-14). HEC-RAS lets the user vary between a Theta of 0.6-1. 0.6 gives the most accurate result but could be less stable. Because of this, testing of Theta value must be done. A value of 1 and 0.8 is compared to the results from theta = 0.6.

3.4.3 Full momentum vs. Diffusion wave

To compare the two different computation methods in HEC-RAS, the diffusion wave and full momentum equation are used to simulate for different cell sizes. The cell sizes tested were the same as for the parameter testing for cell sizes (3.4.1). As the HEC-RAS 2D Modeling manual states that the Diffusion wave will have shorter computation time, this is also interesting to check. The difference between the two computation methods was found by subtracting the values of the raster created by Diffusion wave, from the raster created by Full Momentum. The results with the same cell size were compared with the two different computation methods. The comparison was made in ArcMap, as explained in 3.4

3.4.4 Fixed Time Step

In HEC-RAS 5.0.7, the user can set the time step manually, but as earlier mentioned, Courant conditions set the time step done in this model. To test the effect of the Courant conditions, a simulation with a fixed time step was done to compare with the results from simulations with Courant conditions. The results from a simulation with Courant Conditions are used as a reference for the different time steps.

Time step 5 seconds, 3 seconds, 1 second, and 0.1 seconds is tested. Time steps above 5 seconds are not possible to run, because of a Courant Number that exceeds 3.

3.4.5 Eddy viscosity

In HEC-RAS, the turbulence is expressed through the eddy viscosity, which is modeled as a gradient diffusion process. In the default settings for HEC-RAS, the Eddy Viscosity Mixing coefficient is not used. By changing the eddy coefficient to greater than zero, this feature is turned on. The coefficient requires calibration to get an appropriate value for the situation (Brunner & CEIWR-HEC, HEC-RAS 2D Modeling User's Manual, CPD-68A, 2016, ss. 4-16). Table 2 in Chapter 2.5 presents values for the coefficient found appropriate.

Mixing coefficient 0.2, 0.3, and, 5 is tested. That means a mixing coefficient for each of the tree situations given by HEC-RAS are tested (table 2). The maximum D_T is 5, which indicates strong meanders and rough surface. Even though this is not the situation for Manddalselva, it is interesting to see how the model reacts.

3.4.6 Initial Conditions Rampup Fraction Time and Initial Conditions Time

Rampup time is the option to ramp up the water surface from dry conditions to wet conditions in the 2D area. In modeling of Manndalselva, a hydrograph is used as external boundary conditions. The flow hydrograph has lower values than the intended water flow, to avoid instability and that cells outside of the river are filled because of the first wave that reaches the empty river. The initial conditions ramp up time does this for the modeler so that this it is not needed to increase the flow hydrograph as mentioned above. The option slowly transitions the flow from zero to the initial value in a specified time set by the modeler. If the ramp up time is set to 0.5, it means that 50% of the initial conditions time is used to ramp up the flow to the initial flow. The rest of the time is used to keep the boundary conditions constant.

A ramp up time of 50 % was tested.

3.4.7 Friction Slope

In Normal depth downstream boundary conditions, the friction slope is set. As a rule of thumbs, a friction slope of 0.01 can be used here. To test this, a slope of 0.05 and 0.05 are compared to 0.01. The actual slope of the river is 0.05.

3.5 Flood Simulation

After parameter testing and calibration of the model, the model could be used to simulate different flooding scenarios. Figure 9 illustrates the size of the catchment. The catchment is 201.1 km² (NVE, 2018), and the figure presents how the catchment is affected by the steep mountainsides in Manndalen.



Figure 9: The catchment for Manndalen River

The catchment to Manndalselva has a mean discharge of 29.5 l/(s•km²). The full NEVINA rapport is found in Appendix G. Note that NEVINA uses NIFS. NIFS (NATURFARE – infrastruktur, flom og skred) is a national formula network that estimates mean average flood and water flow with bigger return periods for small catchments in Norway. Small catchment means catchment smaller than 50 km², which is not the case for Manndalen. The values given from NEVINA can only be used as guiding values.

For catchments bigger than 50 km², flood estimates from *Reginale flomfrekvensanalyse* (RFFA-2018) should be used. The results from these calculations are found in Appendix H.

NVE has three security classes for flood-prone areas, which indicates the flood scenario it should be dimension for. The classes are listed in table 4

Table 4: Security classes for flood dimensioning given by the NVE

Security class flood	Consequence	Largest nominal annual probability
F1	Small	1/20
F2	Medium	1/200
F3	Big	1/1000

Security class F1 involves areas where lives are not in danger, small economic losses and other consequences to the society. F2 area areas with a medium consequence, with buildings used for housing, schools, kindergartens, and office buildings. Areas, where particularly vulnerable groups of people reside (ex. Retirement homes), are in class F3. Buildings that house emergency instances (fire department, hospitals, et cetera.) are also in F3 (Stenius, Glad, Wang, & Væringstad, 2015).

The area around Mandalselva contains houses, school, and kindergartens, and is because of this in class F2. The area should minimum endure a 200-year flood. A 200-year flood means that there is a 0.5 % probability that a flood of this size will happen in a year. That means a 200-year flood can happen two years in a row, though the probability for that event is small.

A return period of 200 years with a climate change projection of 1.4%, $Q_{200Klima} = 190$ m³/s will be simulated for Mandalen.

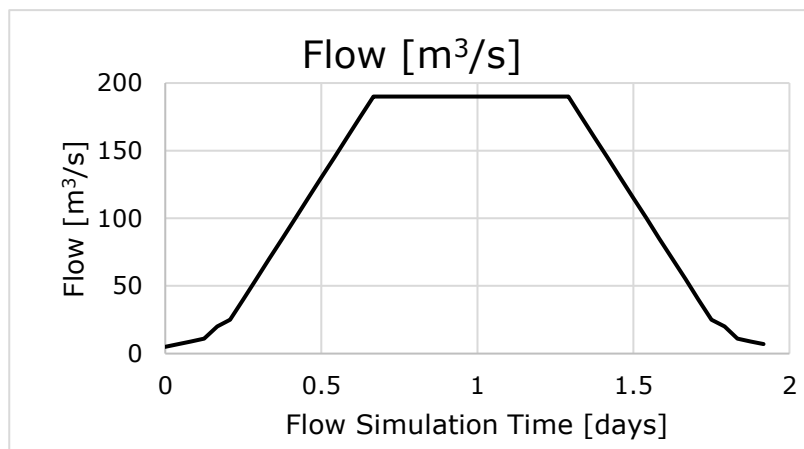


Figure 10: Flow hydrograph used for flood simulation

The simulation was done with a grid size of 3 meters, and the upper boundary condition used is shown in figure 10. This provided a stable running of the model

3.6 Validation of Model

May 30th, the gauging station in Mandalen registered a high water flow. Anders Bjordal in NVE was able to measure the water surface elevation during this event. When the measurements were taken the water flow had decreased, but there were clear signs where the water had reached when the flow was at its highest. GPS points were measured for a flow of 14.7 m³/s and 24.2 m³/s. This data is used to validate the model,

as the calibration data is not completely accurate. The graph of the river flow can be found in Appendix I.

4 Results

Here the results from the calibration, sensitivity analysis, flood simulation and validation will be given.

4.1 Calibration

For each simulation, the difference from the observed WSE was calculated and made into a matrix for each cell size. Green color indicates a difference under 0.01; yellow is 0.01-0.05, orange is 0.05-0.1, bright red is 0.1-0.3, while dark red indicates a difference bigger than 0.3. As grid size 10 meters needed the shortest simulation time, the most crucial changes were done with that grid size. Table 5 holds the results.

Table 5: Result from calibration with grid size 10 meters

Cross-section	Difference between measured and simulated WSE [m]						
	Sim. 1	Sim. 2	Sim. 3	Sim. 4	Sim. 5	Sim. 6	Sim. 7
2	-0.116	-0.146	-0.146	-0.116	-0.116	-0.106	-0.106
3	-0.007	0.013	0.013	0.013	0.013	0.003	0.003
5	0.150	0.160	0.160	0.160	0.160	0.160	0.160
7	0.064	0.054	0.064	0.044	0.054	0.034	0.034
8	0.175	0.265	0.265	0.265	0.265	0.245	0.245
10	0.150	0.140	0.140	0.150	0.140	0.140	0.140
11	0.058	0.078	0.078	0.078	0.078	0.078	0.078
12	0.132	0.102	0.122	0.152	0.182	0.172	0.172
13	0.197	0.157	0.177	0.187	0.187	0.217	0.217
17	0.074	0.044	0.064	0.064	0.064	0.054	0.054
19	-0.025	-0.035	-0.045	-0.025	0.015	0.005	0.005
20	0.205	0.225	0.235	0.325	0.385	0.265	0.265

Sim. 1 is an abbreviation for simulation 1. Simulation 1 indicates the first simulation done, and simulation 2 is the next one, et cetera. For some of the cross-section, the results are quite close to the observed WSE. For cross section 20, the difference is the more significant. The manning's number used in each simulation are found in Appendix J.1

Table 6 shows the result for calibrations with grid size 5.

Table 6: Result calibration with grid size 5 m

Cross-section	Difference between measured and simulated WSE [m]							
	Sim. 1	Sim. 2	Sim. 3	Sim. 4	Sim. 5	Sim. 6	Sim. 7	Sim. 8
1	-0.126	-0.126	-0.106	0.086	-0.086	-0.086	-0.086	0.086
2	-0.017	-0.027	-0.007	0.013	0.013	0.013	0.013	0.013
3	0.150	0.150	0.150	0.170	0.170	0.170	0.170	0.150
4	0.054	0.054	0.054	0.084	0.084	0.084	0.084	0.064
5	0.165	0.175	0.175	0.215	0.185	0.185	0.185	0.165
6	0.150	0.150	0.150	0.170	0.170	0.150	0.150	0.150
7	0.048	0.048	0.048	0.068	0.068	0.068	0.068	0.068
8	0.102	0.092	0.122	0.202	0.202	0.202	0.172	0.172
9	0.157	0.157	0.177	0.287	0.397	0.317	0.247	0.317
10	0.064	0.064	0.064	0.104	0.084	0.084	0.074	0.074
11	-0.025	-0.025	-0.025	0.005	-0.005	-0.005	-0.005	0.005
12	0.185	0.185	0.205	0.325	0.305	0.245	0.205	0.245

The Manning's n from sim.1 were tested with smaller grid size as this gave the best result. The different Manning's number used are in Appendix J.2.

For grid size 3 x 3, the simulation time varied around 20 minutes, and the fine-tuning of the Manning's number were done here. Table 7 presents the results. As the adjusting of a Manning's n affects the WSE in the nearby area, several simulations were done.

Table 7: Result for calibration with grid size 3 meters

Cross-section	Difference between measured and simulated WSE [m]							
	Sim. 1	Sim. 5	Sim. 10	Sim. 15	Sim. 20	Sim. 25	Sim. 28	Sim. 29
1	-0.136	-0.116	-0.116	0.024	0.004	0.009	0.001	0.001
2	-0.007	0.003	0.003	0.003	0.003	0.002	-0.014	-0.021
3	0.140	0.120	0.090	0.050	0.110	0.123	0.064	0.048
4	0.064	0.034	0.014	-0.076	-0.156	-0.081	-0.122	-0.120
5	0.185	0.165	0.145	0.055	-0.015	0.033	0.002	0.001
6	0.150	0.140	0.140	0.070	0.090	0.065	0.067	0.060
7	0.058	0.048	0.048	0.048	-0.002	-0.010	-0.011	-0.017
8	0.212	0.082	0.022	0.022	0.022	0.001	-0.011	-0.014
9	0.267	0.117	0.067	0.057	0.047	0.028	0.010	0.010
10	0.074	0.054	0.034	0.014	0.054	0.032	0.018	-0.024
11	0.005	-0.065	-0.065	-0.065	-0.035	-0.015	-0.042	-0.012
12	0.235	0.085	0.085	0.085	0.085	0.058	-0.005	-0.004

Only highlights are shown in table 7, as there were conducted 29 calibration simulations. The complete result is found in Appendix J.3. The Manning's number used are in Appendix J.4-J.6.

Simulation 30 with grid size 3 meters gave results where a majority of the cross sections had acceptable differences in WSE. Manning's number from simulation 29 was used for simulations with smaller mesh. Since simulation 28 also gave good results, the corresponding Manning's number was run with a grid resolution of 2 meters. Manning's values for simulation 28 grid size 3 meters correspond with simulation 4, grid size 2 meter. Simulation 29 (3 meters) corresponds with Manning's n for simulation 1 (2 meters).

The result from simulations with a grid size of 2 x 2 meters is found in table 8.

Table 8: Result for calibration with grid size 2 m

Cross-section	Difference between measured and simulated WSE [m]			
	Simulation 1	Simulation 2	Simulation 3	Simulation 4
1	-0.003	-0.003	0.005	0.004
2	-0.027	-0.027	0.056	0.016
3	0.032	0.031	0.108	-0.053
4	-0.115	-0.113	-0.112	0.118
5	0.009	0.024	0.024	-0.005
6	0.062	0.230	0.231	-0.071
7	-0.020	0.064	0.093	0.014
8	-0.006	0.052	0.064	0.006
9	0.021	0.021	0.021	-0.021
10	0.001	0.001	0.001	-0.001
11	-0.004	-0.004	-0.004	0.036
12	-0.007	-0.007	-0.007	0.007

The best overall result was from simulation 1. As mentioned in Chapter 3.3, a modeled WSE equal to the measured WSE cannot be expected. The Manning's n for simulation 1 was used for the sensitivity analysis, as well as the flood simulation. The values for n are found in table 9. The other Manning's numbers tested are listed in Appendix J.7.

Table 9 The final Manning's numbers. n has unit $s/m^{1/3}$

Manning's n region	n	Manning's n region	n
river 1	0.1	river 11	0.05
river 2	0.06	river 12	0.06
river 3	0.18	river 13	0.06
river 4	0.01	river 14	0.045
river 5	0.05	river 15	0.045
river 6	0.04	river 16	0.045
river 7	0.14	river 17	0.041
river 8	0.06	river 18	0.01
river 9	0.045	river 19	0.14
river 10	0.068	river 20	0.04

Figure 11 a) shows the depth of the river at the water flow used for the calibration. The picture to the right is the velocity for the same flow. The highest velocity is in the Manning's region *River 3* (see chapter 3.3), where the Manning's n is $0.18 s/m^{1/3}$. The same area is shallower than the area upstream and downstream.

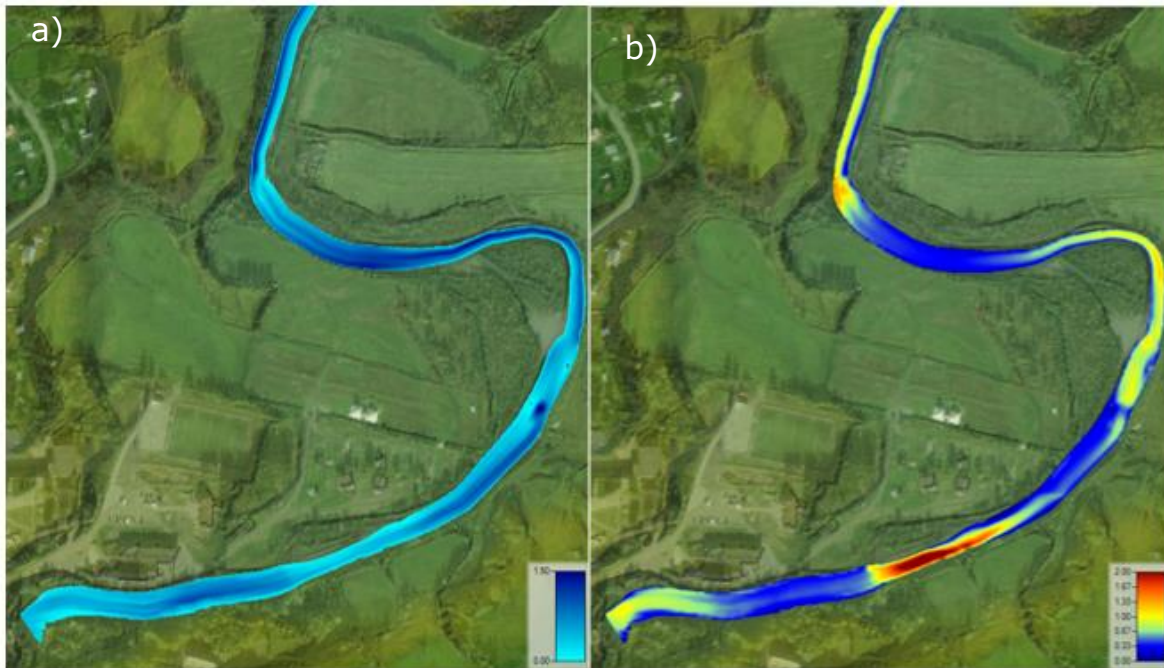


Figure 11: a) The depth and b) velocities for the calibration simulation.

4.2 Sensitivity analysis

4.2.1 Grid size

The different cell sizes tested were 0.5 meters, 1 meter, 3 meters, 5 meters, and 10 meters. The computation period for the simulations varies a lot, as table 10 shows. A grid size of 3 meters was used as a reference value for comparison of the water surface elevation. Table 10 shows a correlation between cell size and computation time. A cell size of 10 meters uses nearly double the time as 1 meter. 1 meter takes almost nine times as much time as 2 meters. The computation time makes a 0.5 and 1 meter grid unpractical to use when many computations are to be made.

Table 10: Computation time for different grid sizes

Cell size	10 m	5m	3 m	2 m	1 m	0.5 m
Computation time	00:00:57	00:08:53	00:28:24	01:07:54	09:10:02	17:47:25

The maximum difference, mean difference, and standard deviation for the different grid sizes compared to a grid of 3 meters are listed in table 11.

Table 11: Statistical data, grid size

Cell sizes compared to 3 m	Maximum difference [m]	Mean [m]	Standard deviation [m]
0.5	0.154	0.001	0.023
1	0.115	0.006	0.015
2	0.122	0.001	0.008
5	0.116	0.007	0.010
10	0.250	0.007	0.024

The maps in figure 12-14 illustrates where the differences in water surface elevation for the different cell sizes are. Figure 12 a) illustrates the difference between 3 meters and 1 meter and figure 12 b) shows the difference between 3 meters and 0.5 meters. The differences are more significant for 3 meters and 0.5 meters. The maximum difference between 3 meters and 0.5 meters is 0.154 meters, while for 3 meters and 1 meter it is 0.115 meter. The mean difference for 0.5 meters is 0.001 m. For 1-meter grid the difference is 0.006 m.

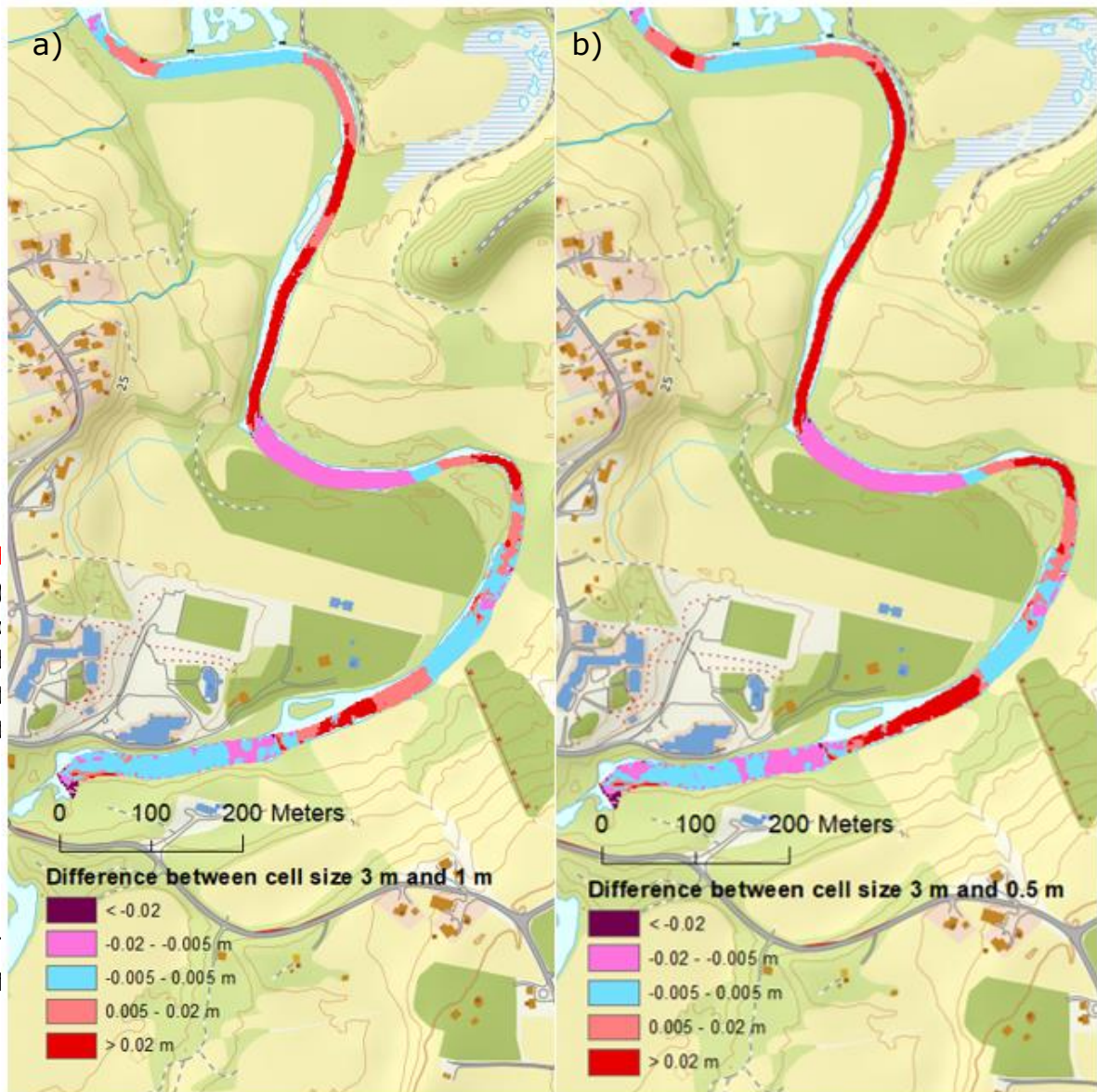


Figure 12: The difference in WSE between grid size 3 m and a) 1 m and b) 0.5 m.

Figure 13 a) shows small differences between cell size 2 meters and 3 meters. For the upstream part of the river there are nearly no differences bigger than 0.02 meters. Some areas occurs where there are bigger differences in WSE than 0.02, but only for small sections. In the middle part of the river shown in the figure, there are a long distance of the river where the differences vary between 0.005 and 0.02, and also parts where the difference is bigger. For the most downstream part, there are small differences. 13 b) shows some of the same trends as 13 a), but the differences are bigger. The differences are more speckled spread for 13 b) than for 13 a). For both 13 a) and b) the differences varies between having a higher WSE than the reference result of 3 meter grid, or a lower WSE. A hypothesis could have been that a finer grid size would have given a lower WSE than the reference, and a bigger grid size would give a higher WSE. As figure 13 shows, that hypothesis does not seems to be correct.

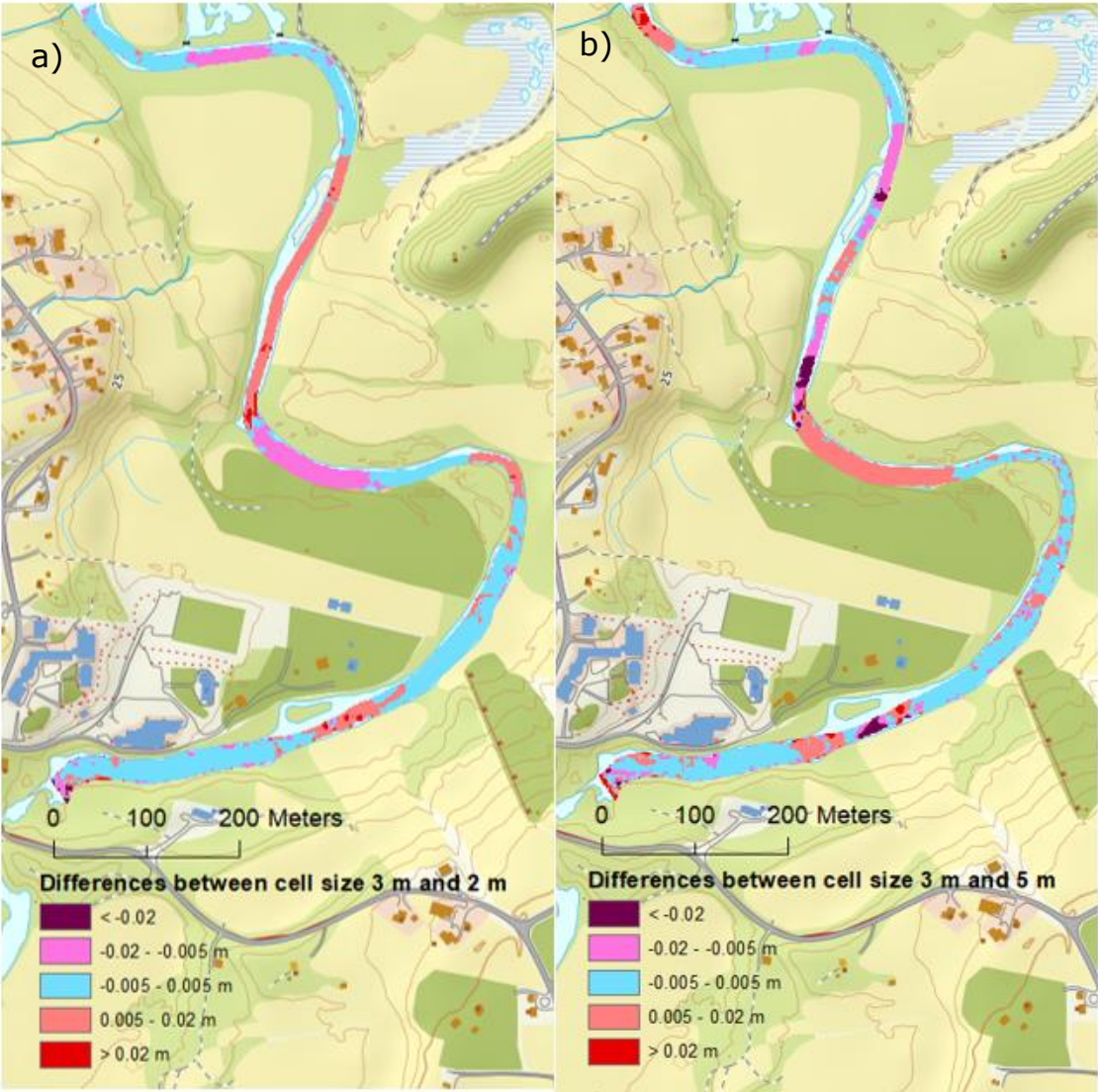


Figure 13: Difference in WSE between 3 m and a) 2 m and b) 5 m

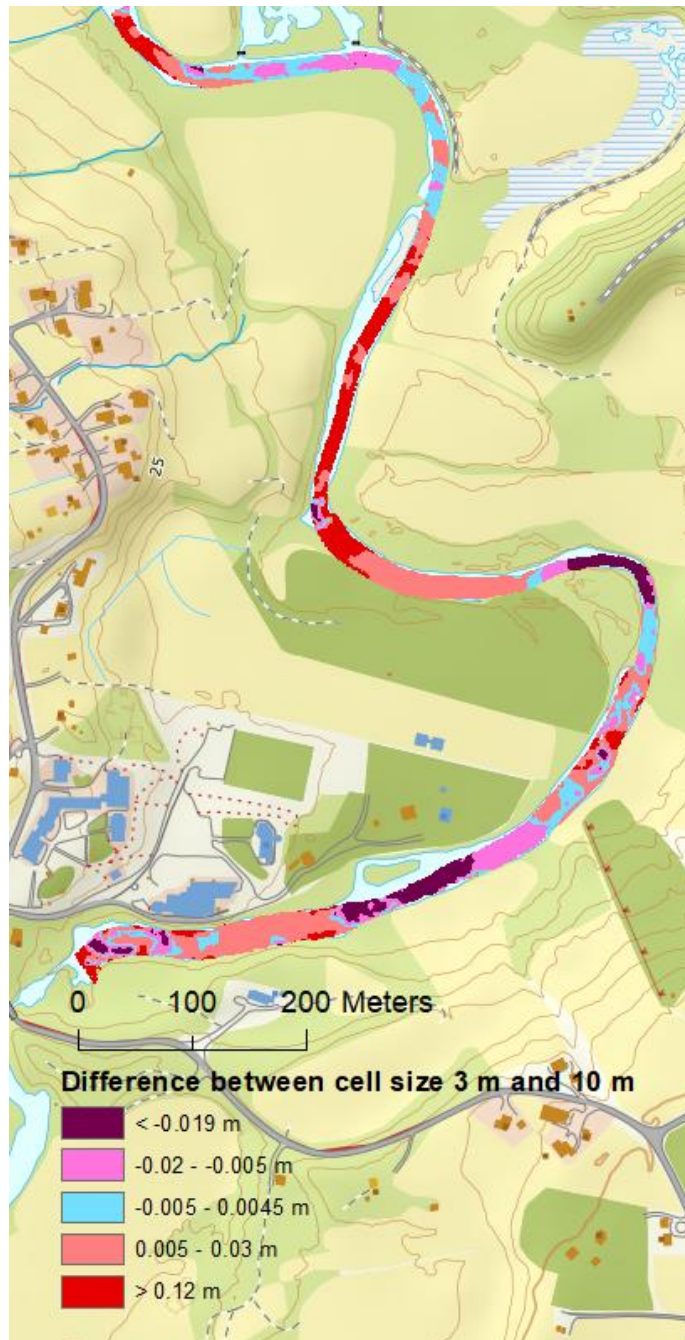


Figure 14: Difference in WSE between 3 m and 10 m

As figure 14 shows, there are more differences in the water surface elevation, than equal water surface elevations. There are bigger differences between these two grid sizes than for the other sizes tested. The maximum difference is 0.25 meters, and that is the highest value for all of the comparisons done. Bigger maps are found in Appendix L.

4.2.2 Theta

Theta of 1 and 0.8 was tested and compared to a computation with Theta of 0.6, as used in the calibration. Theta equal 1 is the default setting for HEC-RAS.

Table 12: Statistical data, theta

Theta compared to 0.6	Maximum difference [m]	Mean [m]	Standard deviation[m]
0.8	0.045	-0.00013	0.00057
1	0.044	-0.000001	0.0006

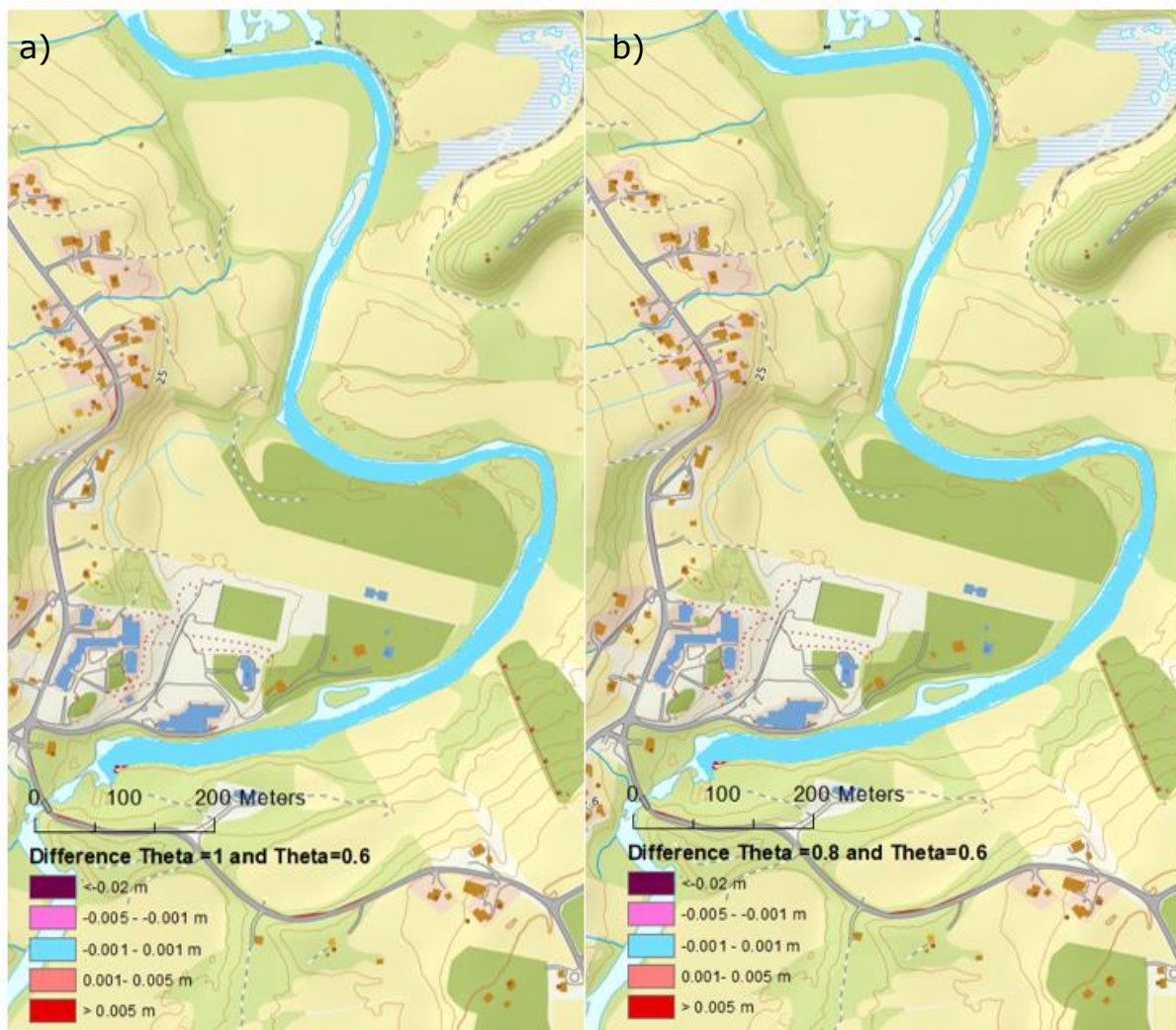


Figure 15: The difference in WSE between theta 0.6 and a) 1 and b) 0.8.

Figure 15 shows minimal differences for both situations Theta equal 1 and 0.8 compared to Theta=0.6. The most observable difference is upstream of the river, but as the differences are minimal, this is considered to be negligible. The maximum difference is 4.5 centimeters. The model runs stable with all values of Theta. The 2D modeling User's Manual states that Theta of 0.6 and 1 will give about the same answer, as this sensitivity analysis shows. The simulations were run over a time window of six hours, and Theta=1 used 9 minutes, Theta=0.8 used 14 minutes, and Theta=0.6 used 24 minutes. Bigger maps are found in appendix M. The difference in computation time cannot be proven to be caused by the difference in Theta. Lars Skeie did a similar analysis in his master

thesis *Hydraulisk modellering av kraftversdrift i Tokkeåi* (Skeie, 2017), where the different Theta did not affect the simulation time.

4.2.3 Full momentum vs. Diffusion wave

The diffusion wave computational method is the default equation used by HEC-RAS, and it performs faster computations with greater stability than full momentum.

Table 13 shows the computation time for each of the cell sizes for the two different computational methods.

Table 13: Computation time for Diffusion wave and full momentum

Cell size	10 m	5 m	3 m	1 m	0.5 m
Diffusion wave					
Computation time	00:00:55	00:08:43	00:11:26	04:35:20	15:23:37
Full momentum					
Computation time	00:00:57	00:08:53	00:28:24	09:10:02	17:47:25

What stands out in the table is the computation time for a grid of 0.5 meters. For both Diffusion wave and Full momentum, the computation time is significantly higher than for the other sizes. For the finer grids, the computation time is similar for the computation methods, but the difference starts increasing at 3 meters.

Table 14 : Statistical data, computation method

Cell size	Maximum difference [m]	Mean [m]	Standard deviation [m]
0.5	0.563	0.185	0.179
1	0.178	0.0261	0.0253
3	0.177	0.0325	0.0294
5	0.161	0.0313	0.0298
10	0.21	0.0292	0.029

From the data in table 14, it appears that the largest difference is for cell size 0.5. The mean difference is also highest for the finer grid size. The smallest difference occurs for the comparison of cell size 5 meters.

Closer inspection of the differences in WSE is given in the maps in figure 16-18. Bigger maps are found in appendix N

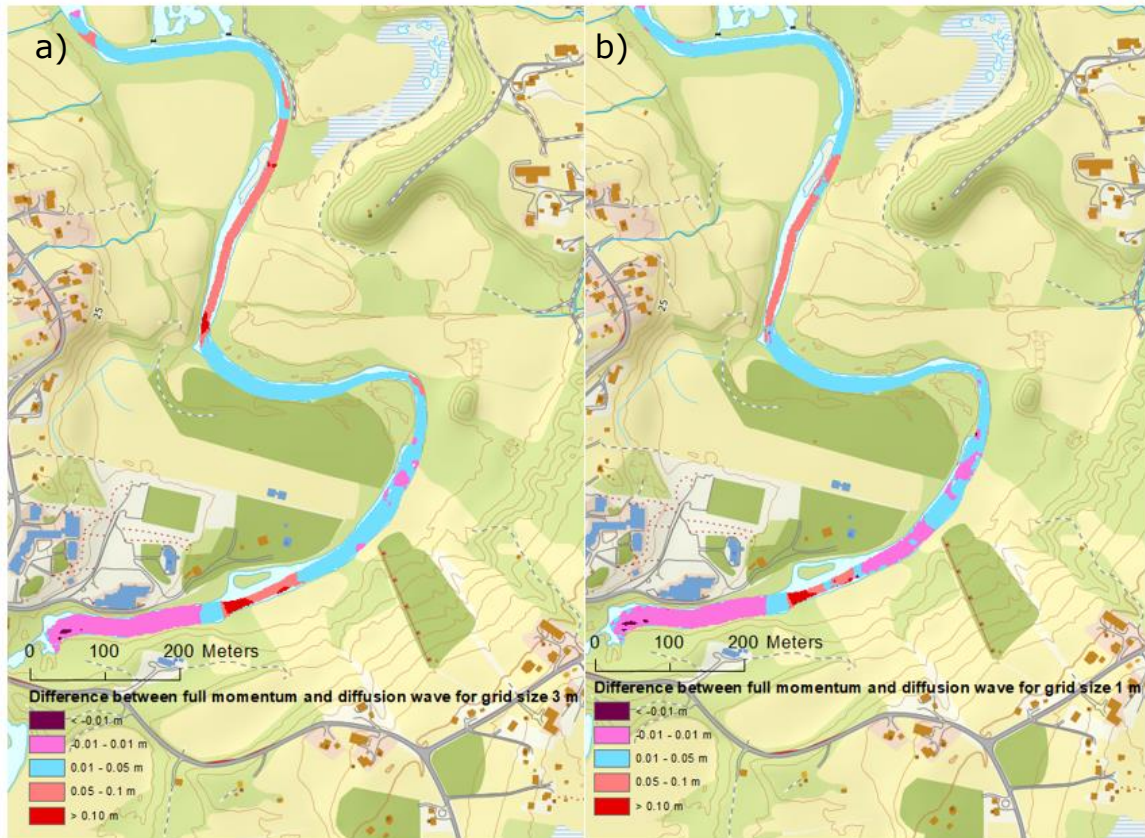


Figure 16: Differences in WSE for full momentum and diffusion with cell size a) 3 m b) and 1 m.

Figure 16 presents the differences between full momentum and diffusion wave for 3-meter grid size and 1 meter. For both comparisons, the main difference between the computation methods occurs in the same areas. For both grid sizes, the maximum difference is 0.18 meters. 3 meter has more extended areas with differences than 1 meter.

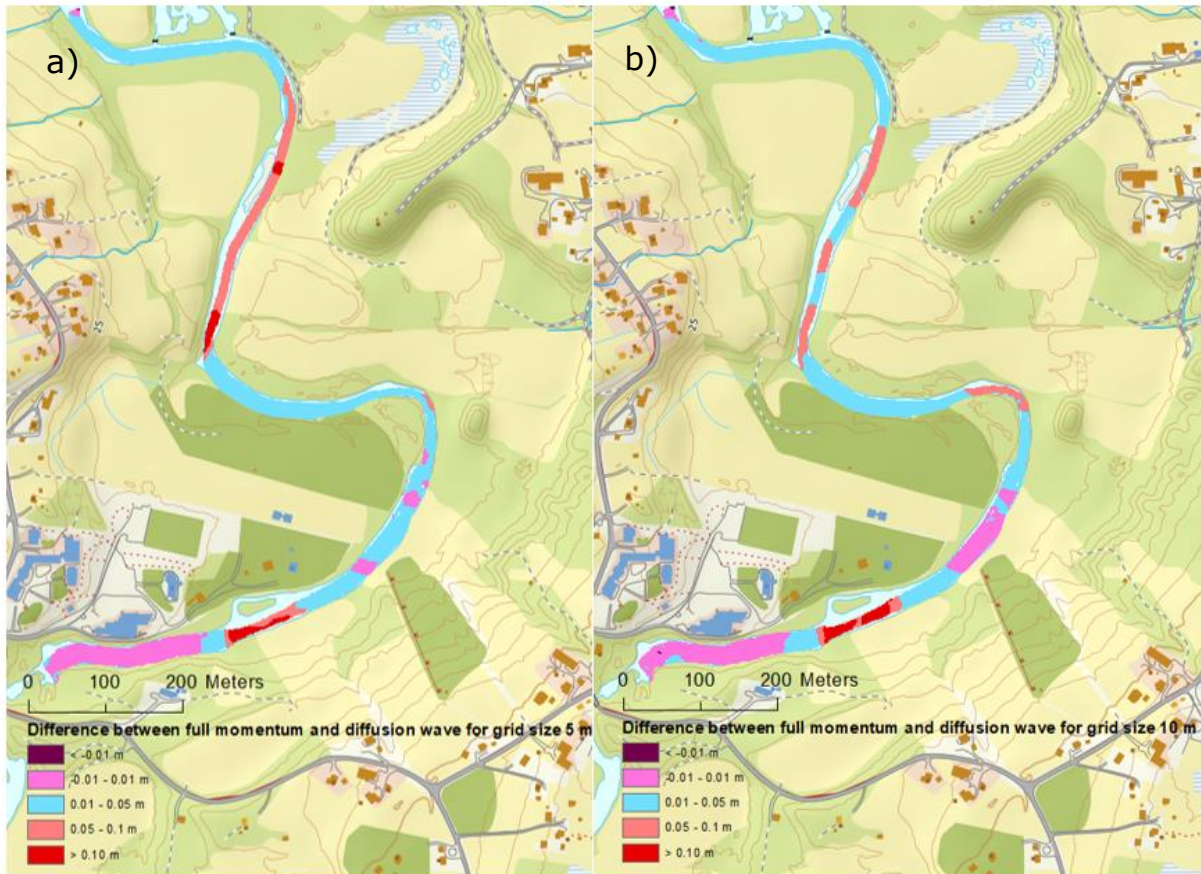


Figure 17: Difference in WSE for full momentum and diffusion wave with cell size a) 5 m and b) 10 meters.

Figure 17 compares the two computation methods for 5 meters and 10 meters. The results for 5 meters are similar to 3 meters, and the maximum difference, mean, and standard deviation are close in value. What is surprising is that 10 meters has fewer differences in certain areas, and there are small differences. The maximum difference is 0.21 meters and occurs close to the island below the kindergarten

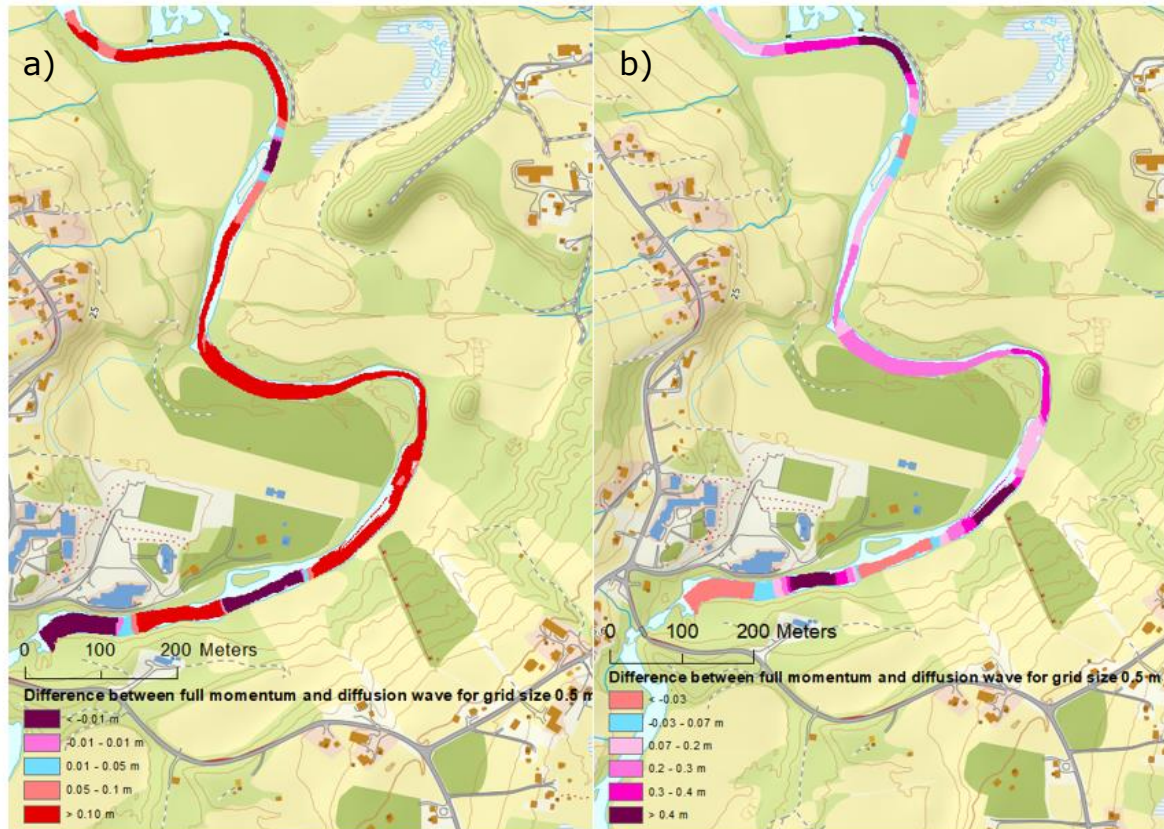


Figure 18: Difference in WSE for full momentum and diffusion wave for grid 0.5

Figure 18 a) shows that there are differences in WSE for nearly the whole river. Only small sections of the river have a nearly equal WSE for diffusion wave and full momentum. As the variation of differences were difficult to obtain with the color scheme used for the earlier comparisons, a new color scheme was made. In figure 18 b) the variations are easier to distinguish. The figure shows there are relatively long distances of the river where the WSE from full momentum simulation is over 0.4 meters.

Bigger figures of the maps are found in Appendix N.

4.2.4 Fixed Time Step

For the fixed time step option, a finer mesh needs a corresponding smaller time step. For simulations tested with a time step bigger than 5 seconds, the simulation crashed (see Appendix O.5). Most likely, this is because of the Courant number exceeded 2, which indicates an unstable computation.

Table 15: Computation time Fixed Time Step

Computation interval [s]	0.1	1	3	5
Computation time	04:14:13	00:31:58	00:10:11	01:18:08

As expected, the highest computation time was for 0.1 seconds. More surprisingly is that the computation time for 5 seconds is higher than for 1 second and 3 seconds.

Table 16: Statistical data, Courant Conditions and Fixed Time step

Time Step compared to Courant Conditions [s]	Maximum difference [m]	Mean [m]	Standard deviation [m]
5	0.0920	0.0098	0.0130
3	0.0840	0.0040	0.0093
1	0.0599	-0.0004	0.0012
0.1	0.0440	0.0005	0.0015

The WSE from the fixed time step computation was compared to simulations with time steps controlled by Courant conditions, as shown in figures 19 and 20. Bigger maps are found in Appendix O.

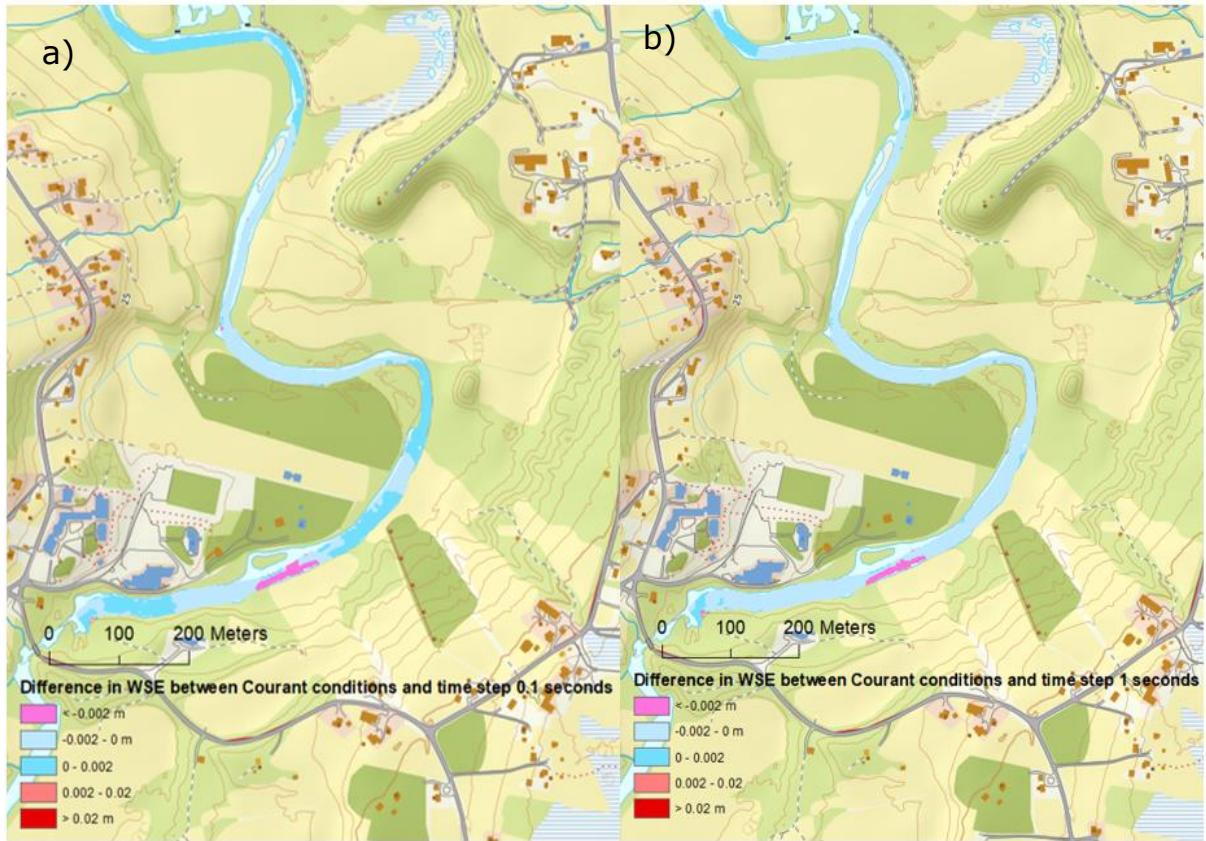


Figure 19: The difference in WSE for Courant conditions and time step a) 0.1 second and b) 1 second

There are minimal differences for both 0.1 second and 1 second. The differences occur in the same areas for the two simulations. The maximum differences for figure 19 a) are 0.044 m, and 0.06 m for figure 19 b).

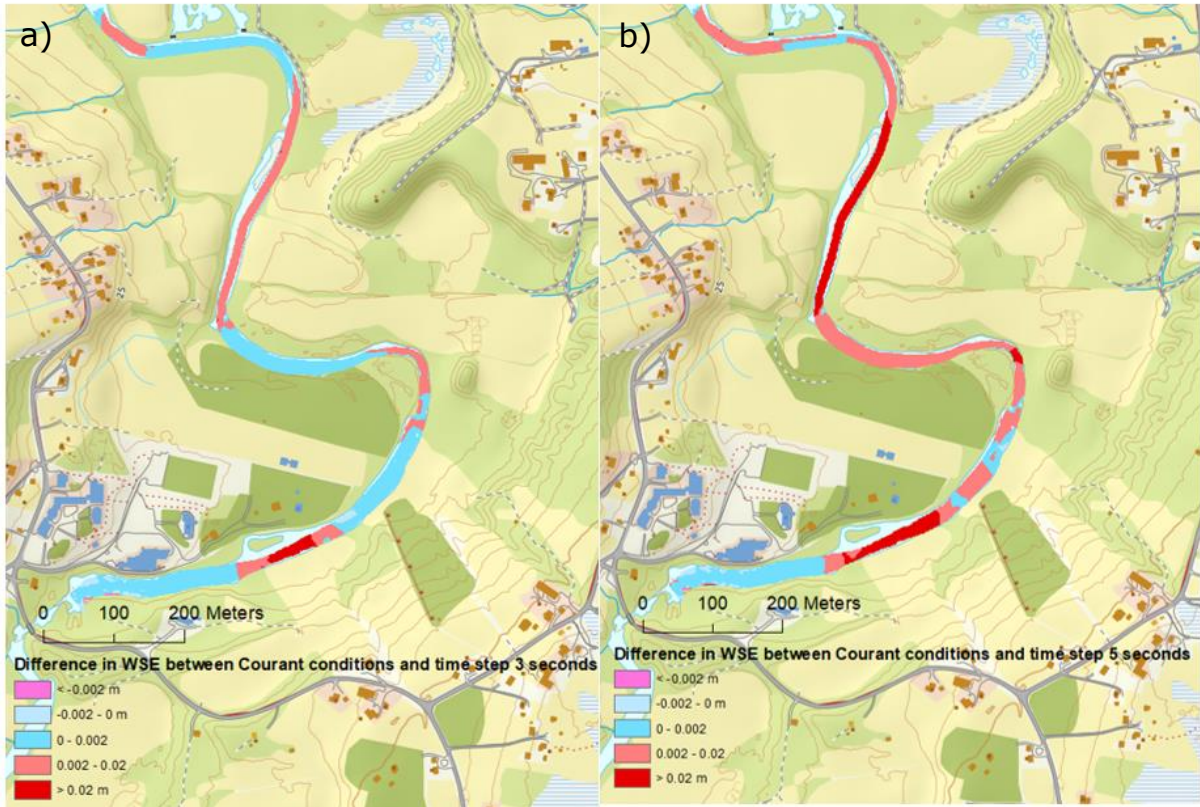


Figure 20: Difference in WSE for Courant Condition and a) 3 seconds and b) 1 second

As shown in figure 20 the difference in WSE between Courant Conditions and 3 seconds and 5 seconds are more significant than for 1 and 0.1 seconds. The biggest difference in WSE is between Courant conditions and a time step of 5 seconds. As the differences were biggest, and the computation time were long, a 5-second time step is not advisable for this model.

The result for the simulation done with Courant Conditions has an adaptive maximum time step of 02:51.429, and a minimum adaptive time step of 00:00.335. The initial adaptive time step is 00:05:357. The complete computation process took 20 minutes. The adaptive time steps for Courant conditions are found in the Compute Message created by HEC-RAS when the simulation is done.

4.2.5 Eddy Viscosity

The values tested for Eddy viscosities were 0.2, 0.3, and 5. The computation times are listed in the table below. The different coefficients were compared to a simulation with the turbulence term off.

Table 17: Simulation time for Eddy Viscosity

Eddy Viscosity Mixing				
Coefficient	Off	0.2	0.3	5
Simulation time	00:23:51	00:14:13	00:25:58	00:27:18

Table 17 shows that the computation times are similar for all simulations, except Eddy coefficient of 0.2.

Table 18: Statistical data, Eddy viscosity

Eddy Viscosity compared to 0 (off)	Maximum difference [m]	Mean [m]	Standard deviation [m]
0.2	0.0338	-0.0093	0.021
0.3	0.034	-0.003100	0.0033
5	0.085	-0.00042	0.00086

Table 18 present the differences for the computations. The maximum differences are small for all simulations, and the mean values are also minimal. The figures below illustrate where the differences in WSE are located.

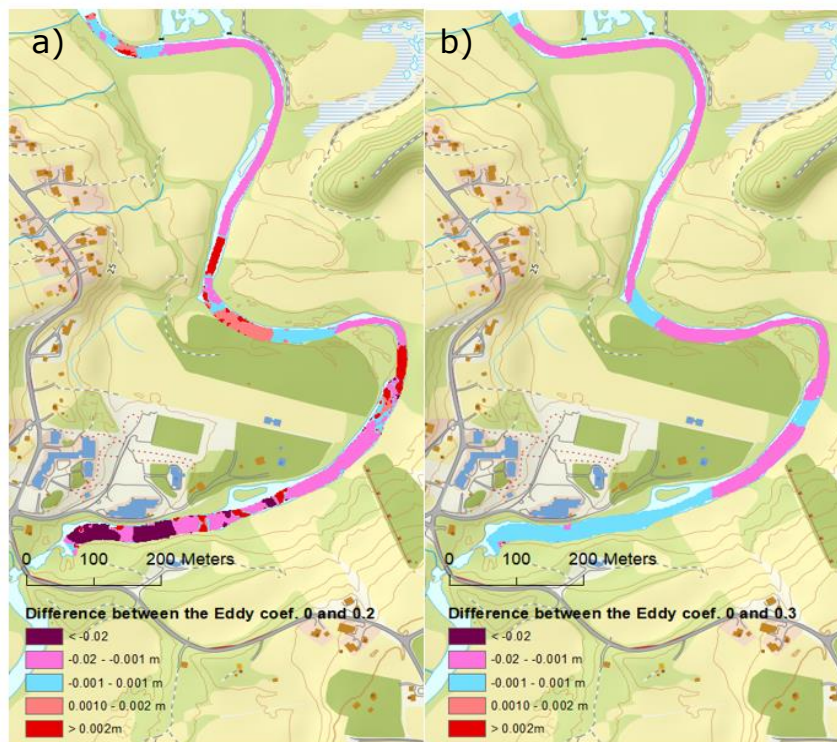


Figure 21: Difference in WSE for Eddy coefficient value of a) 0 and 0.2 and b) 0 and 0.3.

The differences are more significant for an Eddy viscosity of 0.2 compared to a value of 0.3. In the upstream part of the river, there are nearly no differences for eddy coefficient of 0.3. For an eddy of 0.2, the upstream area has more differences over a severe area. Even though there are differences, they are still minimal.

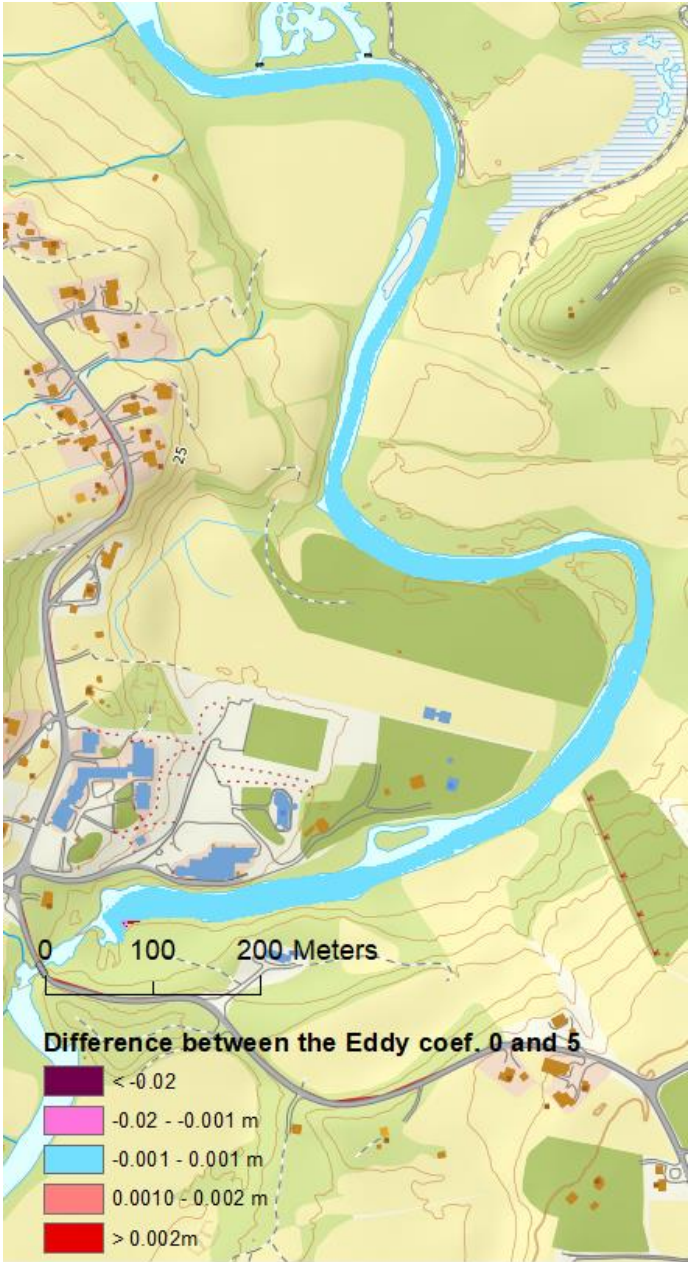


Figure 22: Difference in WSE for eddy coefficient of 0 and 5

For the Eddy velocity equal 5, the biggest difference for the test values occur. The difference is upstream in the river, but in a small area. For the rest of the river, the difference is minimal. Bigger maps of figure 21 and 22 are found in Appendix P.

4.2.6 Initial Conditions Rampup Fraction Time

For the calibration, an increasing flow hydrograph was used. To validate if there is a significant difference between a ramp up time and an increasing flow. Table 19 holds the results. The simulation time was 24 minutes.

Table 19: Statistical data Rampup time

Rampup time	Maximum difference	Mean	Standard deviation
0.5 (50%)	0.044	0	0.00049

Figure 23 shows where the differences in WSE are found.

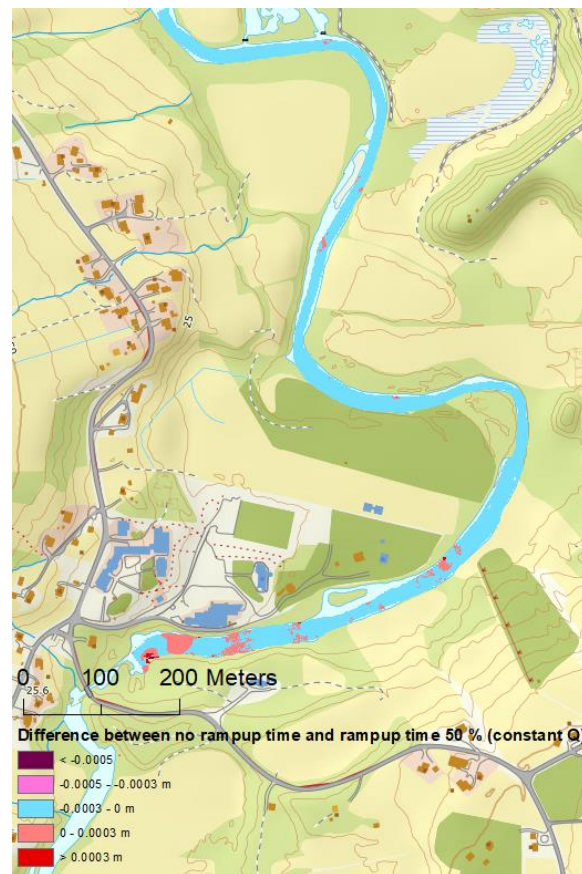


Figure 23: Differences in WSE between an increasing flow hydrograph and a rampup time

The maximum difference is located upstream in the river. Smaller differences occur throughout the river, but these are minimal.

4.2.7 Friction Slope

The actual slope for the river is 0.05, but a friction slope of 0.01 is used. To check if this will affect the result, a comparison between 0.01 and 0.05 is conducted, as well as a comparison of 0.01 and 0.5. The summary of the comparison is found in the table below.

Table 20: Statistical data, friction slope

Friction slope	Maximum difference [m]	Mean [m]	Standard deviation [m]
0.05	0.135	0.00087	0.0071
0.5	0.26	0.00047	0.0112

The difference between a friction slope of 0.01 and 0.05 are minimal for most of the river, as shown in figure 24. The difference occurs at the most upstream part of the river as well as furthest downstream. For the comparison of 0.5 and 0.01, the differences are more significant. The maximum difference is 0.26 meters, and by the downstream boundary condition.

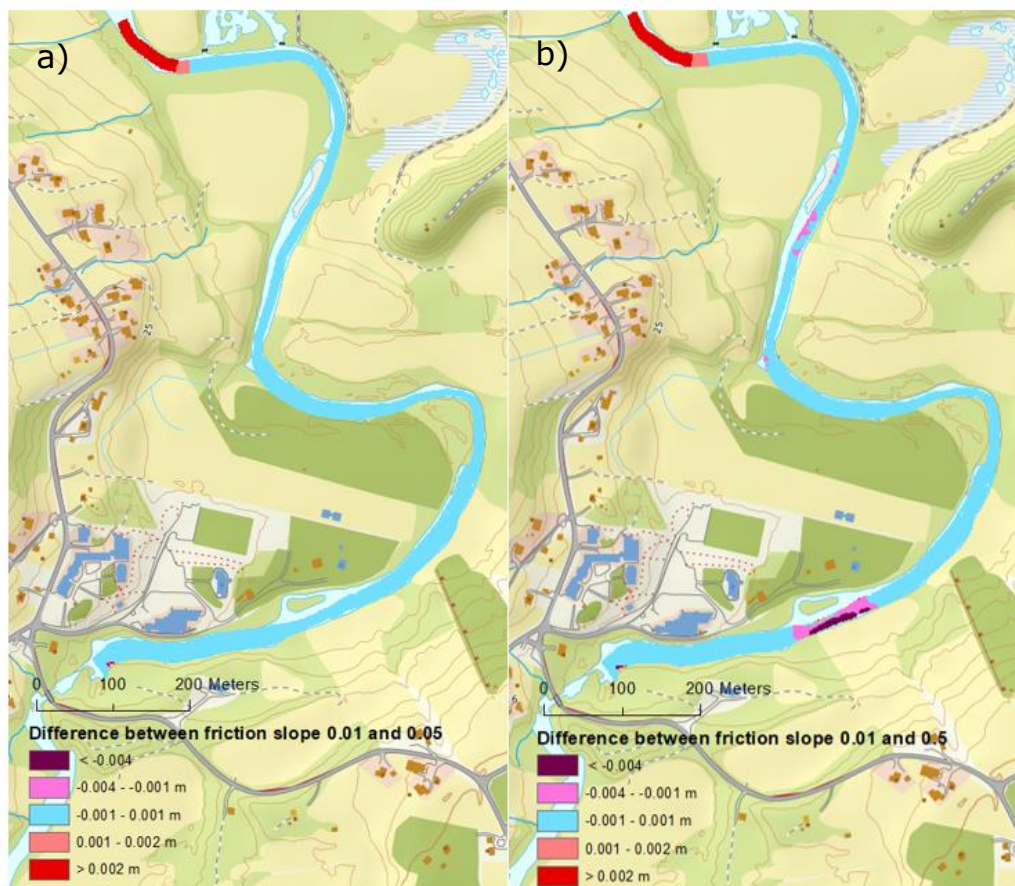


Figure 24: Difference in WSE for a friction slope of a) 0.01 and 0.05 and b) 0.01 and 0.5.

0.5 was checked to see if the friction slope effects the results, as the differences were minimal for 0.05 and 0.01 meter. The computation time is presented in table 21

Table 21: Computation time Friction slope

Friction slope	0.01	0.05	0.5
Simulation time	00:28:24	00:28:46	00:40:54

The simulation time were longer for a friction slope of 0.5 than the two other values

4.3 Flood Simulation

Figure 25 shows the flood simulation for the 200-year flood with climate change projection ($Q=190 \text{ m}^3/\text{s}$). As figure 25 shows, the flood does not flood the Center of Northern People or the kindergarten. A picture of the flooding of the whole area can be found in Appendix S.

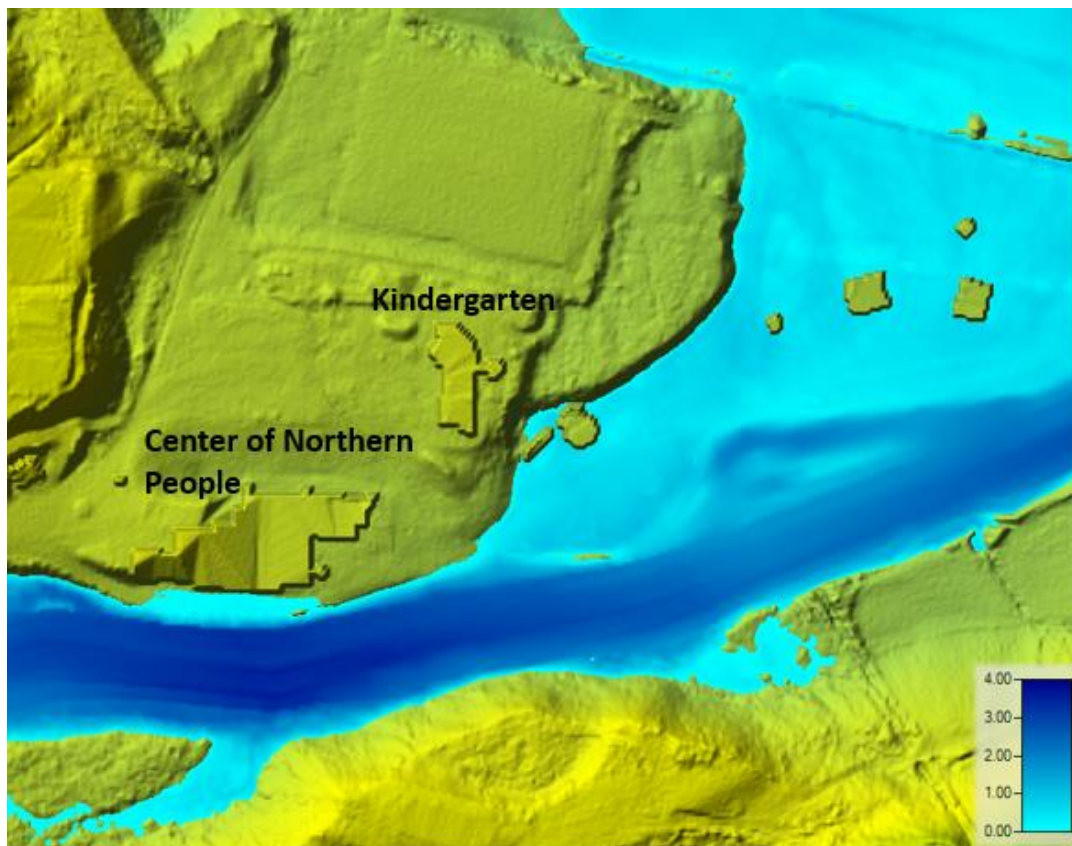


Figure 25: Center of Northern People and the kindergarten in a flooded situation

Cross-sections in the flooded area were studied to see the depth of the water. Figure 26 illustrates the selected cross-sections. Cross-section A, B, C, E, and, H are given in this chapter, while D and G are found in appendix T.

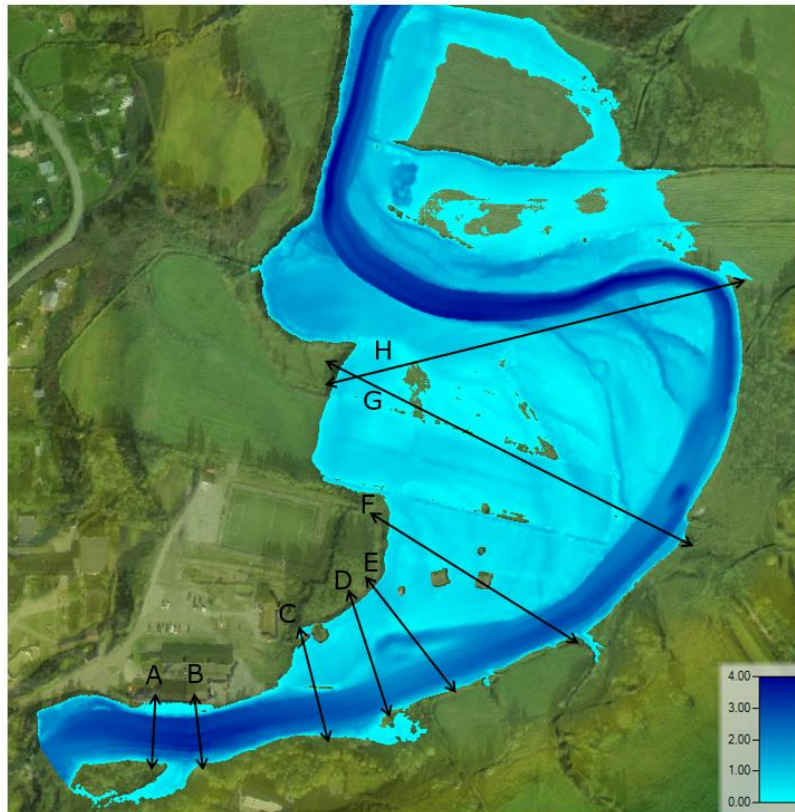


Figure 26: Flood simulation with an overview of cross-sections further investigated.

Cross-section A is close to the Center of Northern People. The steep area in the terrain in the figure at station 6 is the wall of the center. The flat area following the wall is a gravel road. With a water flow of $6.33 \text{ m}^3/\text{s}$, the water surface elevation is 8.4 m and is at station 17. The maximum depth of the flooded area in station 6-13 is 0.12 m. The river has a depth of around 3.3 meters.

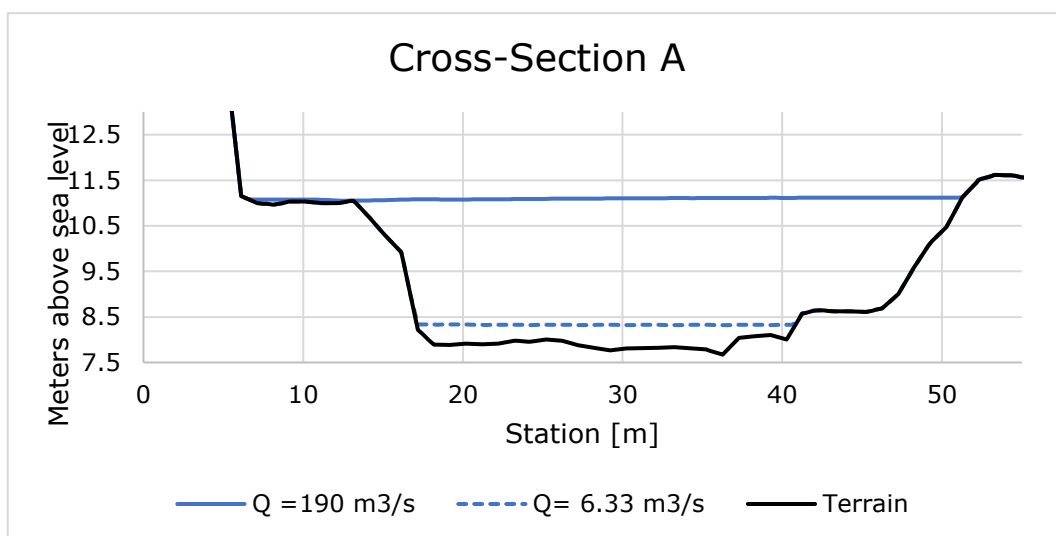


Figure 27: Cross-section A flood simulation

In cross-section B, the maximum depth of the flood in the terrain is 0.09 meters (station 9-10). The river has a depth of 3.4 meters. At station 3, the same wall and road as in figure 27 are found. The dashed line is the WSE for a flow of $6.33 \text{ m}^3/\text{s}$, the flow used for calibration and sensitivity analysis.

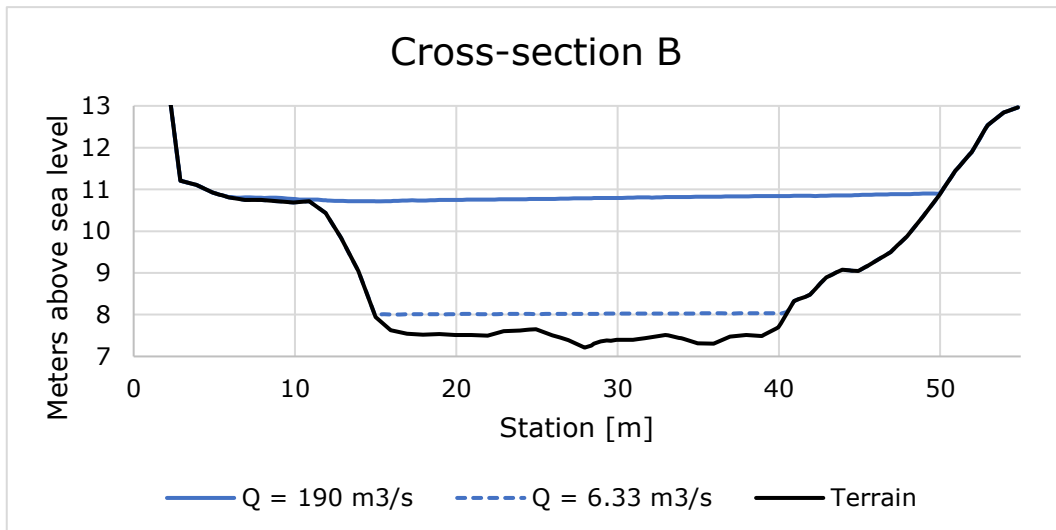


Figure 28: Cross-section B flood simulation.

In cross-section C, the depth at station 9 is 0.16 meters, while at station 45 it is 0.94 meters. Over the flood embankment in station 49 the depth is 0.6 meters. The maximum depth in the river is 2.92 meters. The elevation is station 11-18 is a house used under the festival Riddu Riddu.

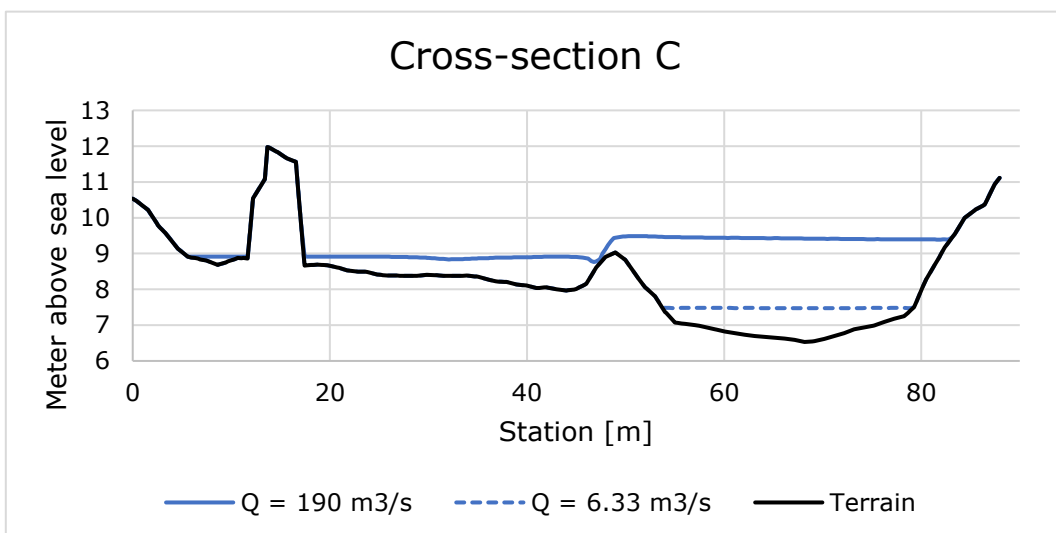


Figure 29: Cross-section C flood simulation.

For cross-section E the depth at station 20 is 0.76 meters, while the river has a depth of 2.34 meters. The water surface elevation reaches the terrain at station 91 with a flow of 6.33 m³/s.

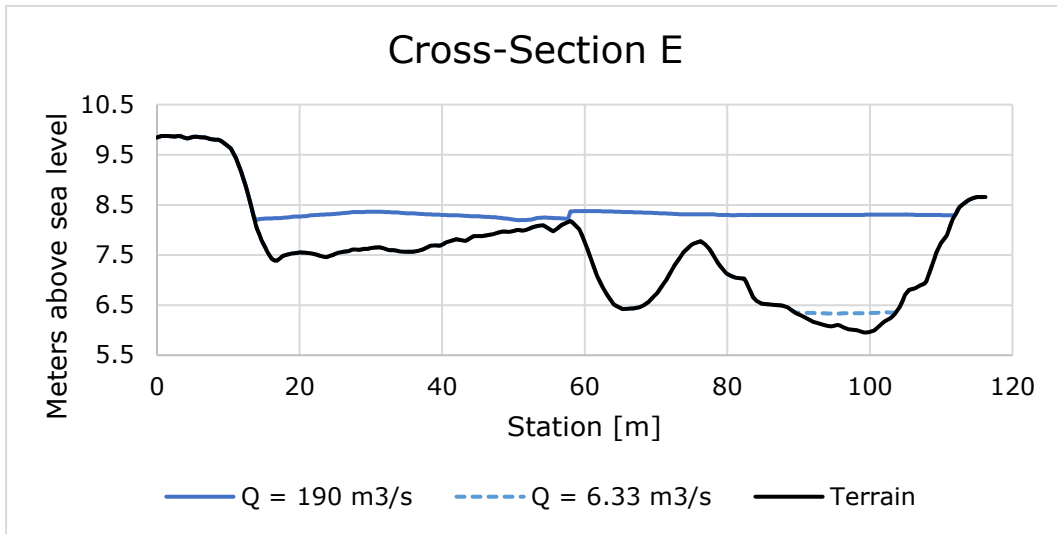


Figure 30: Cross-section E flood situation.

In Cross-section H the depth of the river is 2.75 m. At station 40 the depth of the flood is 0.67 meters, and at station 19 it it is 0.7 meters. With a flow of 6.3 m³/s, the WSE reaches the terrain at station 300.

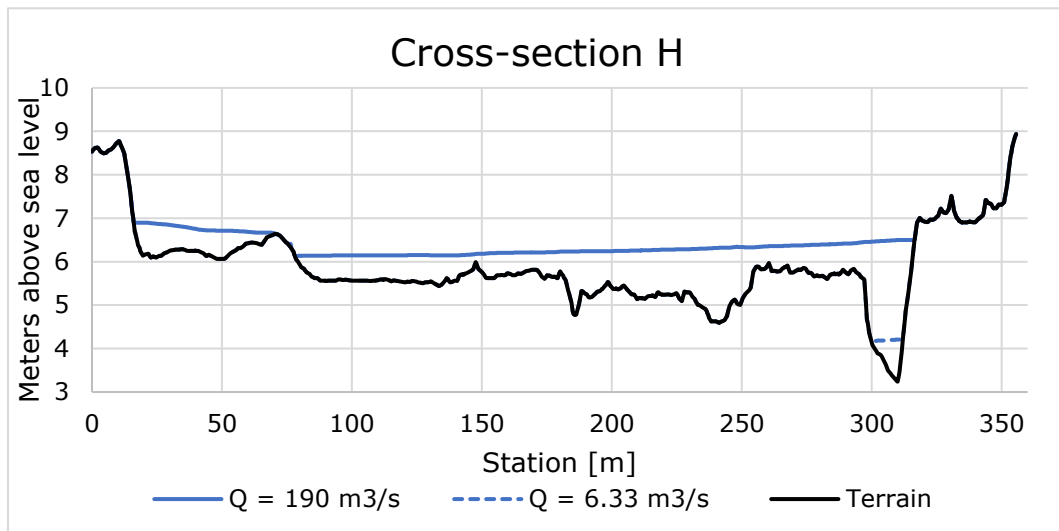


Figure 31: Cross-section H flood situation

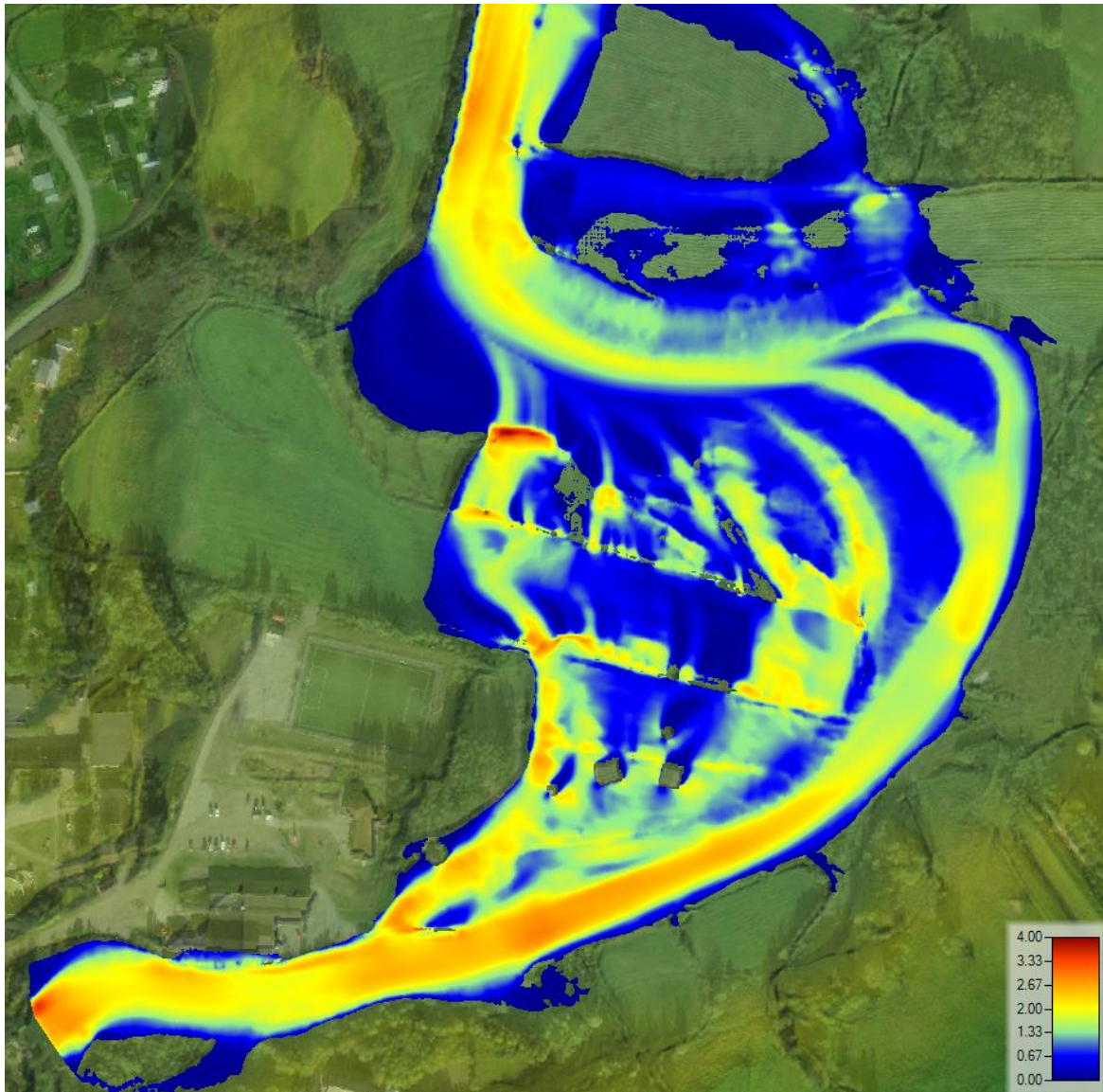


Figure 32: Velocity in flood simulation.

Figure 32 shows the velocity of the flow in a flooding situation. The velocity below the Center of Northern Peoples and the kindergarten is low but needs to be taken into account.

4.4 Terrain

The pictures to use for photogrammetry were collected, but the processing of the raw data was not finished in time for submission of the thesis. Instead, a comparison of the raw LIDAR data and the interpolated bathymetry and terrain was performed. The reason for the comparison was to see if it is sufficient to only use raw LiDAR data for flood simulation. The extent on the flood for the original and interpolated terrain can be found in Appendix S and U.

Cross-sections A, C, and G are compared for a flow of $6.33 \text{ m}^3/\text{s}$ and the 200-year flood. Cross-section A-G are found in V and W for both situations.

4.4.1 The water flow of $6.33 \text{ m}^3/\text{s}$

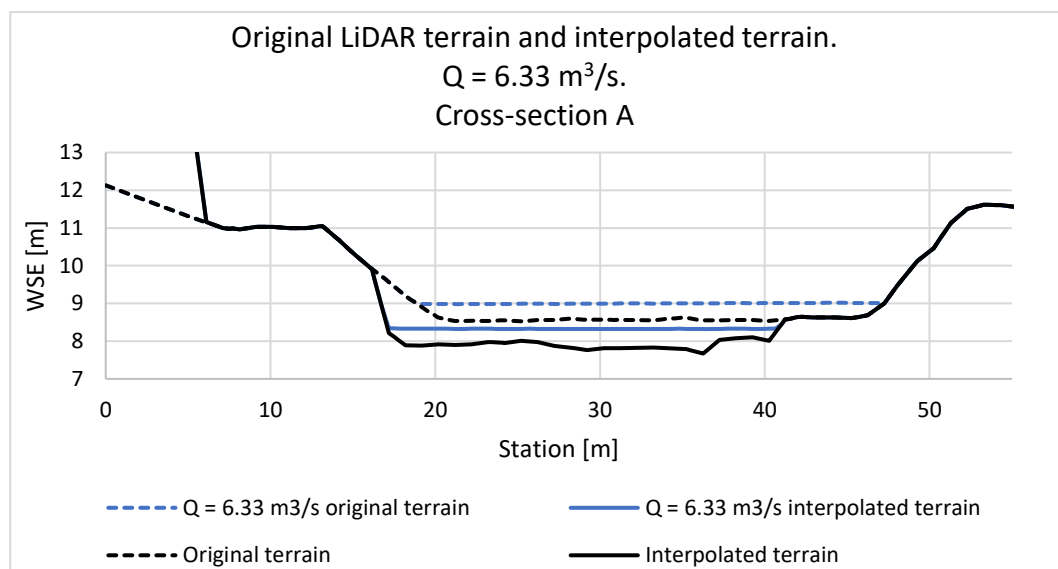


Figure 33: Cross-section A for original LiDAR terrain and interpolated terrain. $Q = 6.33 \text{ m}^3/\text{s}$

As figure 33 shows, the original terrain is above the WSE for the interpolated terrain. The same results are found in cross-section C and G.

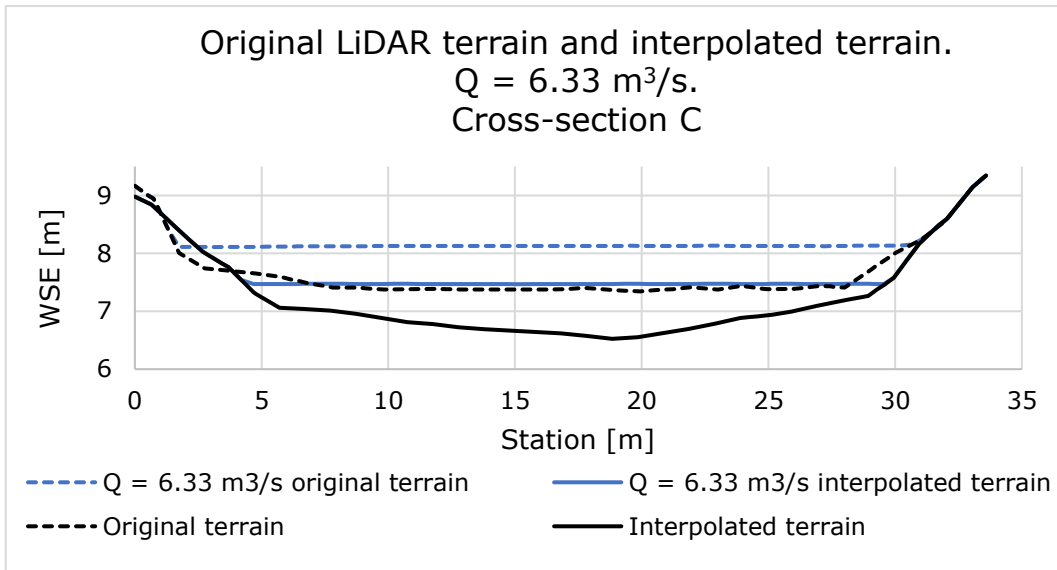


Figure 34: Cross-section C for original LiDAR terrain and interpolated terrain. $Q=6.33 \text{ m}^3/\text{s}$

Figure 34 shows that the LiDAR registered a flat surface of the river, nearly equal to the simulated WSE for the interpolated terrain. As the LiDAR data was collected at a time when the flow was $3.23 \text{ m}^3/\text{s}$, it is unexpected that the simulated WSE should be below the LiDAR terrain.

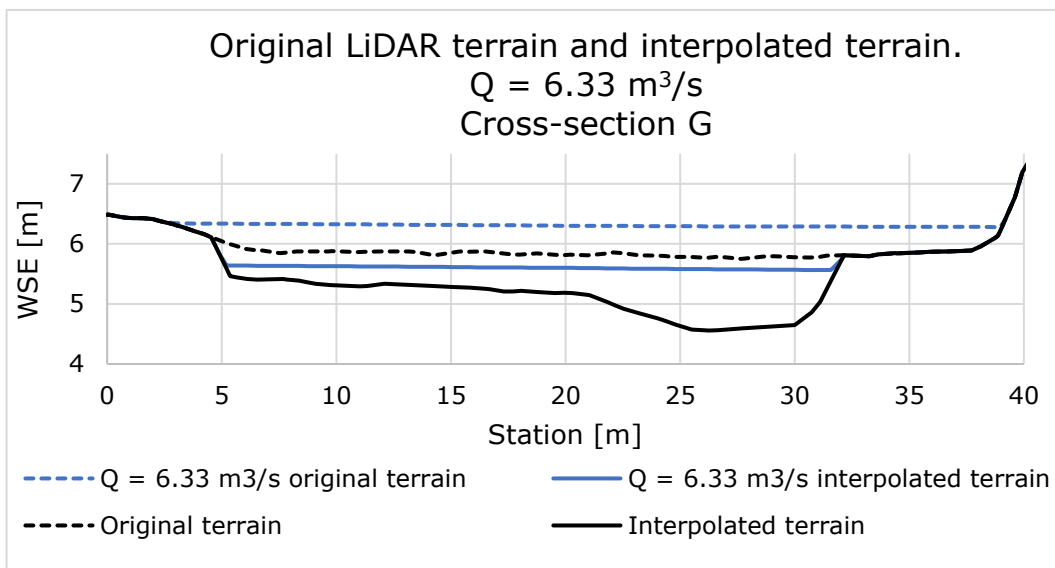


Figure 35: Cross-section G for original LiDAR terrain and interpolated terrain. $Q = 6.33 \text{ m}^3/\text{s}$

4.4.2 200-year flood

With the original terrain, the flood would reach the Center of Northern Peoples. The original terrain does not have the houses integrated into the terrain, but the wall of the building is at station 6. The difference between the two WSEs varies around 0.45 meters in cross-section A.

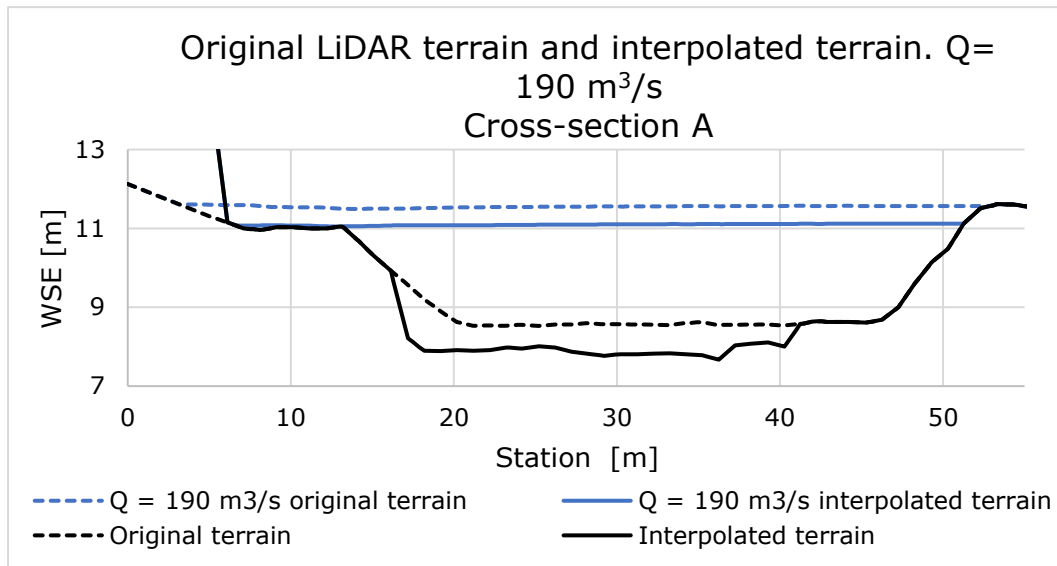


Figure 36: Cross-section A for original LiDAR terrain and interpolated terrain - $Q=190 \text{ m}^3/\text{s}$

In Figure 36 the WSE is higher for the original terrain than the interpolated terrain, while the WSE are more similar for cross-section G in figure 38. In cross-section G the flood is spread over a more extended area, and the river channel is a small fraction of the total area. The effect of the lower bathymetry is less decisive for cross-section G than A and C.

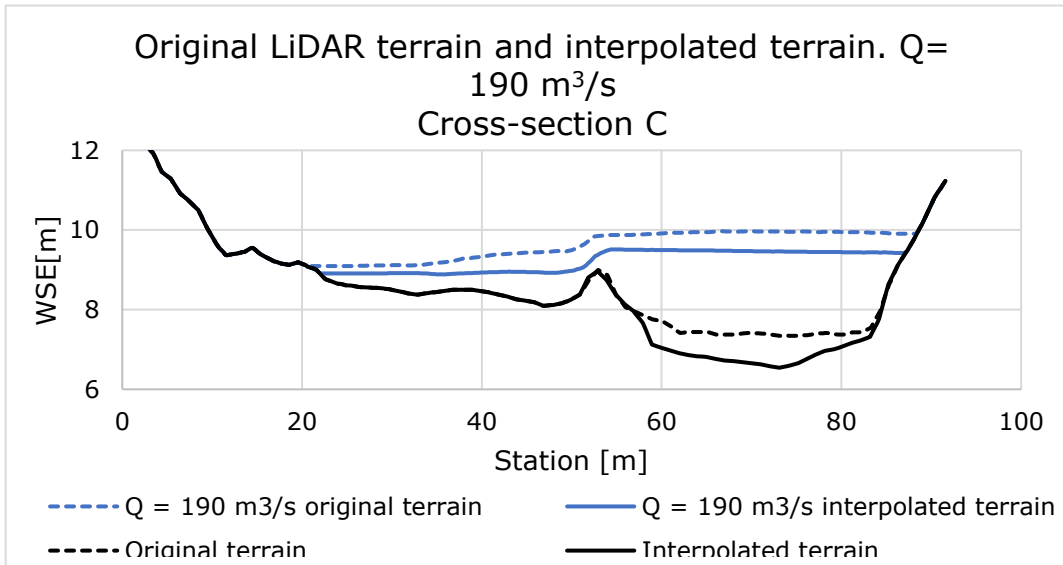


Figure 38: Cross-section C for original and interpolated terrain. $Q = 190 \text{ m}^3/\text{s}$

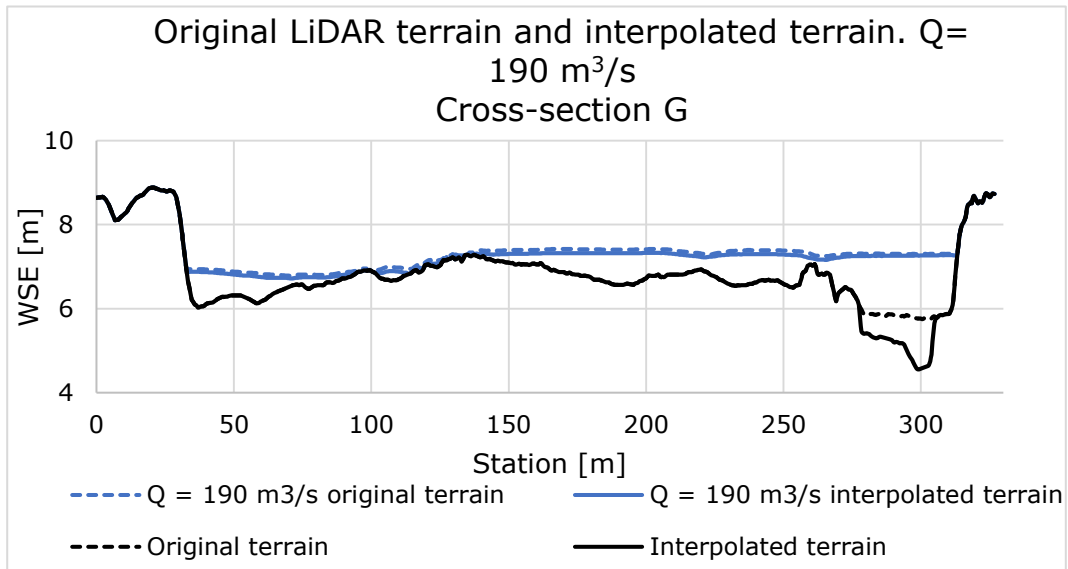


Figure 37: Cross-section G for original and interpolated terrain. $Q = 190 \text{ m}^3/\text{s}$

4.5 Validation of Model

Five points were measured with a water flow of $14.7 \text{ m}^3/\text{s}$. The measured points are highlighted as red dots on figure 39.



Figure 39: Measured and modeled WSE, $Q=14.7 \text{ m}^3/\text{s}$

Points number 2 and 3 fit the simulation, while the water surface elevation for the modeled river is higher than the measured WSE in point 1 and 4. For point number 5, the measured WSE is higher than the modeled WSE.

The result of the simulation with a water flow of 24.2 m³/s are shown in figure 40



Figure 40: Measured and modeled WSE, Q=24.2 m³/s

The same situation as for a flow of 14.7 m³/s happens for 24.2 m³/s; the model computes a higher WSE than the real situation for point number 1. For point number 2, the simulation and the measured point reach the terrain at the same height.

Table 22: Data measured and simulated WSE

Q=14.7 m³/s			
Point	Measured WSE [m.a.s.l.]	Simulated WSE [m.a.s.l.]	Difference [m]
1	7.306	7.99	-0.684
2	5.974	6.37	-0.396
3	4.191	3.98	0.211
4	3.661	3.89	-0.229
5	3.826		

Q=24.2 m³/s			
Point	Measured WSE [m.a.s.l.]	Simulated WSE [m.a.s.l.]	Difference [m]
1	7.486	8.29	-0.804
2	6.126	6.69	-0.564

The differences in WSE were significant, and especially for the situation with a high flow. The model was checked for differences and error in the coordination system and height system, but EUREF89 and NN2000 were used for all features.

5 Discussion

5.1 Calibration

The measurements for the real-time WSE were done by handheld GPS. The method used was prone to human errors, and an accurate calibration cannot be expected. The GPS points were measured by placing the GPS at the waterfront of the river, and then the time of day of the measurements was written down. As the GPS points of the waterfront were collected simultaneously as the cross-section was measured, human mistakes could lead to the wrong point being set as the waterfront, or the GPS could have been placed on rocks, etc. The gauging station giving the information of the water flow is placed above the area of interest and runs through a waterfall before reaching the start of the modeled area. That means the flow goes from over supercritical to subcritical before it reaches the Center of Northern Peoples. That means a possible inaccurate flow was used for calibration data. The water flow in the calibration is an average for the flow over the time of period the measurements were taken, which also indicates that an accurate result cannot be expected. Calibration against a flood scenario, with measurements or pictures of the area, might have given a better result.

Since the river was divided into several Manning's regions, it is difficult to be sure how the regions affect each other. Some of the Manning's number decided by calibration is reasonable. Values between 0.14-0.025 are expected for a natural river (NVE, 2017). The Manning's number in River 3 is 0.18 ($M=5.56$) and indicates that the actual n for this area might be lower. The same goes for the lowest value, 0.01 ($M=100$). A Manning's number this high usually occurs in smooth channels in concrete or metal pipes. The calibration for the middle part of the river gave reasonable n 's that varies between 0.04-0.14.

Even though there are many uncertainties applied to the calibration process, the result from the calibration is still on a centimeters level. Cross-section 7 has the highest difference of 11.5 centimeters. Based on the other results from the calibration, this difference is acceptable.

5.2 Sensitivity analysis

As the sensitivity analysis is done after the calibration, the sensitivity analysis shows how the parameters will affect the model used for flood simulations. As the calibration was done at low water flow and could be affected by human mistakes, the errors from calibration would also be in the sensitivity analysis.

In a majority of the parameters tested in the sensitivity analysis, the most significant difference occurred in the same area. To find the reason for the differences, the terrain for the areas are investigated, as seen in figure 41.

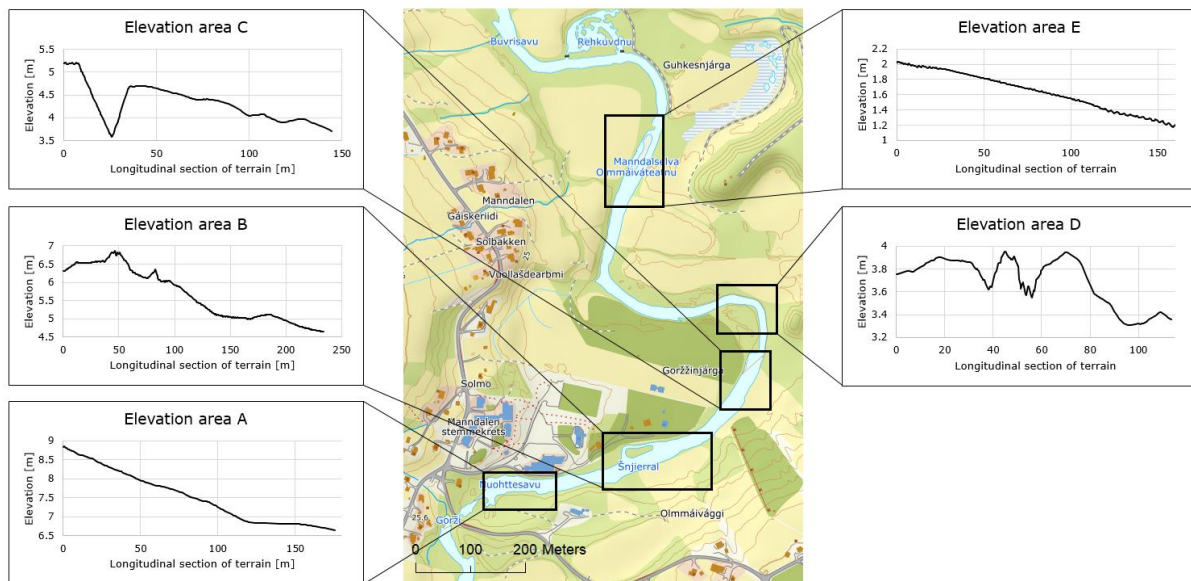


Figure 41: Terrain in problematic areas (a bigger picture is found in appendix X)

Area A inclines 0.036. HEC-RAS has a limit of 0.1 inclination, so area A is within this limit. The river is bending in the area, which can affect the result. In area B the inclination is 0.01, also within the limit. The Manning's number in area B is quite high, at $n=0.18 \text{ s/m}^{1/3}$. The high number would in natural rivers indicate extensive vegetation or deep pools. From fieldwork, this is known not to be true. The high Manning's number could affect the differences observed in the sensitivity analysis.

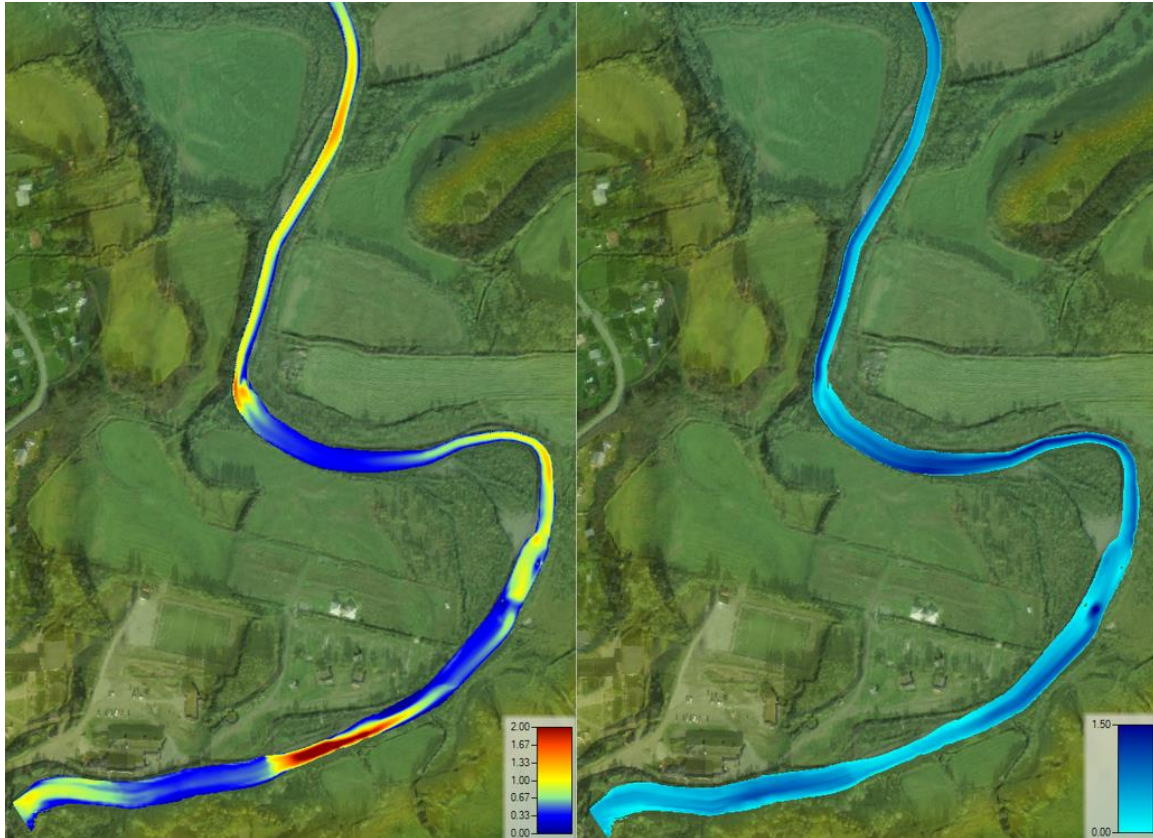


Figure 42: a) Depth and b) velocities with a flow= 6.33 m³/s and settings from the calibration.

Figure 42 a) shows a higher velocity in area B than in the areas upstream and downstream.

Area C has a pool that could create differences in the result. The pool is visible from figure 42 b). Area C is in Manning's region *River 6* and *River 7*, where the Manning's number is accordingly 0.04 and 0.14. The Manning's number is for *River 6* as expected for this type of river, while 0.14 is higher than expected.

Area D is similar to B, with a varying riverbed. The area is in a river bend, which creates different flow lines than for the straight sections. The velocity is higher here than the upstream and downstream part of the river. The same goes for the river bend between area D and E. The Manning's number in the upstream part of the river is 0.06, while the n for area D is 0.045. The downstream area has Manning's number of 0.068. All of these Manning's numbers are within reason for this type of river.

The Manning's numbers in area E is 0.045 and 0.041. The downstream part of the river has a low n , $n=0.01$. Figure 42 a) shows a high velocity in this part of the river

5.2.1 Cell size

The larger the grid cell is, the shorter computation time is, and vice versa. An explanation for this is that there are more cells that need to be computed.

The current study found that cell sizes bigger than the cell size of 3 (as used as reference), had areas that had a higher WSE. For cell size 0.5, 1, and 2 meters the areas where the WSE was higher than the result for the reference grid size were minimal, and only occurring furthest upstream of the river. For the grid size 10 meters, the higher WSEs than the reference are located in area B and D (figure 41). For the grid size of 5 meters, the differences are in area B and E.

The same parts of the river that had a lower WSE than the reference for grid size 5 m and 10 meters, have a higher WSE than the reference for the results from a grid size of 0.5 meters, 1 meter, and 2 meters. A grid size of 5 meters and 2 meters were the grid sizes with least differences compared to the reference, while 10 meters had the most differences. This indicates that grid cells with similar sizes give similar results. Even though cell size 10 had the most differences, the result from 0.5 also stands out. There are big areas with lower WSE than 3 meters, but also relatively big areas with higher WSE. Here, small and big are used relatively, as the difference vary between 0.02 meters to 0.154 meters.

As Goodell stated in Chapter 3.2.1, the river should be covered by 5-7 cells. Hence, a grid size of 3 meters would meet this requirement, as well as giving a result with small differences compared to a finer grid. The computation is shorter, which is also of great importance.

A comparison of the geometric data without breaklines should have been conducted, as the study did not investigate the effects of these. As more knowledge of HEC-RAS was obtained during the study, it was too late to perform a sensitivity analysis for breaklines at the time of the awareness of its possible effects on the results.

5.2.2 Theta

The differences between theta of 1 and theta of 0.6 and 0.8 are so low that they can be ignored. The differences do not affect the quality of stability on the results for Mandalen. The 2 D HEC RAS User's manual states that value for theta should be 0.6 if the model runs stable, and this recommendation is followed for the later simulations. The simulations done in this study is using constant flows, and the result might have been different if there were sudden changes in flow.

5.2.3 Diffusion wave

In the diffusion wave equation, some terms of the Saint Venant equation are neglected. Since the turbulence and Coriolis Effect are off for the full momentum simulations, the difference between the two computations must originate from the unsteady and advection term. The difference is greater for a grid size of 0.5 meters than 10 meters, and the cause of this can be that the bigger cells are not able to compute the details as well as a grid of 0.5 meters. Note that the legends for the figures in 4.2.3 do not have the same scale. The results for grid 0.5 have the biggest span in differences. It spans from -0.21 to 0.56 meters, which is a significant difference. There are more areas with large differences in WSE than small in WSE, so the modeler must be careful if using diffusion wave for the finer mesh. For 1, 2 and, 3-meter grid size, the results are similar. The differences occur in the same areas. Grid size 1 meter has the least differences, followed by 3 and 5 meters. Even though the grid size with 10 meters returned similar results with the two computation methods, there are uncertainties as details might be missing. A resolution of 10 meters does not meet the requirement of 5-7 cells crossing the river, and the results from the simulation might be misleading.

A grid resolution of 1 meters gives the lowest difference between the two computation methods. 10 meters also gave low differences, but as earlier mentioned, using this cell size for simulation of Mandalselva is not adequate.

What is surprising is that for the largest cell sizes, the difference is negligible, but for finer grids, the difference is more significant. These findings were unexpected and suggested that something went wrong with the simulations. Several simulations were done, and the results were the same.

5.2.4 Fixed Time Step

Surprisingly, it was found that the time-step of 5 seconds used a longer computation time than 1 and 3 seconds. The longer time steps make fewer computations when using a set time window for simulation. A possible explanation of this might be that the number of convergence errors increases; hence the computation process gets slower. 0.1 seconds had by far the longest computation time, at 5 hours and 14 minutes. A time step of 5 seconds used 1 hour and 18 minutes, while 3 seconds used 10 minutes. The low simulation time leads to thinking that something must have been done incorrectly. Investigations did not find the cause of the short computation time

The differences between the Courant Conditions and fixed time step were most significant for the increasing time steps. 0.1 seconds were most similar to the adjust time step based on Courant, and 5 seconds had the biggest differences. As it was not possible to run with higher time steps with a grid size of 3 meters, the modeler is locked when it comes to deciding time steps. A bigger grid size could have been used, but that would have been at the expense of the level of details in the terrain.

In area B, the differences are greatest. This could be in correlation to the high Manning's number for this area, as mentioned in chapter 5.3 or the high velocity.

It is interesting to note that with the Courant Conditions, the time step varied between 0.35 seconds and 2 minutes and 51 seconds. This means the lowest time step used, is still higher than the lowest time step tested. The time step used as a base for Courant Conditions was 10 seconds, and the settings used allowed HEC-RAS to perform 4 halving of the base time step. To achieve a minimum time step a 0.1, a base time step would

have to be 1 second. Further research should be undertaken to investigate the effects of a lower time base for Courant Conditions.

5.2.5 Eddy Viscosity

An Eddy viscosity of 0.3 gives the overall closest result to the viscosity coefficient turned off. For 0.2 and 0.3, the WSE is higher than for a Viscosity of 0. An Eddy viscosity of 0.2 has areas of differences in the WSE that 0.3 does not have. This finding was unexpected since the numbers are so close. It could suggest that a lower Eddy number is more affected by the velocities, as the highest differences occur where there is high velocity. A low eddy indicates a straight channel with smooth surfaces and low mixing intensity, and as Mandalen Rivers have gentle meanders and irregularities, this might be the reason. Since the eddy of 0.2 is compared to the turbulence term turned off, this study has been unable to prove that the geometry and surface of the river are the reasons for the differences. The result from the comparison of WSE for an eddy of 5 and 0 was surprising, as a eddy of 5 indicates a high mixing intensity, as well as strong meanders and a rough surface. Why the simulation for the turbulence term being set to 0 and 5 gave nearly the same result, this study is not able to answer. A more calibrated model should be used to investigate this further.

5.2.6 Initial Conditions Ramp up Fraction time

The difference between an increasing flow and a 50 % ramp up time was investigated, and the differences found were minimal. The results of this study are not able to explain the reasons for the differences found, and a more thorough study should be conducted to answer this. The HEC-RAS Manual or Reference manual does not discuss the differences between the two options, and no literature has been found on the subject.

A possible explanation for the difference might be that with a ramp up time, the model can settle down to water surface elevations and flow that is consistent when the unsteady flow equation is applied. With an increasing flow, this consistency is not quarantined.

5.2.7 Friction Slope

The difference between a friction slope of 0.01 and 0.05 are minimal. As 0.05 is the actual slope for the area, but 0.01 is used in simulations, this shows that the accuracy of the results will not be affected by the difference. The friction slope of 0.5 showed a bigger difference but is not surprising since a slope of 0.5 is quite significant compared to 0.01. Using a friction slope of 0.5 was never intended to use for the actual modeling, but it was interesting to see how a high friction slope affected the result. The reason for 0.01 being used for the calibration was a mistake that was discovered too late in the process, as the calibration was already finished. Fortunately, the sensitivity analysis showed that this did not have much impact of the results.

5.3 Flood Simulation

A part of the thesis was to get terrain data from photogrammetry. As the processing was not finished at the date of the submission of the Master's thesis, the comparison of the LIDAR data and the drone footages was not possible to conduct. One of the objectives for the photogrammetry was to get better data for the riverbed, because the measurements from fieldwork was not as accurate as intended.

Cross-section A-H shows a visible river channel for Manndalelva. When the river floods over and rises above the channel, big parts of the terrain around the river is flat. This leads to a big spread of the river, and especially in the Riddu Riddu festival area and the fields close to it. Apart from the river channel, there is no elevation on the left side of the river to stop the water flooding. One exception of this is the flood embankment visible in cross-section C (figure 29). The embankment was built during the Riddu Riddu festival in 2012, as a flood reached the festival area.

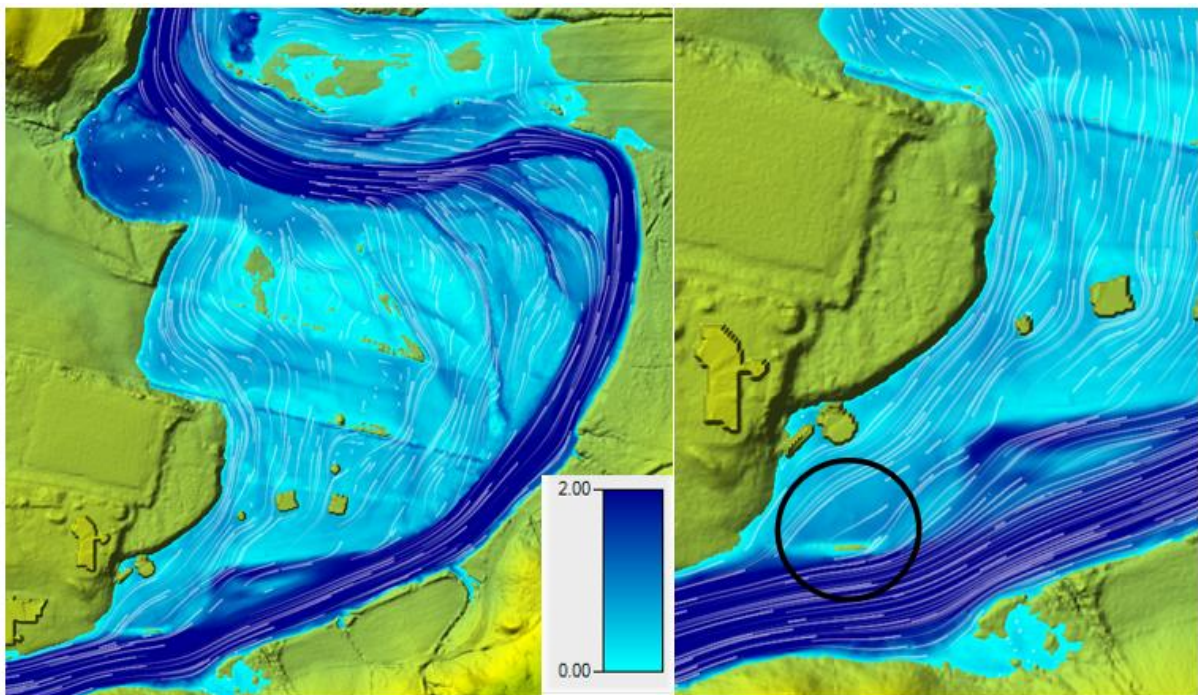


Figure 43: Flow patterns for flood simulation.

In figure 43, the top of the flood embankment is above the water surface. The white lines show the flood pattern. As flows to the fields from the upstream part of the river, higher and longer flood embankment can be a solution for the Riddu Riddu festival area. The existing flood bank is between 0.7 to 1 meter high. The processes in rivers are complex, and to find the best possible solution the whole picture must be taken into account. Safety measures upstream of the river can have consequences for the downstream part of the river. The flow pattern can change as a result of security measures, and that can lead to problematic areas downstream. In the simulation, sediments have not been accounted for, but the effect of sediments in the river should also be investigated. The environment also plays an important role in the decision of security measurement, as every security measurement is also an intervention in nature. Flood measurements should be taken, but the goals must be established. How is the area used today, and

what plans lay ahead for the area? It is not possible to safeguard for every event, and the societal, economic, and ecological interest must be balanced.

As figure 25 shows, the buildings around the area are not over flooded. However, the river cuts close to Center of Northern People. A solution can be to raise the road between the river and the house, as there is not much room for a flood embankment here. The simulation showed a depth in cross-section A of 12 centimeters. If the road were to be raised, erosion control measures must be taken in the river channel. The area between the river channel and the road is steep and consists of stone, gravel, and vegetation. A retaining wall of stone can be built, or ripraps could be built to armor the riverside. The kindergarten is on an elevation in the terrain, and will of that reason not be affected.

5.4 Terrain

The result of the comparison between the original and interpolated terrain indicates that simulations with a low water flow give significant differences, while at higher flows, the differences decrease. Cross section 5 with flow $24.2 \text{ m}^3/\text{s}$ has a difference in WSE of nearly 0.5 meters, but it increases downstream the river. The consequences of the simulation the river with raw LiDAR data for the lower flows could result in significant differences, leading to unknown consequences.

For the situation with a flow of $6.33 \text{ m}^3/\text{s}$, the WSE from the result with the interpolated bathymetry is in all cross-sections, except one, under the LiDAR riverbed. In some of the cross-sections, the difference between the LiDAR terrain and the interpolated terrain is over one meter. One meter is higher than the depth of the river on its deepest points for several of the cross-sections.

In some of the cross-sections, the difference between the interpolation and the original terrain leads to assuming the result of the interpolation of the bathymetry was not as successful as first believed.

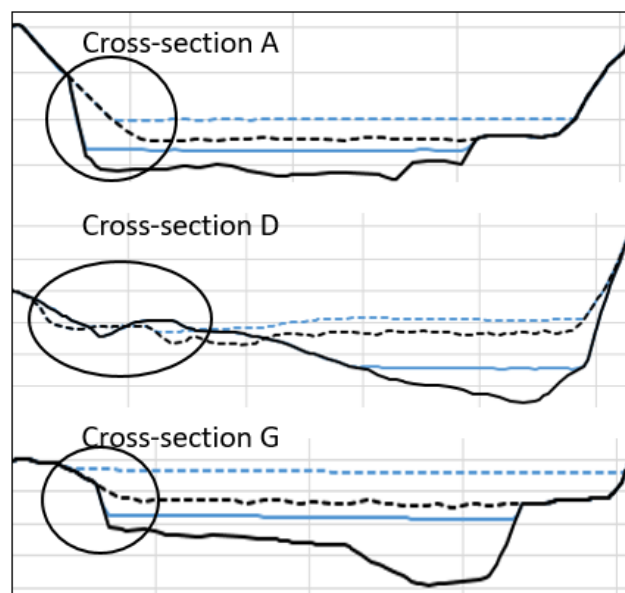


Figure 44: Comparison of original LIDAR terrain and interpolated terrain

If the measured bathymetry represented the real terrain in the river, then the two terrains highlighted in the circles in figure 44 should be equal, as the water flow was

lower the day the LIDAR data was taken than the flow used for the simulations. The reason for LIDAR data being problematic for rivers is its inability to penetrate water. However, even with the inability to penetrate water. The water surface elevation should have been lower than the solid blue line because of the low flow the day the LIDAR was taken.

All simulations are based on the same basis for the terrain around the river, which leads to a relatively similar movement of the river in the flood simulation.

An appealing thought is to check the flow at $3.23 \text{ m}^3/\text{s}$ to see if the surface is close to the bathymetry. $2.33 \text{ m}^3/\text{s}$ was the flow when the LIDAR data was collected.

5.5 Validation of model

The validation of the model was not able to demonstrate that the model reflects reality as well as hoped for. As discussed earlier, the interpolated bathymetry is exposed to several sources of error. The GPS could have been placed on top of rocks or in deep pools, or the measurement for the WSE can have been mixed with other measurements. As the WSE measurement and the measurement of the riverbed were taken at the same time, there are several measurements for each cross-section. To be able to know which one was the WSE, and not a cross-section measurement, the number for the point were written down. The wrong number could have been written down, leading to an inaccurate result for the calibration.



Figure 45: Difference between aerial photo (Kartverket) and integrated terrain for Mandalselva

Figure 45 shows the differences between the actual river and terrain and the modeled terrain. The interpolated terrain is missing aspects of the river, like sandbanks and the eroded area in the river bend. The downside of using GPS for measuring of the

bathymetry is that the situation between the cross-sections are lost, as figure 45 illustrates.

The gauging station is upstream of the measurements, and it cannot be assumed that the flow scenario will be the same for all the cross-sections. In addition, the gauging station is above a waterfall, which means the river goes from supercritical to subcritical flow before it reaches the Center of Northern People. To calibrate the model against the flow from the gauging station can lead to wrong flow-situation for the downstream area.

6 Conclusion

The depth for the flooded area in front of the Center for Northern People is below 0.5 meters, and for the Riddu Riddu festival area, the depth of the flood varies 0.5 to 1 meter. As shown by the existing flood embankment, there is a possibility that an embankment of 1 meter would be sufficient. Further research should be made to investigate if an embankment is sufficient for the festival area. The flood does not reach the kindergarten, as the kindergarten is on an elevation in the terrain. According to the modeling of Manndalselva, the kindergarten is safe for most flooding events. The sensitivity analysis showed that the choices made during the setup can have a significant effect on the results and that an in-depth knowledge of HEC-RAS and the complexities of a river should be known before performing important simulations. As this knowledge was obtained throughout working with the thesis, some of the choices made were not necessarily the right ones. As the photogrammetry was not completed, the terrain data was not as good as hoped for. As a 2D HEC-RAS model is entirely dependent on the terrain, this affected all the simulation. The 1D model from the Specialization project was not calibrated and should therefore not be used for flood modeling. Compared to the 1D model, the 2D model performs better.

Based on these conclusions, raw LiDAR data can be considered used for flood simulations, as long as the modeler shows caution and the water flow is low at the time of collecting data. If there is urgent need for a flood simulation, raw data is better than no data or insufficient bathymetry measurement. The study was not able to investigate if UAV gives better results than LiDAR data, but it proved that UAV is depending on many factors that are impossible to control, like weather and water flow in rivers.

Future work should be to investigate if the UAV data performs better for 2D numerical modeling of rivers in HEC-RAS. Flow measurement should be taken in each cross-section, to endure better calibration data.

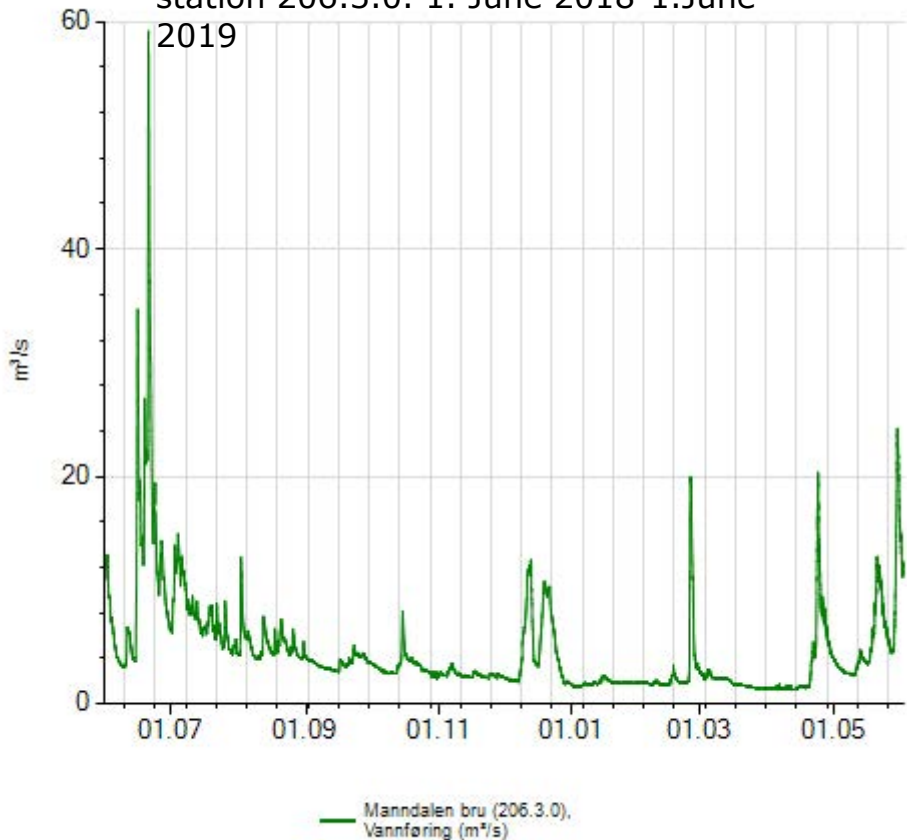
7 References

- Arcement, G. J., & Schneider, V. (1984). *Guide for Selecting Manning's Roughness Coefficients for Natural Channels and Flood Plains* .
- Bjerke, P. L., Majala, G. D., & Forsgren, E. F. (2017). *Dambruddsanalyse - skredgenerert dam i Manndalselva, Troms*. NVE.
- Brunner, G. W. (2016, February). *HEC-RAS Reference Manual*. Retrieved from HEC-RAS Reference Manual: <https://www.hec.usace.army.mil/software/hecras/documentation/HEC-RAS%205.0%20Reference%20Manual.pdf>
- Brunner, G. W., & CEIWR-HEC. (2016). *HEC-RAS 2D Modeling User's Manual, CPD-68A*.
- Böhme, M., Bunkholt, H., Dehls, J., Oppikofer, T., Hermanns, R. L., Dalsegg, E., . . . Eriksen, H. Ø. (2016). *Geologisk modell og fare- og risikoklassifisering av det ustabile fjellpartiet Gamanjuni 3 i Manndalen, Troms*. NVE.
- Casey, M., & Wintergerste, T. (2000). *ERCRAFT: Best Practice Guidelines*. ERCRAFT.
- Casey, M., & Wintersgerste, T. (2000). *ERCRAFT Best Practice Guidelines*.
- CivilGEO. (2019, February 6). *CivilGEO Engineering Software*. Retrieved from CivilGEO Engineering Software: <https://www.civilgeo.com/knowledge-base/hecras-2d-flow-area-modeling/>
- Deal, E. C., Parr, A. D., & Young, B. (2017). *A Comparison Study of One- and Two-Dimensional Hydraulic Modeling for River Environments* . Kansas .
- Gary W. Brunner, C.-H. (2018, April). *US Army Corps of Engineers*. Retrieved from HEC-RAS 5.0.4 Supplemental Users Manual: https://www.hec.usace.army.mil/software/hecras/documentation/HEC-RAS_5.0.4_Supplemental_UsersManual.pdf
- Gharbi, M., Soualmia, A., Dartus, D., & Masbernat, L. (2016). Comparison of 1D and 2D Hydraulic Models for Flood Simulation on the Medjerda River in Tunisia. *Journal of Environmental Sciences*, 7.
- Kartverket. (n.d.). *Norgebilder*. Retrieved from Norgebilder: <https://www.norgebilder.no/>
- NVE. (2003). *Miljøtiltak i Manndalselva skal gi bedre elvemiljø*.

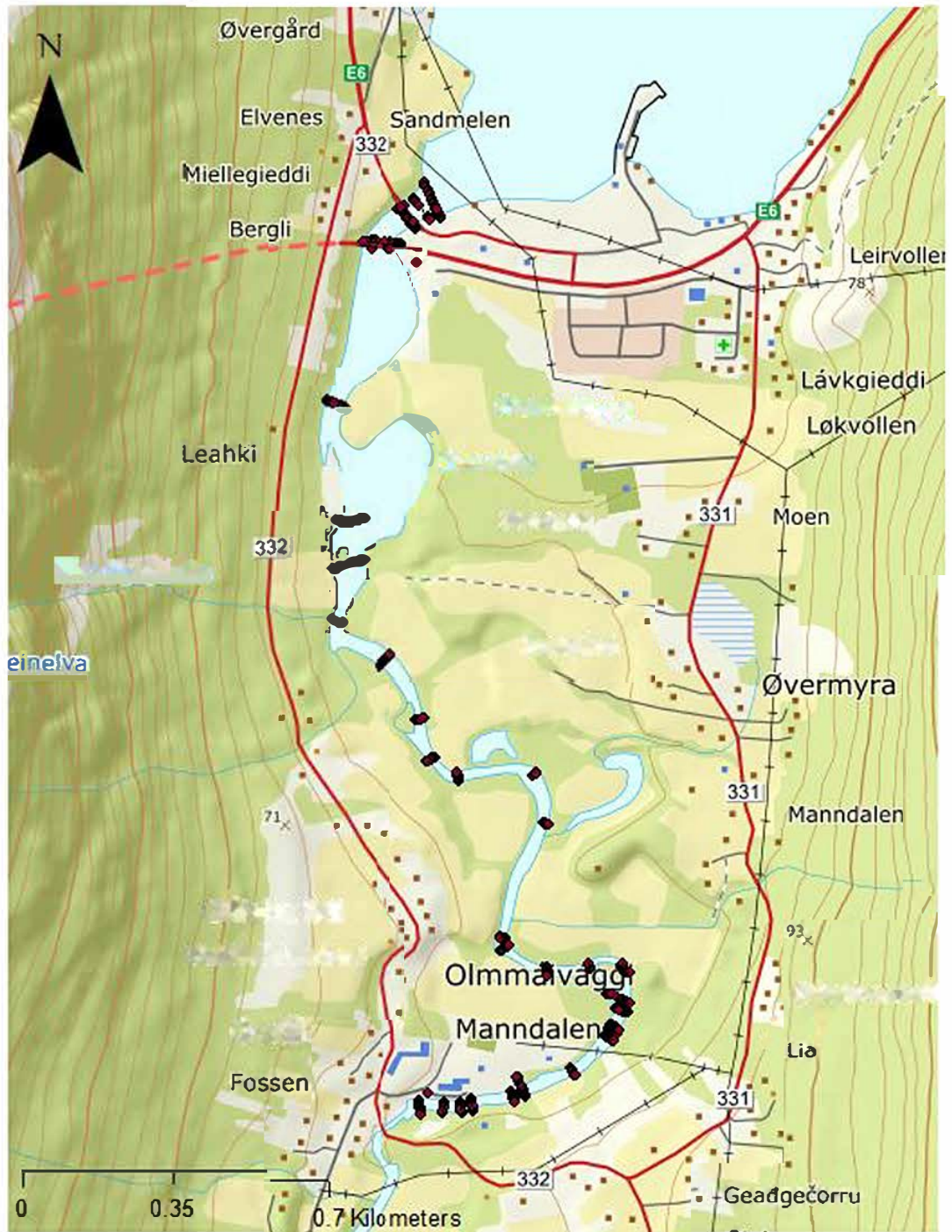
- NVE. (2017). *Vassdragshåndboka. Håndbok i vassdragsteknikk*. Bergen: Fagbokforlaget.
- NVE. (2018, November 9). *Gamanjunki 3*, NVE. Retrieved from NVE:
<https://www.nve.no/flaum-og-skred/fjellskredovervaking/gamanjunki-3/>
- NVE. (2018, February 12). *Målestasjon 206/1 Manndalen*, NVE.no. Retrieved from NVE:
<https://www.nve.no/vann-vassdrag-og-miljo/verneplan-for-vassdrag/troms/206-1-mannselva-olmmaivateatnu/>
- NVE. (2018, July 9). *NEVINA*. Retrieved from NEVINA:
<http://atlas.nve.no/Geocortex/Essentials/REST/TempFiles/NevinaRapport.pdf?guid=e3d91785-0ec6-4098-9290-e28ffaaaa6c4&contentType=application%2Fpdf>
- NVE. (2019). *Sildre.nve.no*. Retrieved from <http://sildre.nve.no/Sildre/Chart>
- NVE. (2019). *Vannføring for Manndalen bru Nr: 206.3.0*. Retrieved from
<https://www2.nve.no/h/hd/plotreal/Q/0206.00003.000/>
- Olsen, N. R. (2015). *Numerisk modellering av kapasitet på flomløp - et litteraturstudium*. Trondheim.
- Olsen, N. R. (2017). *Numerical Modelling and Hydraulics*.
- Palau, J. F. (2016). *2D River Flood Modeling Using HEC-RAS 5.0*.
- Pettersson, L.-E. N. (2011, August). *Flommen i Nord-Norge juni 2011*. Retrieved from NVE.
- Skeie, L. (2017). *Hydraulisk modellering av kraftverksdrift i Tokkeåi*.
- Statens Kartverk. (2019). *Høydedata*. Retrieved from Høydedata:
<https://hoydedata.no/LaserInnsyn/>
- Stenius, S., Glad, P. A., Wang, T. K., & Væringstad, T. (2015). *Veileder for flomberegning i små uregulerte felt*. NVE.
- US Army Corps of Engineers. (2019, March). *HEC-RAS River Analysis System Release Notes*. Retrieved from US Army Corps of Engineers:
https://www.hec.usace.army.mil/software/hec-ras/documentation/HEC-RAS_5.0.7_Release_Notes.pdf

Appendices

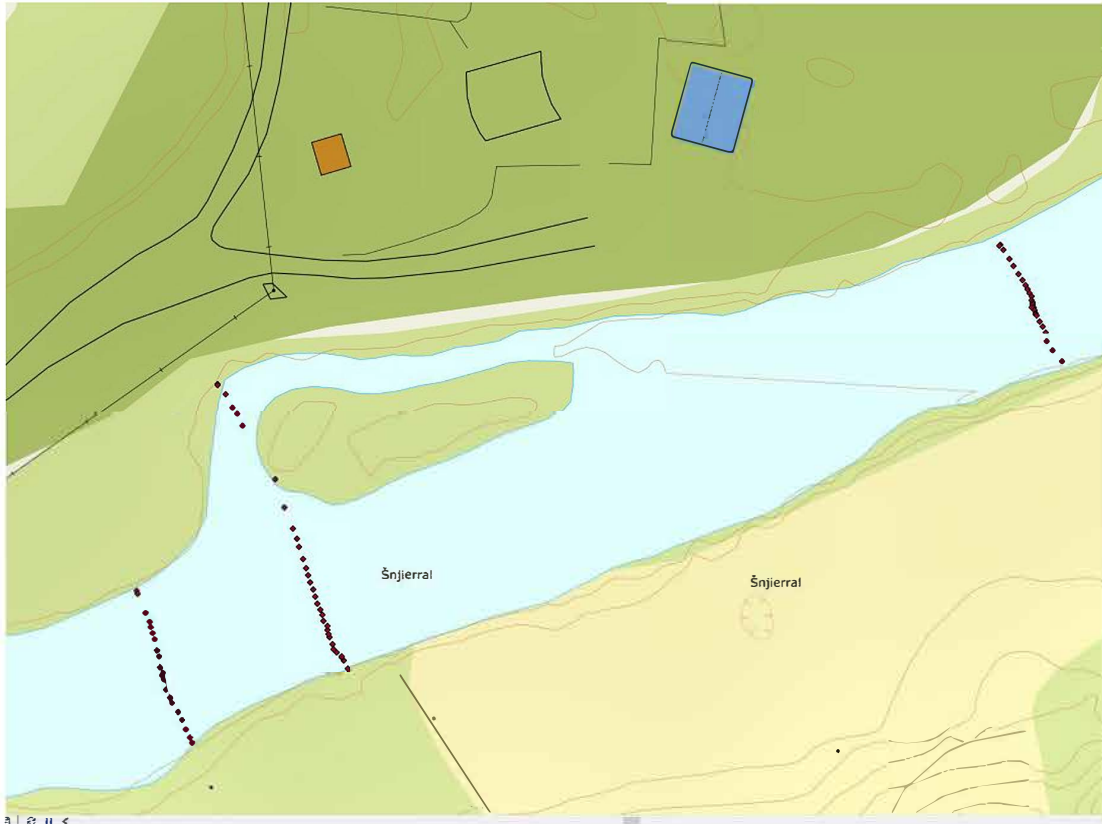
APPENDIX A: Water flow gauging
station 206.3.0. 1. June 2018-1.June
2019



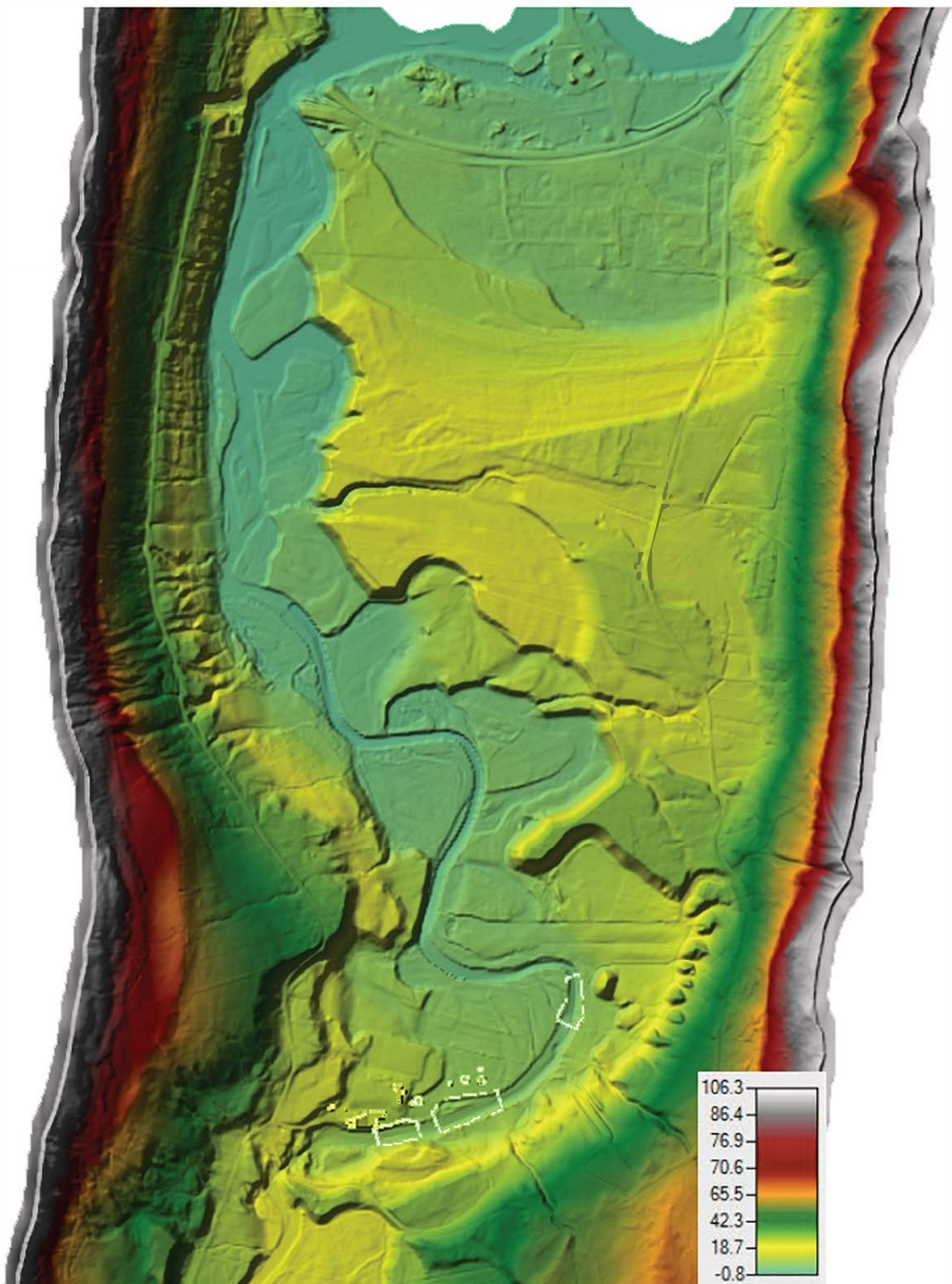
APPENDIX B.1: Location of measured cross-sections



APPENDIX B.2: Location of measured cross-sections



APPENDIX C.1: Interpolated terrain



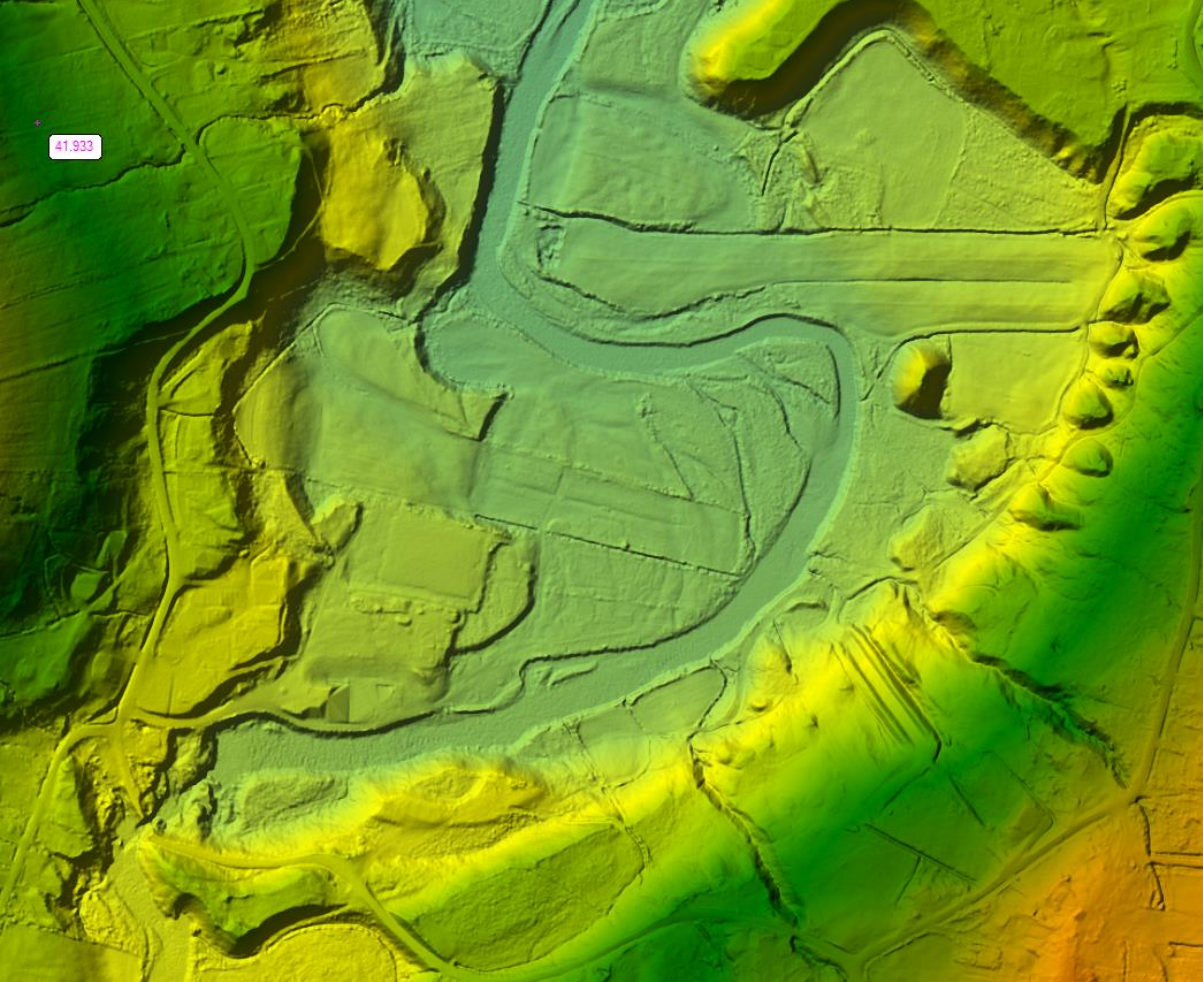
APPENDIX C.2: Interpolated terrain



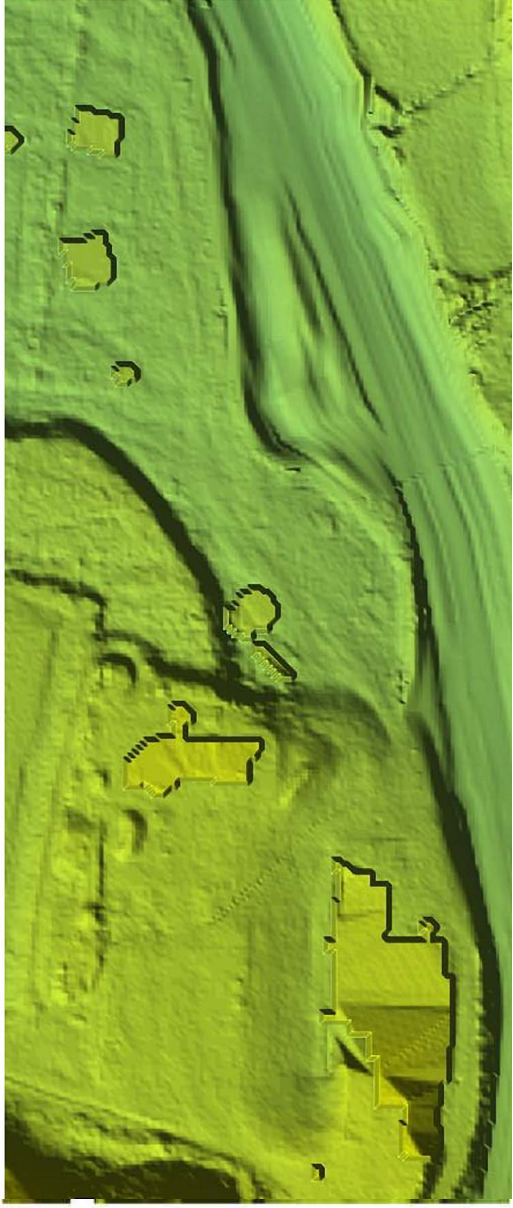
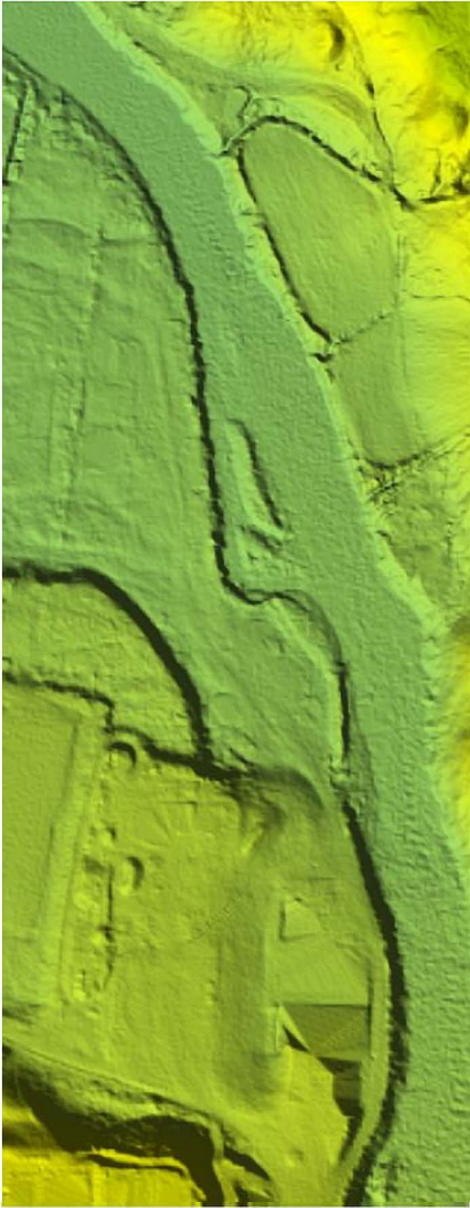
APPENDIX C.3: Interpolated terrain



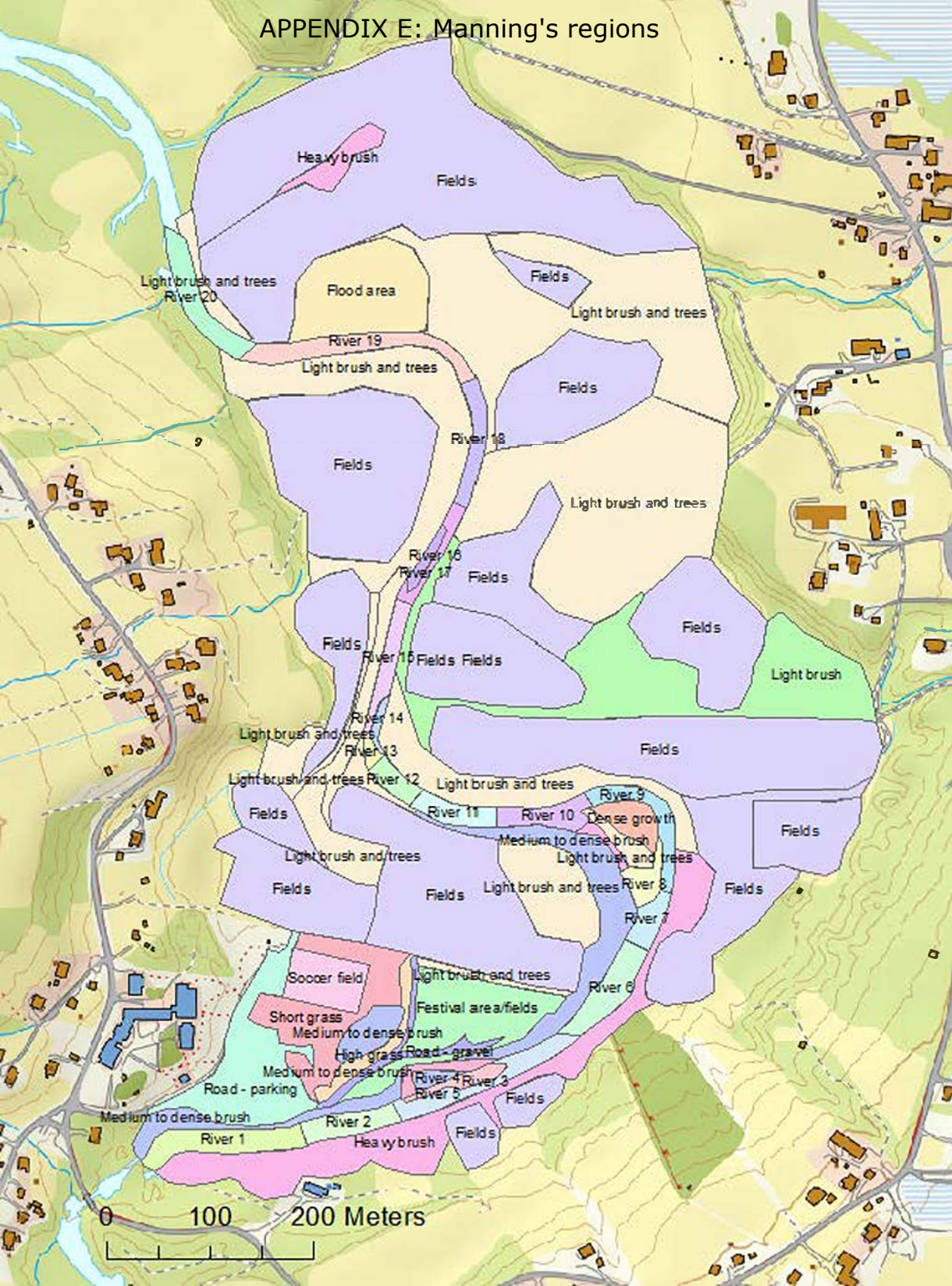
APPENDIX D.1: Terrain from Høydedata



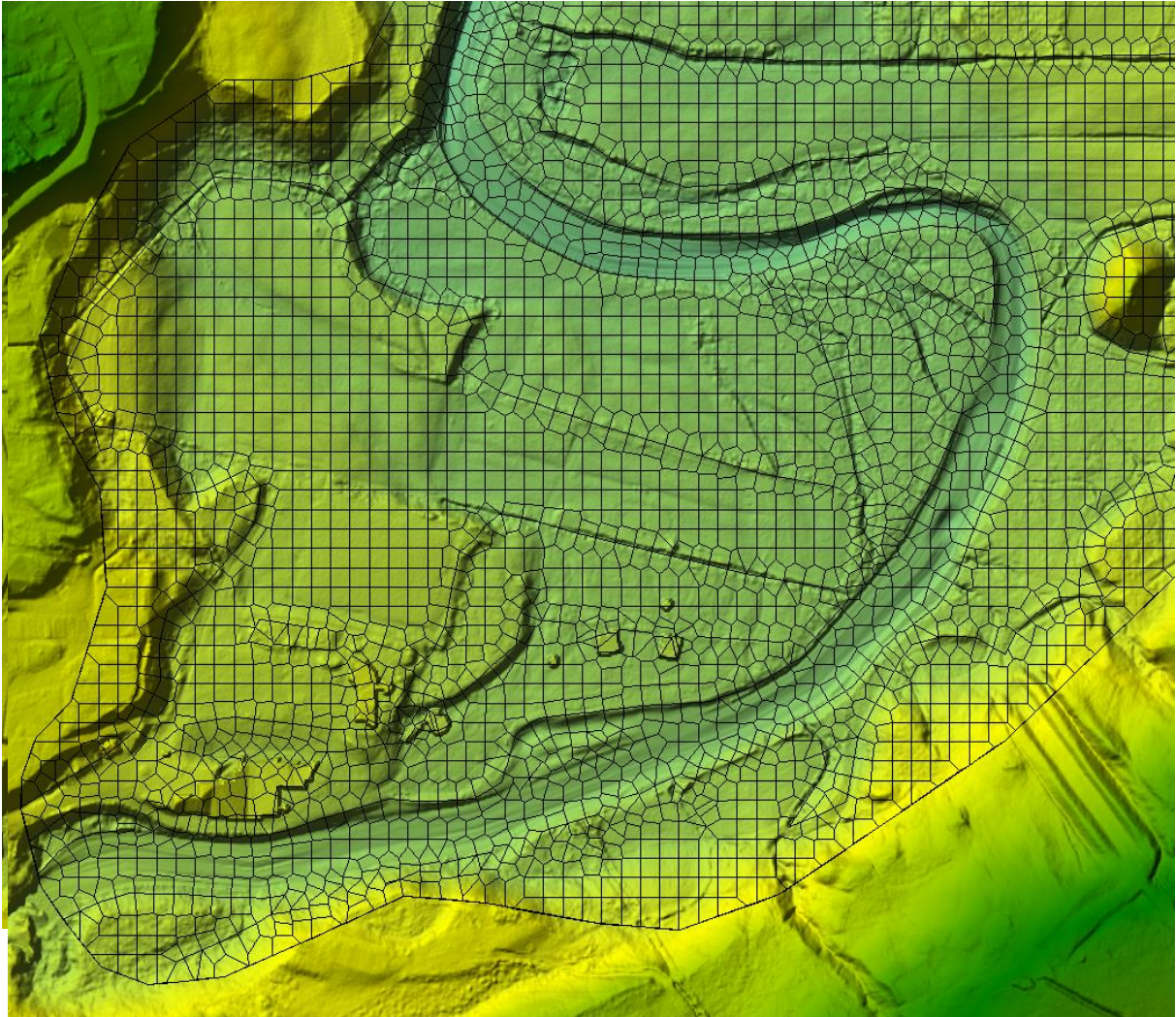
APPENDIX D.2: Original terrain and interpolated terrain



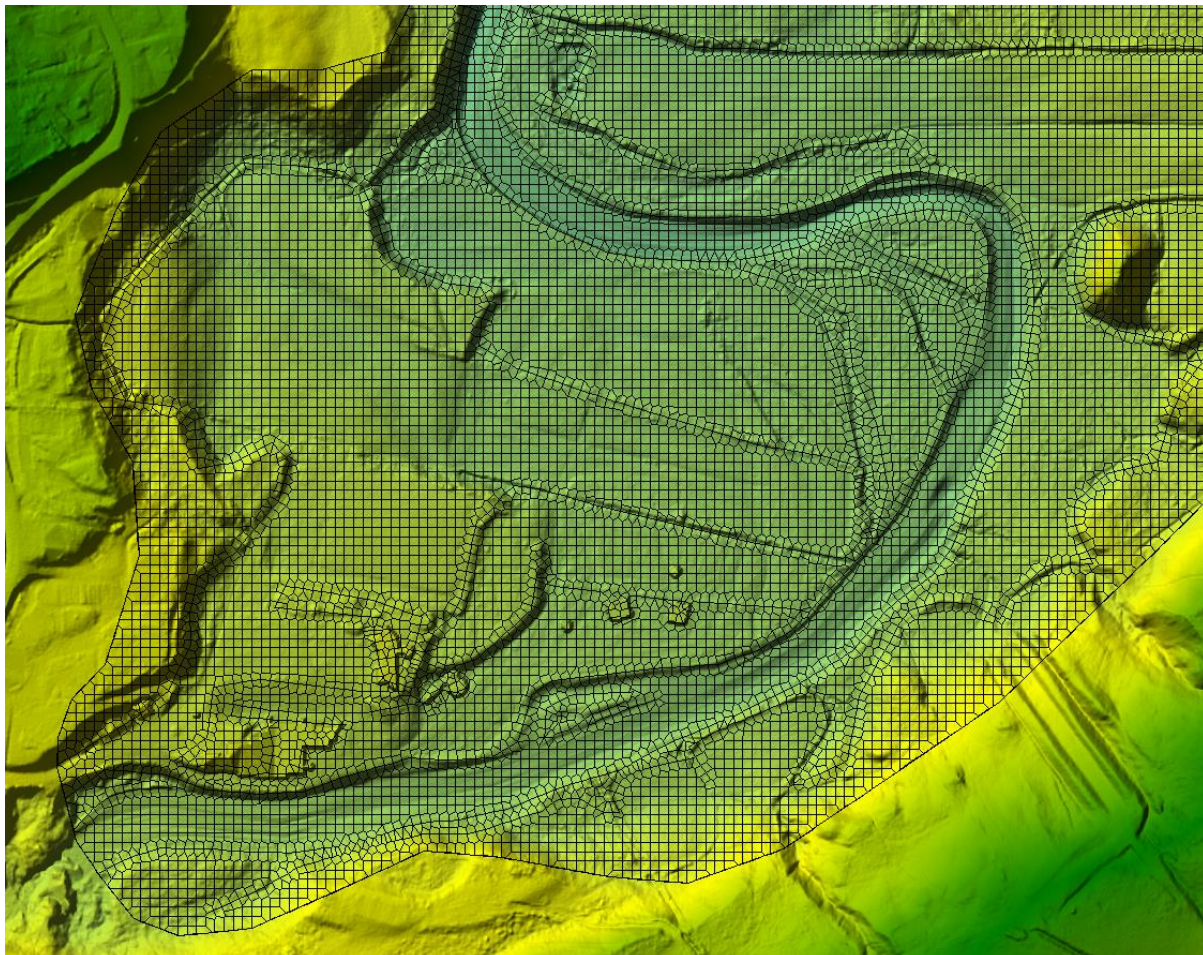
APPENDIX E: Manning's regions



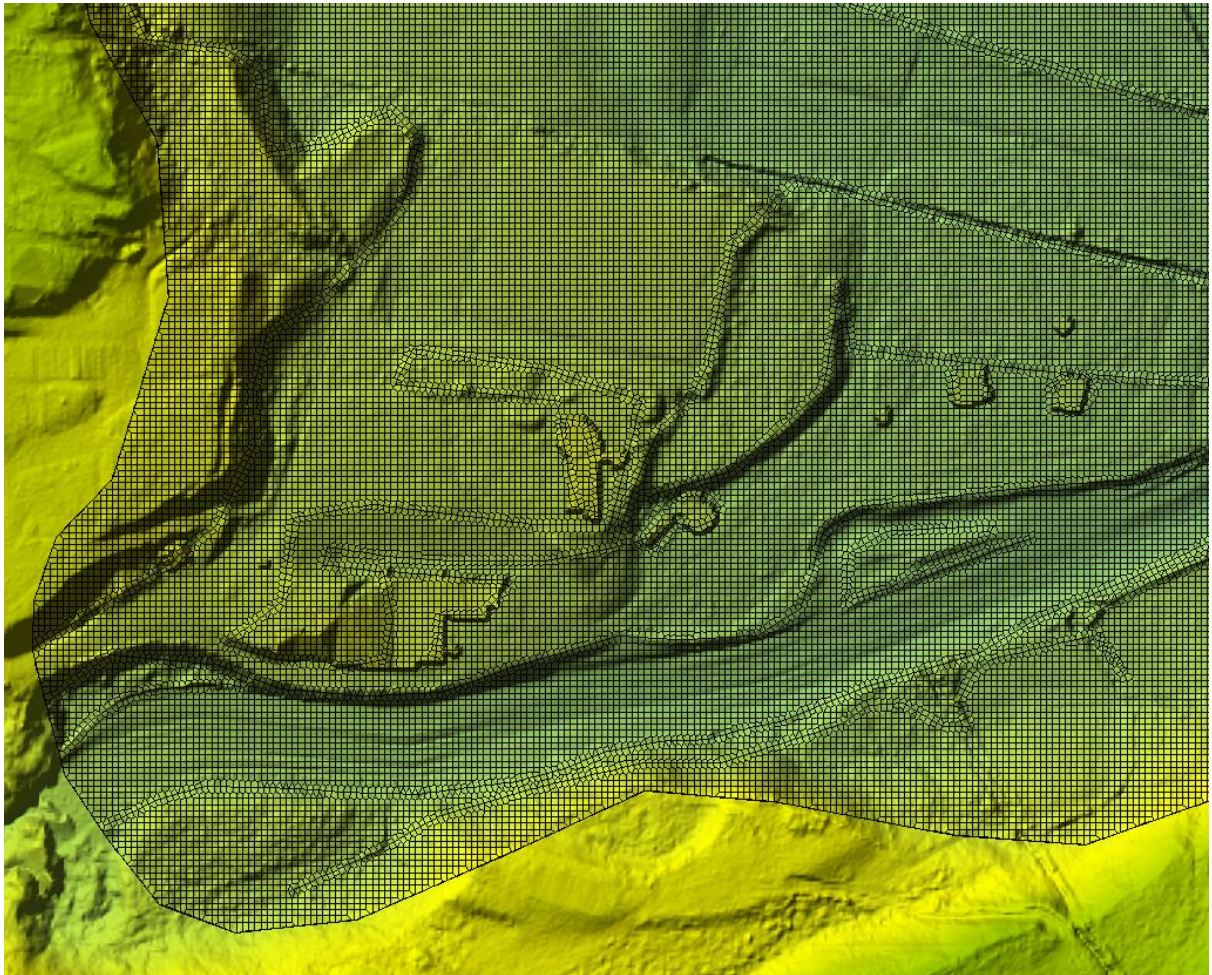
APPENDIX F.1: Geometry grid size 10 meters



APPENDIX F.2: Geometry grid size 5 meters



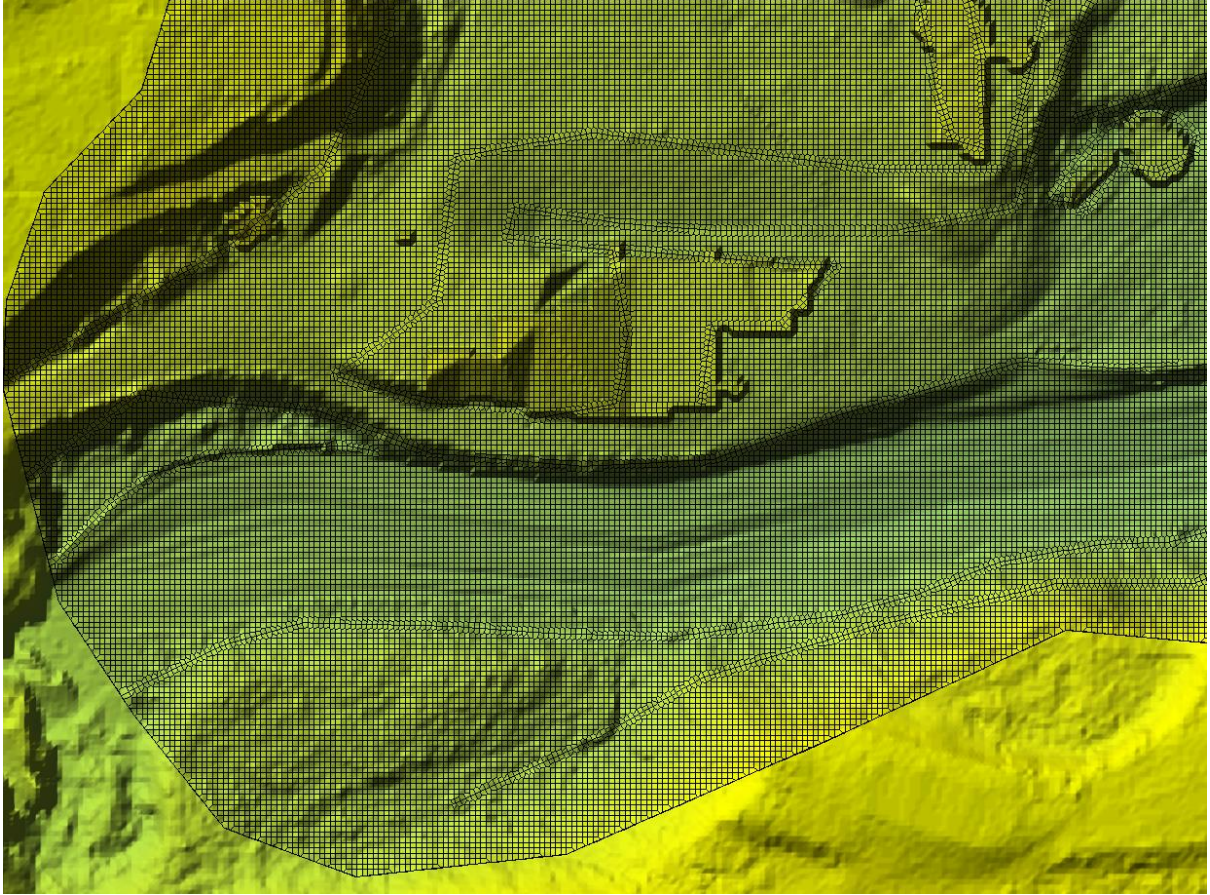
APPENDIX F.3: Geometry grid size 2 meters



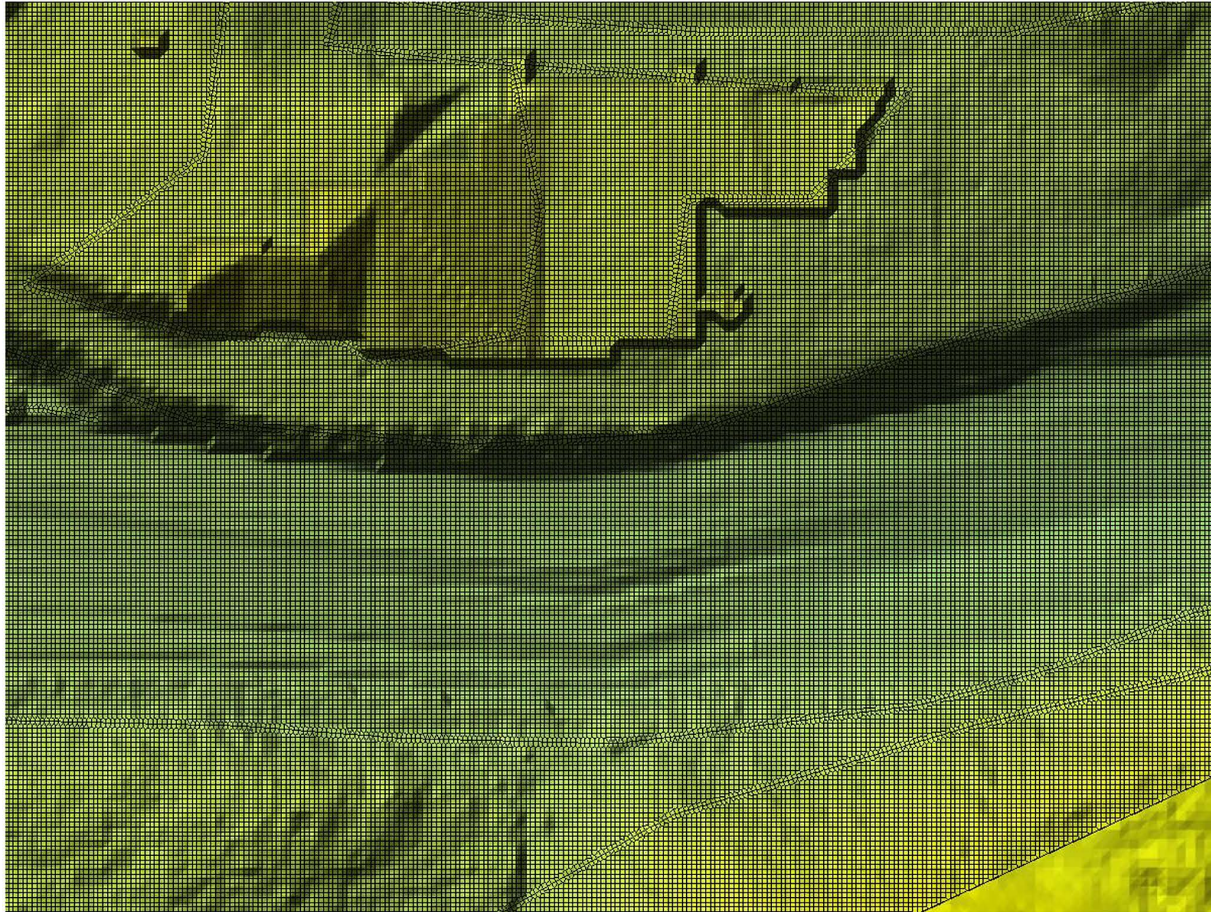
APPENDIX F.4: Geometry grid size 3 meters



APPENDIX F.5: Geometry grid size 1 meters



APPENDIX F.6: Geometry grid size 0.5meters



Regional flomberegning

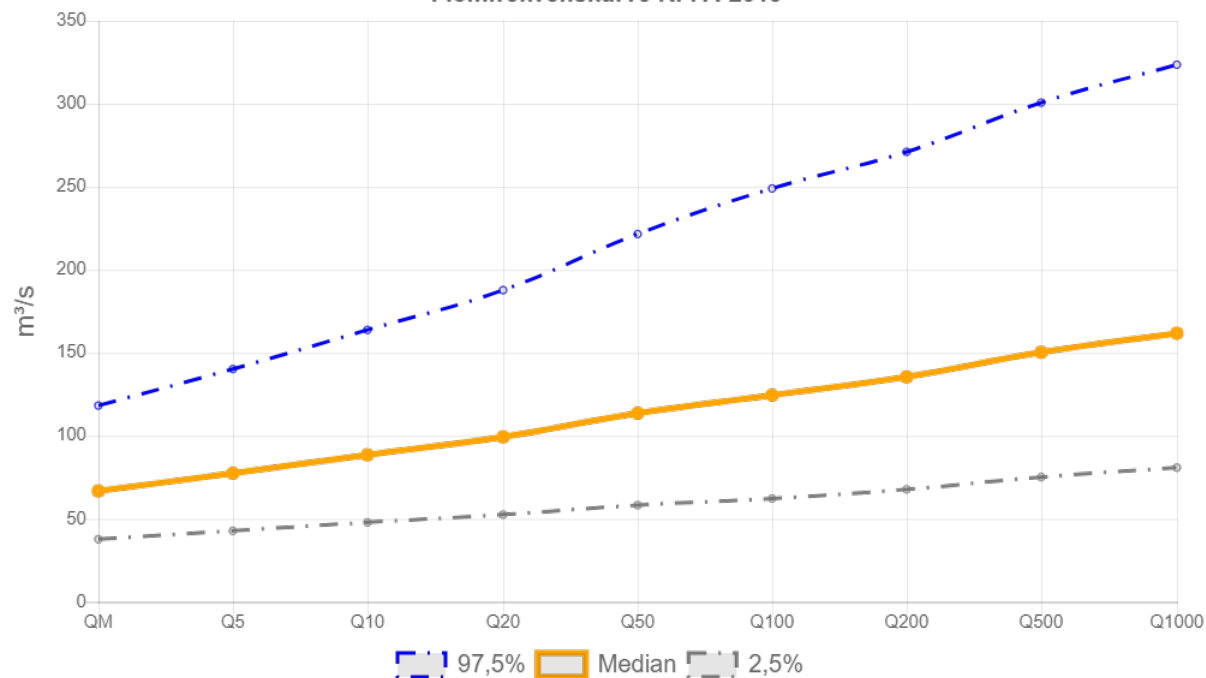
Vassdragsnr.: 206.1A0
 Kommune.: Gáivuotna
 Fylke.: Troms
 Vassdrag.: Manndalselva
 Nedbørfeltareal: 200 km²

Flomestimer er beregnet basert på «Regional flomfrekvensanalyse (RFFA-2018)». Om nedbørfeltet er mindre enn 60 km², er det alternativt beregnet kulminasjonsflommer basert på NIFS-formelverk (2015).

Anbefalinger om klimapåslag er gitt i NVE rapport nr. 81-2016 og klimaprofiler for fylker (se www.klimaservicesenter.no).

Hvordan bruke resultatene fra rapporten, se her.

Flomfrekvenskurve RFFA-2018



RFFA-2018

Tidsoppløsning	-	-
Indeksflom (QM): Medianflom	412.25	l/s*km ²
Klimapåslag	1.4	%
Kulminasjonsfaktor	1.25	-

NIFS-2015

Tidsoppløsning	-	-
Indeksflom (QM): Middelflom	-	l/s*km ²
Klimapåslag	-	%

Annet

Tilløpsflom	Nei	-
-------------	-----	---

RFFA-2018 (døgnmiddel)

	Q _M	Q ₅	Q ₁₀	Q ₂₀	Q ₅₀	Q ₁₀₀	Q ₂₀₀	Q ₅₀₀	Q ₁₀₀₀	Q _{200-klima}
Flomfrekvensfaktor (QM / QT)	1	1.16	1.33	1.49	1.70	1.86	2.03	2.25	2.42	-
Flomverdier, m ³ /s	66.8	77.5	88.6	99.4	114	125	136	150	162	190
Flom usikkerhet (97,5%), m ³ /s	118	140	164	188	222	249	271	301	324	-
Flom usikkerhet (2,5%), m ³ /s	37.8	42.8	47.9	52.6	58.3	62.3	67.8	75.2	80.9	-

NIFS (kulminasjon)

Ikke beregnet pga. areal større enn 60km²

	Q _M	Q ₅	Q ₁₀	Q ₂₀	Q ₅₀	Q ₁₀₀	Q ₂₀₀	Q ₅₀₀	Q ₁₀₀₀	Q _{200-klima}
Flomfrekvensfaktor (QM / QT)										
Flomverdier, m ³ /s										
Flom usikkerhet (97,5%), m ³ /s										
Flom usikkerhet (2,5%), m ³ /s										

Flomverdier er automatisk generert og kan inneholde feil. Resultatene må kvalitetssikres. Verdiene kan ikke benyttes direkte, men må sammenlignes med andre metoder, sammenligningsstasjoner og/eller egne data.



Norges
vassdrags- og
energidirektorat

Kartbakgrunn: Statens Kartverk
Kartdatum: EUREF89 WGS84
Projeksjon: UTM 33N
Beregnpunkt: 715484 E
7722663 N

Nedbørfeltgrenser og feltparametere er automatisk generert og kan inneholde feil.
Resultatene må kvalitetssikres.

Feltparametere

Areal (A)	200	km ²
Effektiv sjø (A _{SE})	0.04	%
Elvleengde (E _L)	34.2	km
Elvegradient (E _G)	30.4	m/km
Elvegradient ₁₀₈₅ (E _{G,1085})	30.4	m/km
Helning	17.4	°
Dreneringstetthet (D _T)	1.6	km ⁻¹
Feltlengde (F _L)	25.7	km

Arealklasse

Bre (A _{BRE})	0	%
Dyrket mark (A _{JORD})	2.1	%
Myr (A _{MYR})	0.3	%
Leire (A _{LEIRE})	0.1	%
Skog (A _{SKOG})	14.9	%
Sjø (A _{SJO})	2.3	%
Snaufjell (A _{SF})	77.4	%
Urban (A _U)	0	%
Uklassifisert areal (A _{REST})	2.8	%

Hypsografisk kurve

Høyde _{MIN}	14	m
Høyde ₁₀	239	m
Høyde ₂₅	604.5	m
Høyde ₅₀	933	m
Høyde ₇₅	1045	m
Høyde _{MAX}	1316	m

Klima- /hydrologiske parametere

Avrenning 1961-90 (Q _N)	29.0	l/s*km ²
Årsnedbør 1961-90 (P _N)	916	mm
Nedbør juni	33	mm
Nedbør juli	50	mm
Regn og snøsmelting mai	184	mm
Regn og snøsmelting juni	124	mm
Regn og snøsmelting årlig 4d	62	mm
Regn og snøsmelting november	7	mm
Temperatur februar	-13.8	°C
Temperatur mars	-11.6	°C

APPENDIX G:Raport NEVINA



Lavvannskart

Vassdragsnr.: 206.1A0
 Kommune: Gáivuotna
 Fylke: Troms
 Vassdrag: Mannåselva

Feltparametere

Areal (A)	200,2 km ²
Effektiv sjø (S _{eff})	0,0 %
Elvelengde (E _L)	34,3 km
Elvegradient (E _G)	30,4 m/km
Elvegradient ₁₀₈₅ (G ₁₀₈₅)	30,2 m/km
Feltlengde(F _L)	25,7 km
H _{min}	11 moh.
H ₁₀	236 moh.
H ₂₀	507 moh.
H ₃₀	697 moh.
H ₄₀	848 moh.
H ₅₀	932 moh.
H ₆₀	976 moh.
H ₇₀	1018 moh.
H ₈₀	1071 moh.
H ₉₀	1134 moh.
H _{max}	1316 moh.
Bre	0,0 %
Dyrket mark	2,1 %
Myr	0,3 %
Sjø	2,3 %
Skog	15,0 %
Snau fjell	77,3 %
Urban	0,0 %

Vannføringsindeks, se merknader

Middelvannføring (61-90)	29,5 l/(s*km ²)
Alminnelig lavvannføring	2,0 l/(s*km ²)
5-persentil (hele året)	1,9 l/(s*km ²)
5-persentil (1/5-30/9)	2,8 l/(s*km ²)
5-persentil (1/10-30/4)	1,6 l/(s*km ²)
Base flow	10,9 l/(s*km ²)
BFI	0,4

Klima

Klimaregion	Finnmark
Årsnedbør	642 mm
Sommernedbør	229 mm
Vinternedbør	412 mm
Årstemperatur	-1,6 °C
Sommertemperatur	4,7 °C
Vintertemperatur	-6,0 °C
Temperatur Juli	8,1 °C
Temperatur August	7,2 °C

1) Verdien er editert



Norges
vassdrags- og
energidirektorat

Kartbakgrunn: Statens Kartverk

Kartdatum: EUREF89 WGS84

Projeksjon: UTM 33N

Nedbørfeltgrenser, feltparametere og vannføringsindekser er automatisk generert og kan inneholde feil. Resultatene må kvalitetssikres.

Det er generelt stor usikkerhet i beregninger av lavvannsindekser. Resultatene bør verifiseres mot egne observasjoner eller sammenlignbare målestasjoner.

I nedbørfelt med høy breprosent eller stor innsjøprosent vil tørrvæsavrenning (baseflow) ha store bidrag fra disse lagringsmagasinene.

Flomberegning

Vassdragsnr.: 206.1A0

Kommune: Gáivuotna

Fylke: Troms

Vassdrag: Manndalselva

Resultat er kun validert for areal mindre enn 60km².
Flomestimatene er derfor nødvendigvis ikke gyldige.

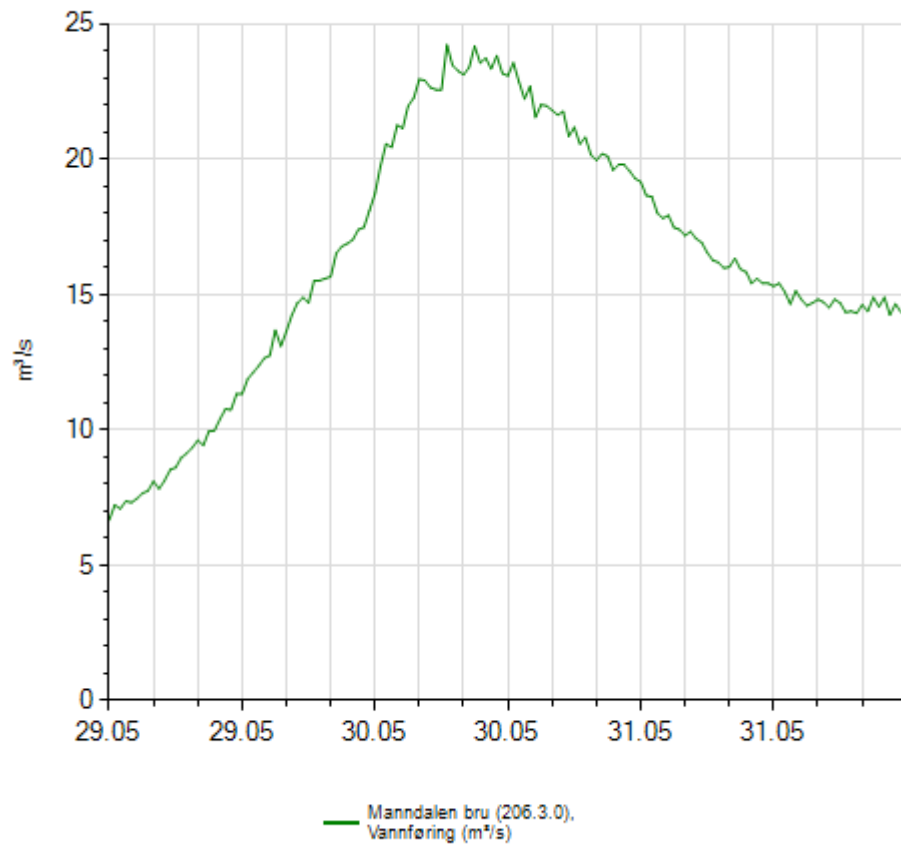
*Flomverdiene viser størrelsen på kulminasjonsflommer for ulike gjentaksintervall. De er beregnet ved bruk av et formelverk som er utarbeidet for nedbørfelt under ca 50 km². Feltparametere som inngår i formelverket er areal, effektiv sjøprosent og normalavrenning (l/s*km²). For mer utdypende beskrivelse av formelverket henvises det til NVE –Rapport 7/2015 «Veileder for flomberegninger i små uregulerte felt». Det pågår fortsatt forskning for å
Det pågår fortsatt forskning for å bestemme klimapåslag for momentanflommer i små nedbørfelt. Frem til resultatene fra disse prosjektene foreligger anbefales et klimapåslag på 1.2 for døgnmiddelflom og 1.4 for kulminasjonsflom i små nedbørfelt.*

Manndalselva	
Areal (km ²)	200,24
Klimafaktor	1,4

	Q ^M		Q ₅	Q ₁₀	Q ₂₀	Q ₅₀	Q ₁₀₀	Q ₂₀₀
	m ³ /s	l/(s*km ²)						
Flomfrekvensfaktorer	-	-	1,24	1,47	1,71	2,06	2,37	2,73
95% intervall øvre grense (m ³ /s)	146,0	729,1	185,7	223,9	265,9	331,7	391,4	449,6
Flomverdier (m ³ /s)	82,5	412	102,6	121,0	140,7	170,1	195,7	224,8
95% intervall nedre grense (m ³ /s)	46,6	233	56,7	65,4	74,4	87,2	97,9	112,4
Flommer med klimapåslag (m ³ /s)	115,5	576,7	102,6	169,4	197,0	238,2	274,0	314,7

Beregningene er automatisk generert og kan inneholde feil. Det er generelt stor usikkerhet i denne typen beregninger. Resultatene må verifiseres mot egne observasjoner eller sammenlignbare målestasjoner. Resultatene er ikke gyldig som grunnlag til flomberegninger for klassifiserte dammer.

APPENDIX I: water flow 29.05.19-31.05.19



APPENDIX J.1: Manning's n grid size 10 meters

Calibration 1

Manning's region	n
river 1	0,15
river 2	0,04
river 3	0,04
river 4	0,04
river 5	0,045
river 6	0,04
river 7	0,04
river 8	0,04
river 9	0,04
river 10	0,04
river 11	0,025
river 12	0,025
river 13	0,04
river 14	0,04
river 15	0,035
river 17	0,033
river 18	0,033
river 19	0,033
river 20	0,03
river 21	0,033

Calibration 2

Manning's region	n
river 1	0,17
river 2	0,038
river 3	0,04
river 4	0,04
river 5	0,045
river 6	0,04
river 7	0,04
river 8	0,04
river 9	0,038
river 10	0,038
river 11	0,025
river 12	0,025
river 13	0,037
river 14	0,038
river 15	0,037
river 17	0,033
river 18	0,033
river 19	0,033
river 20	0,03
river 21	0,033

Calibration 3

Manning's region	n
river 1	0,17
river 2	0,038
river 3	0,04
river 4	0,04
river 5	0,045
river 6	0,036
river 7	0,039
river 8	0,04
river 9	0,035
river 10	0,033
river 11	0,025
river 12	0,025
river 13	0,033
river 14	0,035
river 15	0,033
river 17	0,033
river 18	0,033
river 19	0,035
river 20	0,029
river 21	0,033

Calibration 4

Manning's region	n
river 1	0,17
river 2	0,035
river 3	0,04
river 4	0,038
river 5	0,045
river 6	0,033
river 7	0,037
river 8	0,038
river 9	0,03
river 10	0,025
river 11	0,025
river 12	0,02
river 13	0,033
river 14	0,03
river 15	0,033
river 17	0,033
river 18	0,033
river 19	0,035
river 20	0,02
river 21	0,033

Calibration 5

Manning's region	n
river 1	0,17
river 2	0,035
river 3	0,04
river 4	0,038
river 5	0,045
river 6	0,03
river 7	0,037
river 8	0,038
river 9	0,025
river 10	0,02
river 11	0,025
river 12	0,02
river 13	0,033
river 14	0,03
river 15	0,033
river 17	0,033
river 18	0,033
river 19	0,03
river 20	0,015
river 21	0,03

Calibration 6

Manning's region	n
river 1	0,17
river 2	0,035
river 3	0,04
river 4	0,038
river 5	0,045
river 6	0,04
river 7	0,037
river 8	0,04
river 9	0,027
river 10	0,025
river 11	0,025
river 12	0,025
river 13	0,036
river 14	0,035
river 15	0,033
river 17	0,033
river 18	0,033
river 19	0,03
river 20	0,025
river 21	0,035

Calibration 7

Manning's region	n
river 1	0,17
river 2	0,035
river 3	0,04
river 4	0,038
river 5	0,045
river 6	0,03
river 7	0,037
river 8	0,04
river 9	0,025
river 10	0,015
river 11	0,025
river 12	0,02
river 13	0,036
river 14	0,035
river 15	0,033
river 17	0,033
river 18	0,033
river 19	0,03
river 20	0,025
river 21	0,035

APPENDIX J.2: Manning's n grid size 5 meter

Calibration 1

Manning's region	n
river 1	0,17
river 2	0,035
river 3	0,04
river 4	0,038
river 5	0,045
river 6	0,04
river 7	0,037
river 8	0,04
river 9	0,027
river 10	0,025
river 11	0,025
river 12	0,025
river 13	0,036
river 14	0,035
river 15	0,033
river 16	0,033
river 17	0,033
river 18	0,03
river 19	0,025
river 20	0,035

Calibration 2

Manning's region	n
river 1	0,2
river 2	0,033
river 3	0,038
river 4	0,038
river 5	0,043
river 6	0,028
river 7	0,036
river 8	0,04
river 9	0,02
river 10	0,013
river 11	0,025
river 12	0,02
river 13	0,033
river 14	0,03
river 15	0,033
river 16	0,033
river 17	0,033
river 18	0,033
river 19	0,02
river 20	0,033

calibration 3

Manning's region	n
river 1	0,15
river 2	0,03
river 3	0,038
river 4	0,038
river 5	0,04
river 6	0,03
river 7	0,036
river 8	0,04
river 9	0,015
river 10	0,01
river 11	0,02
river 12	0,02
river 13	0,03
river 14	0,03
river 15	0,03
river 16	0,033
river 17	0,033
river 18	0,033
river 19	0,018
river 20	0,033

calibration 4

Manning's region	n
river 1	0,15
river 2	0,025
river 3	0,038
river 4	0,038
river 5	0,04
river 6	0,025
river 7	0,035
river 8	0,04
river 9	0,025
river 10	0,03
river 11	0,02
river 12	0,02
river 13	0,025
river 14	0,025
river 15	0,025
river 16	0,033
river 17	0,033
river 18	0,033
river 19	0,015
river 20	0,03

calibration 5

Manning's region	n
river 1	0,15
river 2	0,03
river 3	0,038
river 4	0,038
river 5	0,04
river 6	0,03
river 7	0,036
river 8	0,04
river 9	0,015
river 10	0,008
river 11	0,02
river 12	0,02
river 13	0,03
river 14	0,03
river 15	0,03
river 16	0,033
river 17	0,033
river 18	0,033
river 19	0,018
river 20	0,03

calibration 6

Manning's region	n
river 1	0,15
river 2	0,03
river 3	0,038
river 4	0,038
river 5	0,04
river 6	0,025
river 7	0,04
river 8	0,035
river 9	0,02
river 10	0,008
river 11	0,015
river 12	0,025
river 13	0,033
river 14	0,035
river 15	0,033
river 16	0,033
river 17	0,033
river 18	0,033
river 19	0,025
river 20	0,03

calibration 7

Manning's region	n
river 1	0,15
river 2	0,033
river 3	0,038
river 4	0,038
river 5	0,04
river 6	0,03
river 7	0,04
river 8	0,035
river 9	0,03
river 10	0,008
river 11	0,01
river 12	0,025
river 13	0,036
river 14	0,035
river 15	0,036
river 16	0,033
river 17	0,033
river 18	0,033
river 19	0,03
river 20	0,03

Calibration 8

Manning's region	n
river 1	0,15
river 2	0,035
river 3	0,04
river 4	0,038
river 5	0,045
river 6	0,04
river 7	0,037
river 8	0,04
river 9	0,02
river 10	0,025
river 11	0,025
river 12	0,025
river 13	0,036
river 14	0,035
river 15	0,033
river 16	0,033
river 17	0,033
river 18	0,033
river 19	0,025
river 20	0,035

APPENDIX J.3: WSE for Calibration, grid size 3 meter

Cross-section	Observed WSE	Simulated WSE Calibration 1	Difference observed and simulated 1	Simulated WSE Calibration 2	Difference observed and simulated 2	Simulated WSE Calibration 3	Difference observed and simulated 3	Simulated WSE Calibration 4	Difference observed and simulated 4	Simulated WSE Calibration 5	Difference observed and simulated 5	Simulated WSE Calibration 6	Difference observed and simulated 6	Simulated WSE Calibration 7	Difference observed and simulated 7	Simulated WSE Calibration 8	Difference observed and simulated 8
1	8,414	8,55	-0,136	8,55	-0,136	8,53	-0,116	8,54	-0,126	8,53	-0,116	8,53	-0,116	8,53	-0,116	8,53	-0,116
2	7,963	7,97	-0,007	7,97	-0,007	7,96	0,003	7,96	0,003	7,96	0,003	7,96	0,003	7,96	0,003	7,96	0,003
3	7,08	6,94	0,14	6,93	0,15	6,94	0,14	6,96	0,12	6,96	0,12	6,96	0,12	6,97	0,11	6,98	0,1
4	5,844	5,78	0,064	5,78	0,064	5,78	0,064	5,81	0,034	5,81	0,034	5,81	0,034	5,81	0,034	5,81	0,034
5	5,465	5,28	0,185	5,28	0,185	5,29	0,175	5,3	0,165	5,3	0,165	5,32	0,145	5,32	0,145	5,32	0,145
6	5,21	5,06	0,15	5,07	0,14	5,07	0,14	5,07	0,14	5,07	0,14	5,07	0,14	5,07	0,14	5,07	0,14
7	4,828	4,77	0,058	4,78	0,048	4,78	0,048	4,78	0,048	4,78	0,048	4,78	0,048	4,78	0,048	4,78	0,048
8	4,622	4,41	0,212	4,48	0,142	4,5	0,122	4,5	0,122	4,54	0,082	4,57	0,052	4,6	0,022	4,6	0,022
9	4,187	3,92	0,267	4,01	0,177	4,03	0,157	4,03	0,157	4,07	0,117	4,1	0,087	4,12	0,067	4,12	0,067
10	3,384	3,31	0,074	3,31	0,074	3,32	0,064	3,33	0,054	3,33	0,054	3,35	0,034	3,35	0,034	3,35	0,034
11	1,845	1,84	0,005	1,91	-0,065	1,91	-0,065	1,88	-0,035	1,91	-0,065	1,91	-0,065	1,91	-0,065	1,91	-0,065
12	1,705	1,47	0,235	1,62	0,085	1,62	0,085	1,62	0,085	1,62	0,085	1,62	0,085	1,62	0,085	1,62	0,085

Cross-section	Observed WSE	Simulated WSE Calibration 9	Difference observed and simulated 9	Simulated WSE Calibration 10	Difference observed and simulated 10	Simulated WSE Calibration 11	Difference observed and simulated 11	Simulated WSE Calibration 12	Difference observed and simulated 12	Simulated WSE Calibration 13	Difference observed and simulated 13	Simulated WSE Calibration 14	Difference observed and simulated 14	Simulated WSE Calibration 15	Difference observed and simulated 15
1	8,414	8,53	-0,116	8,53	-0,116	8,53	-0,116	8,37	0,044	8,37	0,044	8,39	0,024	8,39	0,024
2	7,963	7,96	0,003	7,96	0,003	8,03	-0,067	7,96	0,003	7,96	0,003	7,96	0,003	7,96	0,003
3	7,08	6,99	0,09	6,99	0,09	6,99	0,09	7,01	0,07	7,03	0,05	7,11	-0,03	7,03	0,05
4	5,844	5,81	0,034	5,83	0,014	5,83	0,014	5,86	-0,016	5,89	-0,046	5,98	-0,136	5,92	-0,076
5	5,465	5,32	0,145	5,32	0,145	5,32	0,145	5,34	0,125	5,36	0,105	5,38	0,085	5,41	0,055
6	5,21	5,07	0,14	5,07	0,14	5,07	0,14	5,07	0,14	5,12	0,09	5,13	0,08	5,14	0,07
7	4,828	4,78	0,048	4,78	0,048	4,78	0,048	4,78	0,048	4,78	0,048	4,78	0,048	4,78	0,048
8	4,622	4,6	0,022	4,6	0,022	4,6	0,022	4,6	0,022	4,6	0,022	4,6	0,022	4,6	0,022
9	4,187	4,12	0,067	4,12	0,067	4,12	0,067	4,12	0,067	4,13	0,057	4,13	0,057	4,13	0,057
10	3,384	3,35	0,034	3,35	0,034	3,35	0,034	3,36	0,024	3,37	0,014	3,37	0,014	3,37	0,014
11	1,845	1,91	-0,065	1,91	-0,065	1,91	-0,065	1,91	-0,065	1,91	-0,065	1,91	-0,065	1,91	-0,065
12	1,705	1,62	0,085	1,62	0,085	1,62	0,085	1,62	0,085	1,62	0,085	1,62	0,085	1,62	0,085

Cross-section	Observed WSE	Simulated WSE Calibration 16	Difference observed and simulated 16	Simulated WSE Calibration 17	Difference observed and simulated 17	Simulated WSE Calibration 18	Difference observed and simulated 18	Simulated WSE Calibration 19	Difference observed and simulated 19	Simulated WSE Calibration 20	Difference observed and simulated 20	Simulated WSE Calibration 21	Difference observed and simulated 21	Simulated WSE Calibration 22	Difference observed and simulated 22
1	8,414	8,4	0,014	8,41	0,004	8,41	0,004	8,41	0,004	8,41	0,004	8,41	0,004	8,41	0,004
2	7,963	7,97	-0,007	7,96	0,003	7,96	0,003	7,96	0,003	7,96	0,003	7,96	0,003	7,96	0,003
3	7,08	7,01	0,07	7,01	0,07	7,01	0,07	7,01	0,07	6,97	0,11	7	0,08	6,98	0,1
4	5,844	6,02	-0,176	6,02	-0,176	6,02	-0,176	6,02	-0,176	6	-0,156	5,97	-0,126	6,01	-0,166
5	5,465	5,5	-0,035	5,5	-0,035	5,5	-0,035	5,48	-0,015	5,48	-0,015	5,45	0,015	5,48	-0,015
6	5,21	5,18	0,03	5,18	0,03	5,18	0,03	5,11	0,1	5,12	0,09	5,12	0,09	5,15	0,06
7	4,828	4,82	0,008	4,83	-0,002	4,83	-0,002	4,83	-0,002	4,83	-0,002	4,83	-0,002	4,84	-0,012
8	4,622	4,61	0,012	4,63	-0,008	4,63	-0,008	4,6	0,022	4,6	0,022	4,6	0,022	4,62	0,002
9	4,187	4,14	0,047	4,15	0,037	4,14	0,047	4,14	0,047	4,14	0,047	4,14	0,047	4,14	0,047
10	3,384	3,38	0,004	3,35	0,034	3,27	0,114	3,27	0,114	3,33	0,054	3,33	0,054	3,34	0,044
11	1,845	1,88	-0,035	1,88	-0,035	1,88	-0,035	1,88	-0,035	1,88	-0,035	1,86	-0,015	1,85	-0,005
12	1,705	1,62	0,085	1,62	0,085	1,62	0,085	1,62	0,085	1,62	0,085	1,62	0,085	1,62	0,085

Cross-section	Observed WSE	Simulated WSE Calibration 23	Difference observed and simulated 23	Simulated WSE Calibration 24	Difference observed and simulated 24	Simulated WSE Calibration 25	Difference observed and simulated 25	Simulated WSE Calibration 26	Difference observed and simulated 26	Simulated WSE Calibration 27	Difference observed and simulated 27	Simulated WSE Calibration 28	Difference observed and simulated 28	Simulated WSE Calibration 29	Difference observed and simulated 29
1	8,414	8,41	0,004	8,405	0,009	8,4047	0,0093	8,4065	0,0075	8,4132	0,0008	8,4132	0,0008	8,4138	0,0002
2	7,963	7,98	-0,017	7,968	-0,005	7,9606	0,0024	7,989	-0,026	7,9689	-0,0059	7,9768	-0,0138	7,9839	-0,0209
3	7,08	7,02	0,06	6,983	0,097	6,9567	0,1233	7,019	0,061	7,0258	0,0542	7,0163	0,0637	7,0317	0,0483
4	5,844	6,01	-0,166	5,928	-0,084	5,9252	-0,0812	5,9961	-0,1521	5,995	-0,151	5,9662	-0,1222	5,9637	-0,1197
5	5,465	5,48	-0,015	5,432	0,033	5,4324	0,0326	5,4778	-0,0128	5,4769	-0,0119	5,4632	0,0018	5,464	0,001
6	5,21	5,15	0,06	5,145	0,065	5,1446	0,0654	5,1424	0,0647	5,1424	0,0676	5,1428	0,0672	5,1503	0,0597
7	4,828	4,84	-0,012	4,838	-0,01	4,8376	-0,0096	4,8376	-0,0096	4,8376	-0,0096	4,8388	-0,0108	4,8449	-0,0169
8	4,622	4,62	0,002	4,621	0,001	4,6214	0,0006	4,6215	0,0005	4,6215	0,0005	4,633	-0,011	4,6356	-0,0136
9	4,187	4,14	0,047	4,157	0,03	4,1587	0,0283	4,1604	0,0266	4,1609	0,0261	4,1768	0,0102	4,1769	0,0101
10	3,384	3,34	0,044	3,333	0,051	3,3518	0,0322	3,3618	0,0222	3,3663	0,0177	3,3657	0,0183	3,36	0,024
11	1,845	1,85	-0,005	1,846	-0,001	1,8601	-0,0151	1,897	-0,0547	1,8986	-0,0536	1,8873	-0,0423	1,8574	-0,0124
12	1,705	1,62	0,085	1,621	0,084	1,6475	0,0575	1,7099	-0,0049	1,7098	-0,0048	1,7098	-0,0048	1,7088	-0,0038

APPENDIX J.4: Manning's n grid size 3 meter

Calibration 1

Manning's region	n
river 1	0,17
river 2	0,035
river 3	0,04
river 4	0,038
river 5	0,045
river 6	0,04
river 7	0,037
river 8	0,04
river 9	0,027
river 10	0,025
river 11	0,025
river 12	0,025
river 13	0,036
river 14	0,035
river 15	0,033
river 16	0,033
river 17	0,033
river 18	0,03
river 19	0,025
river 20	0,035

Calibration 2

Manning's n region	n
river 1	0,17
river 2	0,036
river 3	0,038
river 4	0,038
river 5	0,045
river 6	0,04
river 7	0,042
river 8	0,035
river 9	0,04
river 10	0,03
river 11	0,03
river 12	0,025
river 13	0,036
river 14	0,04
river 15	0,036
river 16	0,033
river 17	0,033
river 18	0,035
river 19	0,045
river 20	0,04

Calibration 3

Manning's n region	n
river 1	0,16
river 2	0,04
river 3	0,04
river 4	0,038
river 5	0,045
river 6	0,044
river 7	0,044
river 8	0,035
river 9	0,045
river 10	0,03
river 11	0,025
river 12	0,025
river 13	0,04
river 14	0,04
river 15	0,036
river 16	0,033
river 17	0,033
river 18	0,033
river 19	0,046
river 20	0,04

Calibration 4

Manning's n region	n
river 1	0,165
river 2	0,042
river 3	0,044
river 4	0,038
river 5	0,05
river 6	0,048
river 7	0,046
river 8	0,035
river 9	0,045
river 10	0,03
river 11	0,023
river 12	0,025
river 13	0,045
river 14	0,045
river 15	0,04
river 16	0,033
river 17	0,033
river 18	0,029
river 19	0,046
river 20	0,04

Calibration 5

Manning's n region	n
river 1	0,16
river 2	0,05
river 3	0,044
river 4	0,038
river 5	0,05
river 6	0,05
river 7	0,047
river 8	0,035
river 9	0,05
river 10	0,04
river 11	0,018
river 12	0,025
river 13	0,045
river 14	0,047
river 15	0,04
river 16	0,04
river 17	0,033
river 18	0,035
river 19	0,046
river 20	0,04

Calibration 6

region	n
river 1	0,155
river 2	0,055
river 3	0,044
river 4	0,038
river 5	0,05
river 6	0,055
river 7	0,047
river 8	0,035
river 9	0,055
river 10	0,04
river 11	0,01
river 12	0,025
river 13	0,05
river 14	0,047
river 15	0,045
river 16	0,045
river 17	0,04
river 18	0,035
river 19	0,046
river 20	0,04

Calibration 7

region	n
river 1	0,155
river 2	0,06
river 3	0,044
river 4	0,038
river 5	0,05
river 6	0,055
river 7	0,047
river 8	0,035
river 9	0,06
river 10	0,045
river 11	0,01
river 12	0,018
river 13	0,05
river 14	0,047
river 15	0,045
river 16	0,045
river 17	0,04
river 18	0,035
river 19	0,046
river 20	0,04

Calibration 8

region	n
river 1	0,155
river 2	0,07
river 3	0,044
river 4	0,038
river 5	0,05
river 6	0,055
river 7	0,047
river 8	0,035
river 9	0,06
river 10	0,045
river 11	0,063
river 12	0,018
river 13	0,05
river 14	0,047
river 15	0,045
river 16	0,045
river 17	0,04
river 18	0,035
river 19	0,046
river 20	0,04

Calibration 9

region	n
river 1	0,155
river 2	0,075
river 3	0,044
river 4	0,038
river 5	0,05
river 6	0,055
river 7	0,047
river 8	0,035
river 9	0,06
river 10	0,052
river 11	0,05
river 12	0,045
river 13	0,05
river 14	0,055
river 15	0,05
river 16	0,045
river 17	0,04
river 18	0,035
river 19	0,046
river 20	0,04

Calibration 10

region	n
river 1	0,155
river 2	0,08
river 3	0,044
river 4	0,038
river 5	0,05
river 6	0,06
river 7	0,047
river 8	0,035
river 9	0,06
river 10	0,055
river 11	0,04
river 12	0,04
river 13	0,05
river 14	0,055
river 15	0,05
river 16	0,05
river 17	0,04
river 18	0,035
river 19	0,046
river 20	0,04

APPENDIX J.5: Manning's n grid size 3 meter

Calibration 11

region	n
river 1	0,155
river 10	0,06
river 11	0,055
river 12	0,04
river 13	0,05
river 14	0,055
river 15	0,05
river 16	0,05
river 17	0,04
river 18	0,035
river 2	0,046
river 19	0,2
river 20	0,04
river 3	0,08
river 4	0,044
river 5	0,038
river 6	0,05
river 7	0,06
river 8	0,047
river 9	0,035

Calibration 12

region	n
river 1	0,08
river 10	0,06
river 11	0,055
river 12	0,03
river 13	0,055
river 14	0,055
river 15	0,05
river 16	0,05
river 17	0,04
river 18	0,035
river 2	0,046
river 19	0,155
river 20	0,04
river 3	0,088
river 4	0,05
river 5	0,038
river 6	0,05
river 7	0,07
river 8	0,047
river 9	0,035

Calibration 13

region	n
river 1	0,08
river 10	0,06
river 11	0,055
river 12	0,02
river 13	0,06
river 14	0,055
river 15	0,05
river 16	0,05
river 17	0,04
river 18	0,035
river 2	0,046
river 19	0,155
river 20	0,04
river 3	0,09
river 4	0,055
river 5	0,038
river 6	0,05
river 7	0,08
river 8	0,047
river 9	0,035

Calibration 14

region	n
river 1	0,09
river 2	0,046
river 3	0,089
river 4	0,085
river 5	0,038
river 6	0,05
river 7	0,09
river 8	0,047
river 9	0,035
river 10	0,06
river 11	0,055
river 12	0,01
river 13	0,06
river 14	0,06
river 15	0,07
river 16	0,05
river 17	0,04
river 18	0,035
river 19	0,155
river 20	0,04

Calibration 15

region	n
river 1	0,09
river 2	0,046
river 3	0,09
river 4	0,05
river 5	0,038
river 6	0,05
river 7	0,1
river 8	0,047
river 9	0,035
river 10	0,06
river 11	0,03
river 12	0,01
river 13	0,06
river 14	0,075
river 15	0,07
river 16	0,05
river 17	0,04
river 18	0,035
river 19	0,155
river 20	0,04

Calibration 16

region	n
river 1	0,094
river 2	0,156
river 3	0,093
river 4	0,046
river 5	0,04
river 6	0,05
river 7	0,15
river 8 -	0,049
river 9	0,04
river 10	0,063
river 11	0,035
river 12	0,01
river 13	0,064
river 14	0,075
river 15	0,07
river 16	0,05
river 17	0,04
river 18	0,03
river 19	0,046
river 20	0,04

Calibration 17

region	n
river 1	0,095
river 2	0,155
river 3	0,095
river 4	0,045
river 5	0,045
river 6	0,055
river 7	0,15
river 8	0,049
river 9	0,045
river 10	0,065
river 11	0,025
river 12	0,01
river 13	0,05
river 14	0,075
river 15	0,075
river 16	0,06
river 17	0,05
river 18	0,03
river 19	0,046
river 20	0,04

Calibration 18

region	n
river 1	0,095
river 2	0,155
river 3	0,095
river 4	0,044
river 5	0,046
river 6	0,053
river 7	0,15
river 8	0,049
river 9	0,045
river 10	0,065
river 11	0,02
river 12	0,01
river 13	0,02
river 14	0,04
river 15	0,045
river 16	0,06
river 17	0,05
river 18	0,03
river 19	0,046
river 20	0,04

Calibration 19

region	n
river 1	0,095
river 2	0,155
river 3	0,095
river 4	0,044
river 5	0,046
river 6	0,053
river 7	0,15
river 8	0,049
river 9	0,045
river 10	0,065
river 11	0,02
river 12	0,01
river 13	0,02
river 14	0,04
river 15	0,045
river 16	0,06
river 17	0,05
river 18	0,03
river 19	0,046
river 20	0,04

Calibration 20

region	n
river 1	0,095
river 2	0,155
river 3	0,095
river 4	0,03
river 5	0,046
river 6	0,053
river 7	0,15
river 8	0,052
river 9	0,045
river 10	0,065
river 11	0,02
river 12	0,01
river 13	0,04
river 14	0,04
river 15	0,045
river 16	0,06
river 17	0,05
river 18	0,03
river 19	0,046
river 20	0,04

APPENDIX J.6: Manning's n grid size 3 meter

Calibration 21

Manning's n	region	n
river 1		0,095
river 2		0,155
river 3		0,095
river 4		0,03
river 5		0,046
river 6		0,053
river 7		0,15
river 8 -		0,052
river 9		0,045
river 10		0,065
river 11		0,018
river 12		0,01
river 13		0,045
river 14		0,04
river 15		0,045
river 16		0,06
river 17		0,05
river 18		0,03
river 19		0,046
river 20		0,04

calibration 22

Manning's n	region	n
river 1		0,095
river 2		0,155
river 3		0,1
river 4		0,04
river 5		0,055
river 6		0,053
river 7		0,13
river 8		0,052
river 9		0,045
river 10		0,065
river 11		0,045
river 12		0,035
river 13		0,045
river 14		0,04
river 15		0,045
river 16		0,06
river 17		0,05
river 18		0,025
river 19		0,046
river 20		0,04

Calibration 23

Manning's n	region	n
river 1		0,095
river 2		0,155
river 3		0,1
river 4		0,035
river 5		0,055
river 6		0,053
river 7		0,15
river 8		0,06
river 9		0,045
river 10		0,065
river 11		0,045
river 12		0,04
river 13		0,047
river 14		0,045
river 15		0,045
river 16		0,045
river 17		0,045
river 18		0,023
river 19		0,046
river 20		0,04

Calibration 24

Manning's n	region	n
river 1		0,095
river 2		0,155
river 3		0,15
river 4		0,03
river 5		0,055
river 6		0,053
river 7		0,15
river 8		0,06
river 9		0,045
river 10		0,065
river 11		0,045
river 12		0,045
river 13		0,047
river 14		0,045
river 15		0,045
river 16		0,045
river 17		0,045
river 18		0,023
river 19		0,046
river 20		0,04

calibration 25

Manning's n	region	n
river 1		0,095
river 2		0,155
river 3		0,12
river 4		0,025
river 5		0,05
river 6		0,053
river 7		0,12
river 8		0,059
river 9		0,045
river 10		0,065
river 11		0,045
river 12		0,05
river 13		0,047
river 14		0,045
river 15		0,045
river 16		0,045
river 17		0,045
river 18		0,023
river 19		0,046
river 20		0,04

Calibration 26

Manning's n	region	n
river 1		0,095
river 2		0,155
river 3		0,1
river 4		0,023
river 5		0,05
river 6		0,053
river 7		0,12
river 8		0,059
river 9		0,045
river 10		0,065
river 11		0,045
river 12		0,055
river 13		0,055
river 14		0,045
river 15		0,045
river 16		0,045
river 17		0,045
river 18		0,023
river 19		0,05
river 20		0,04

Calibration 27

Manning's n	region	n
river 1		0,095
river 2		0,06
river 3		0,16
river 4		0,022
river 5		0,05
river 6		0,053
river 7		0,15
river 8		0,059
river 9		0,045
river 10		0,065
river 11		0,045
river 12		0,06
river 13		0,06
river 14		0,045
river 15		0,045
river 16		0,045
river 17		0,045
river 18		0,023
river 19		0,155
river 20		0,04

Calibration 28

Manning's n	region	n
river 1		0,1
river 2		0,06
river 3		0,16
river 4		0,022
river 5		0,05
river 6		0,04
river 7		0,15
river 8		0,058
river 9		0,045
river 10		0,065
river 11		0,05
river 12		0,06
river 13		0,06
river 14		0,045
river 15		0,045
river 16		0,045
river 17		0,045
river 18		0,023
river 19		0,14
river 20		0,04

Calibration 29

Manning's n	region	n
river 1		0,1
river 2		0,14
river 3		0,16
river 4		0,015
river 5		0,05
river 6		0,04
river 7		0,14
river 8		0,058
river 9		0,045
river 10		0,068
river 11		0,05
river 12		0,06
river 13		0,06
river 14		0,045
river 15		0,045
river 16		0,045
river 17		0,041
river 18		0,02
river 19		0,06
river 20		0,04

APPENDIX J.7: Manning's n grid size 2 meter

Calibration 1

Manning's n	
region	n
river 1	0.1
river 2	0.06
river 3	0.18
river 4	0.01
river 5	0.05
river 6	0.04
river 7	0.14
river 8	0.06
river 9	0.045
river 10	0.068
river 11	0.05
river 12	0.06
river 13	0.06
river 14	0.045
river 15	0.045
river 16	0.045
river 17	0.041
river 18	0.01
river 19	0.14
river 20	0.04

Calibration 2

Manning's n	
region	n
river 1	0.1
river 2	0.14
river 3	0.18
river 4	0.01
river 5	0.02
river 6	0.04
river 7	0.14
river 8	0.01
river 9	0.045
river 10	0.068
river 11	0.05
river 12	0.06
river 13	0.06
river 14	0.045
river 15	0.045
river 16	0.045
river 17	0.041
river 18	0.01
river 19	0.06
river 20	0.04

Calibration 3

Manning's n	
region	n
river 1	0.1
river 2	0.11
river 3	0.12
river 4	0.008
river 5	0.02
river 6	0.04
river 7	0.14
river 8	0.01
river 9	0.02
river 10	0.069
river 11	0.05
river 12	0.06
river 13	0.06
river 14	0.045
river 15	0.045
river 16	0.045
river 17	0.041
river 18	0.01
river 19	0.06
river 20	0.04

Calibration 4

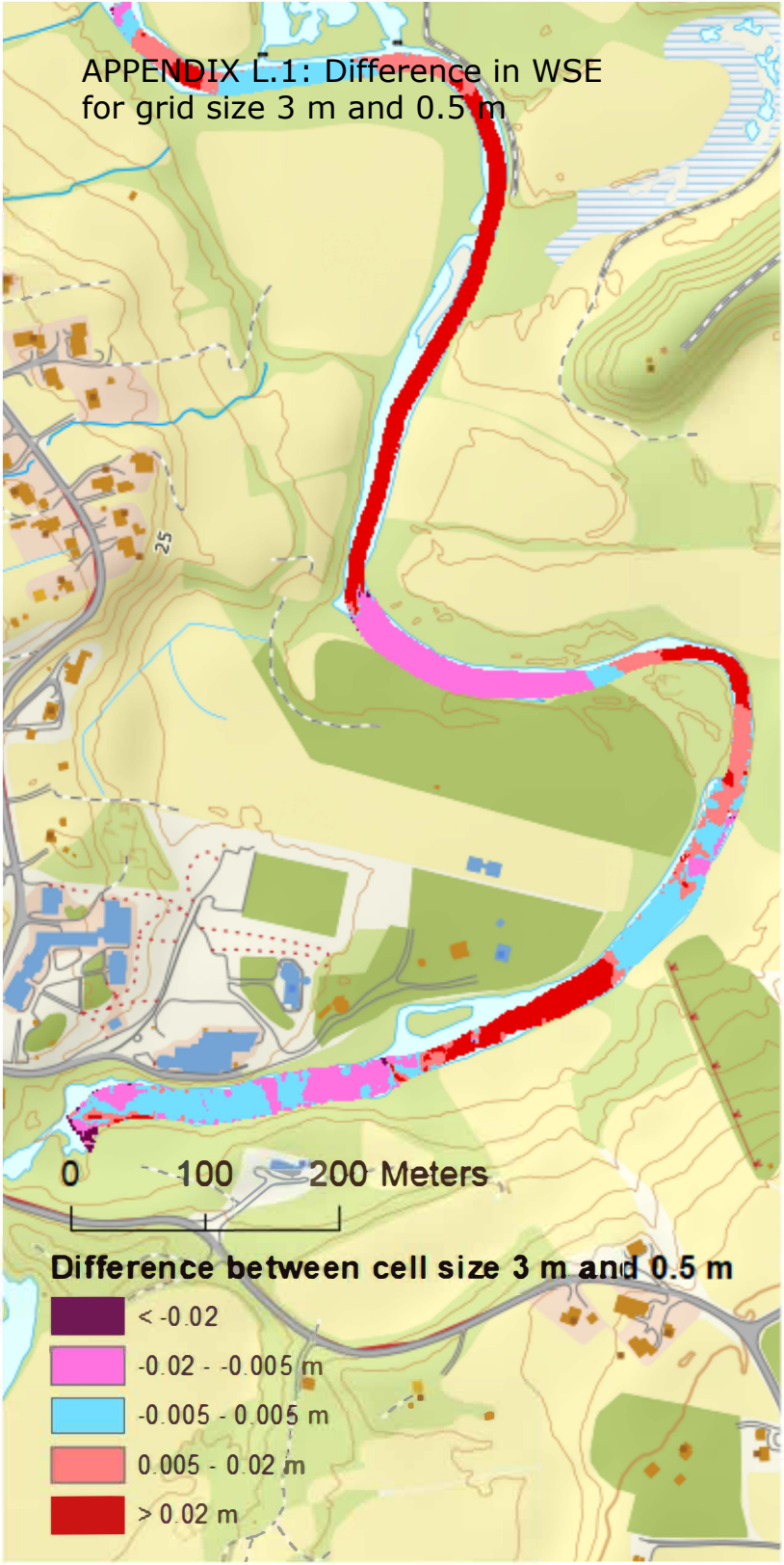
Manning's n	
region	n
river 1	0.1
river 2	0.14
river 3	0.16
river 4	0.015
river 5	0.05
river 6	0.04
river 7	0.14
river 8	0.058
river 9	0.045
river 10	0.068
river 11	0.05
river 12	0.06
river 13	0.06
river 14	0.045
river 15	0.045
river 16	0.045
river 17	0.041
river 18	0.02
river 19	0.06
river 20	0.04

APPENDIX K: Water flow 14.09.2015, day of collection of LIDAR data

Date and time	Flow [m ³ /s]
14.09.2015 23.00	3.263
14.09.2015 22.30	3.255
14.09.2015 22.00	3.255
14.09.2015 21.30	3.263
14.09.2015 21.00	3.263
14.09.2015 20.30	3.272
14.09.2015 20.00	3.263
14.09.2015 19.30	3.272
14.09.2015 19.00	3.272
14.09.2015 18.30	3.28
14.09.2015 18.00	3.28
14.09.2015 17.30	3.272
14.09.2015 17.00	3.28
14.09.2015 16.30	3.296
14.09.2015 16.00	3.296
14.09.2015 15.30	3.305
14.09.2015 15.00	3.305
14.09.2015 14.30	3.305
14.09.2015 14.00	3.313
14.09.2015 13.30	3.313
14.09.2015 13.00	3.313
14.09.2015 12.30	3.329
14.09.2015 12.00	3.329
14.09.2015 11.30	3.329

Date and time	Flow [m ³ /s]
14.09.2015 11.00	3.329
14.09.2015 10.30	3.313
14.09.2015 10.00	3.329
14.09.2015 9.30	3.329
14.09.2015 9.00	3.338
14.09.2015 8.30	3.338
14.09.2015 8.00	3.338
14.09.2015 7.30	3.354
14.09.2015 7.00	3.338
14.09.2015 6.30	3.346
14.09.2015 6.00	3.354
14.09.2015 5.30	3.354
14.09.2015 5.00	3.354
14.09.2015 4.30	3.371
14.09.2015 4.00	3.363
14.09.2015 3.30	3.363
14.09.2015 3.00	3.371
14.09.2015 2.30	3.371
14.09.2015 2.00	3.371
14.09.2015 1.30	3.379
14.09.2015 1.00	3.379
14.09.2015 0.30	3.363
14.09.2015 0.00	3.371
Average flow	3.32

APPENDIX L.1: Difference in WSE for grid size 3 m and 0.5 m

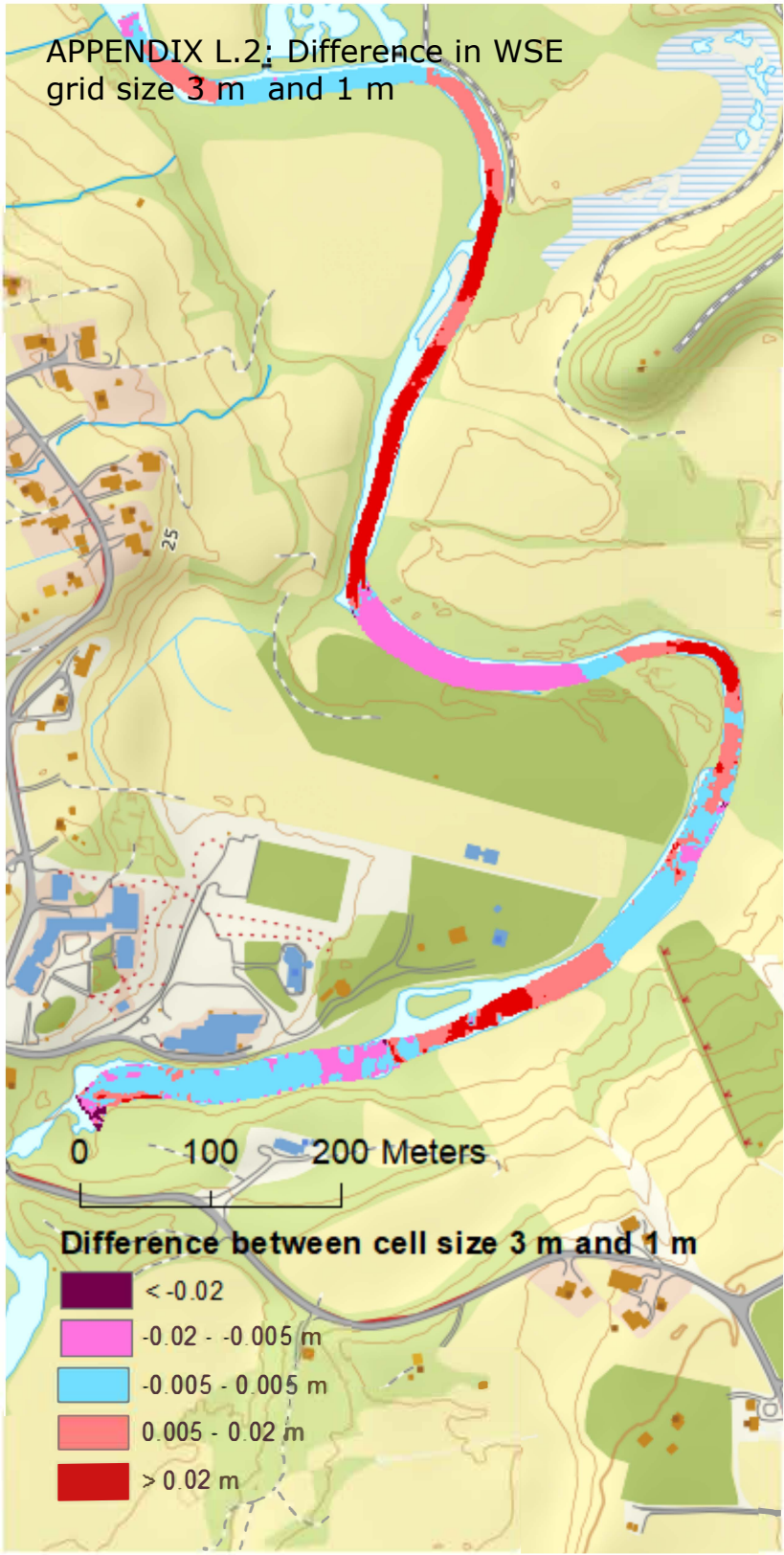


0 100 200 Meters

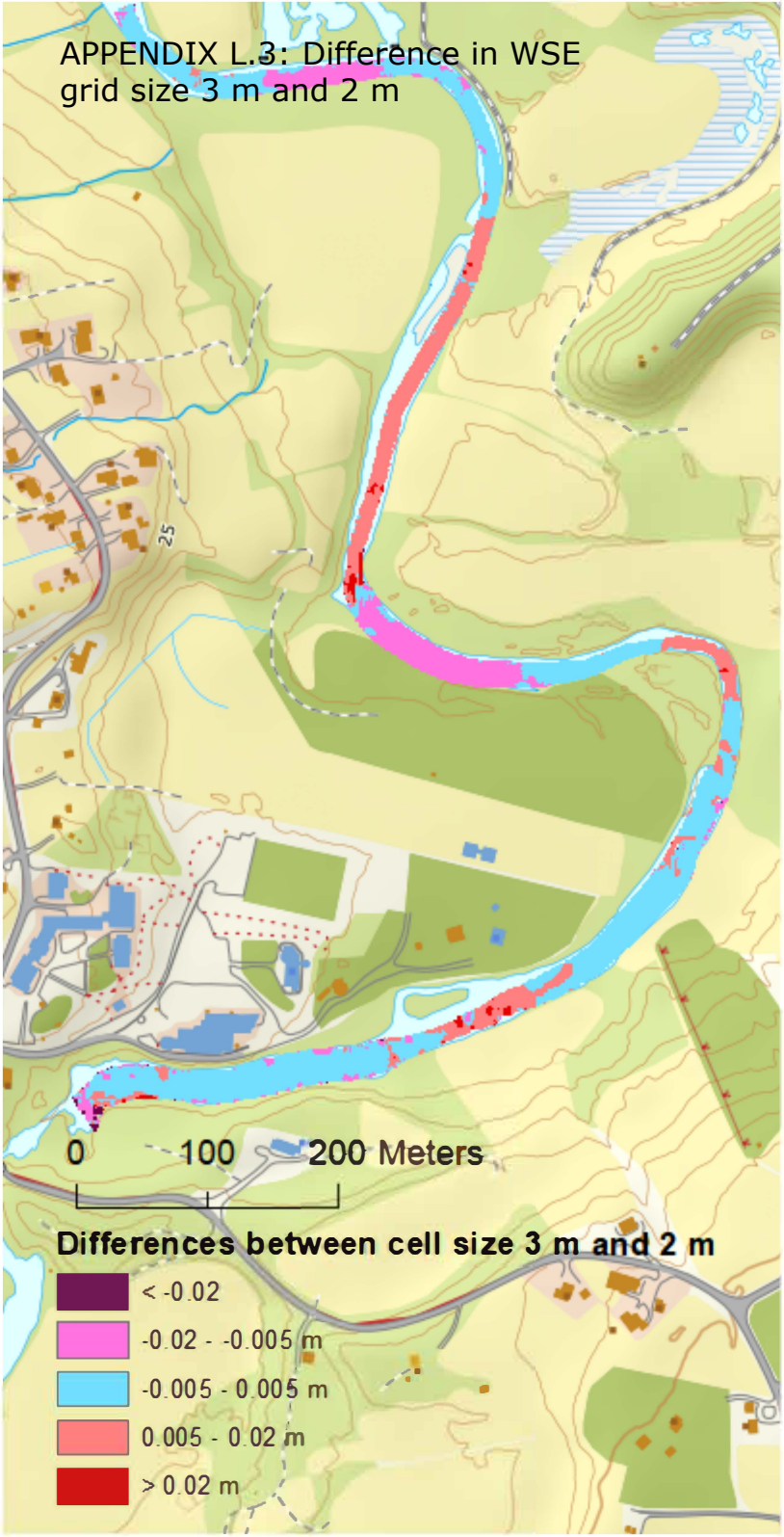
Difference between cell size 3 m and 0.5 m

- < -0.02
- 0.02 - -0.005 m
- 0.005 - 0.005 m
- 0.005 - 0.02 m
- > 0.02 m

APPENDIX L.2: Difference in WSE
grid size 3 m and 1 m



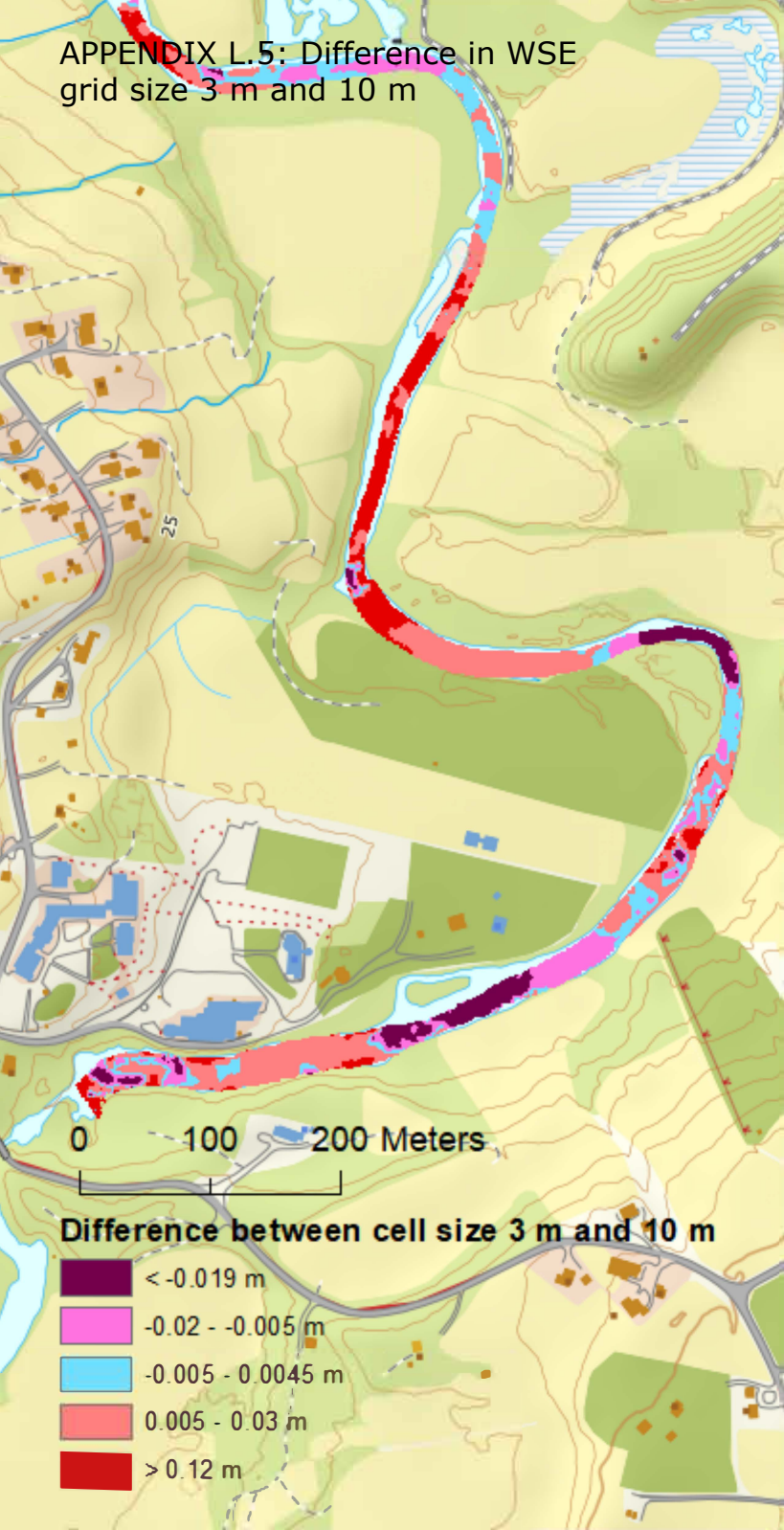
APPENDIX L.3: Difference in WSE
grid size 3 m and 2 m



APPENDIX L.4: Difference in WSE
grid size 3 m and 5 m



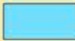
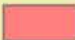



APPENDIX L.5: Difference in WSE
grid size 3 m and 10 m



0 100 200 Meters

Difference between cell size 3 m and 10 m

-  < -0.019 m
-  -0.02 - -0.005 m
-  -0.005 - 0.0045 m
-  0.005 - 0.03 m
-  > 0.12 m

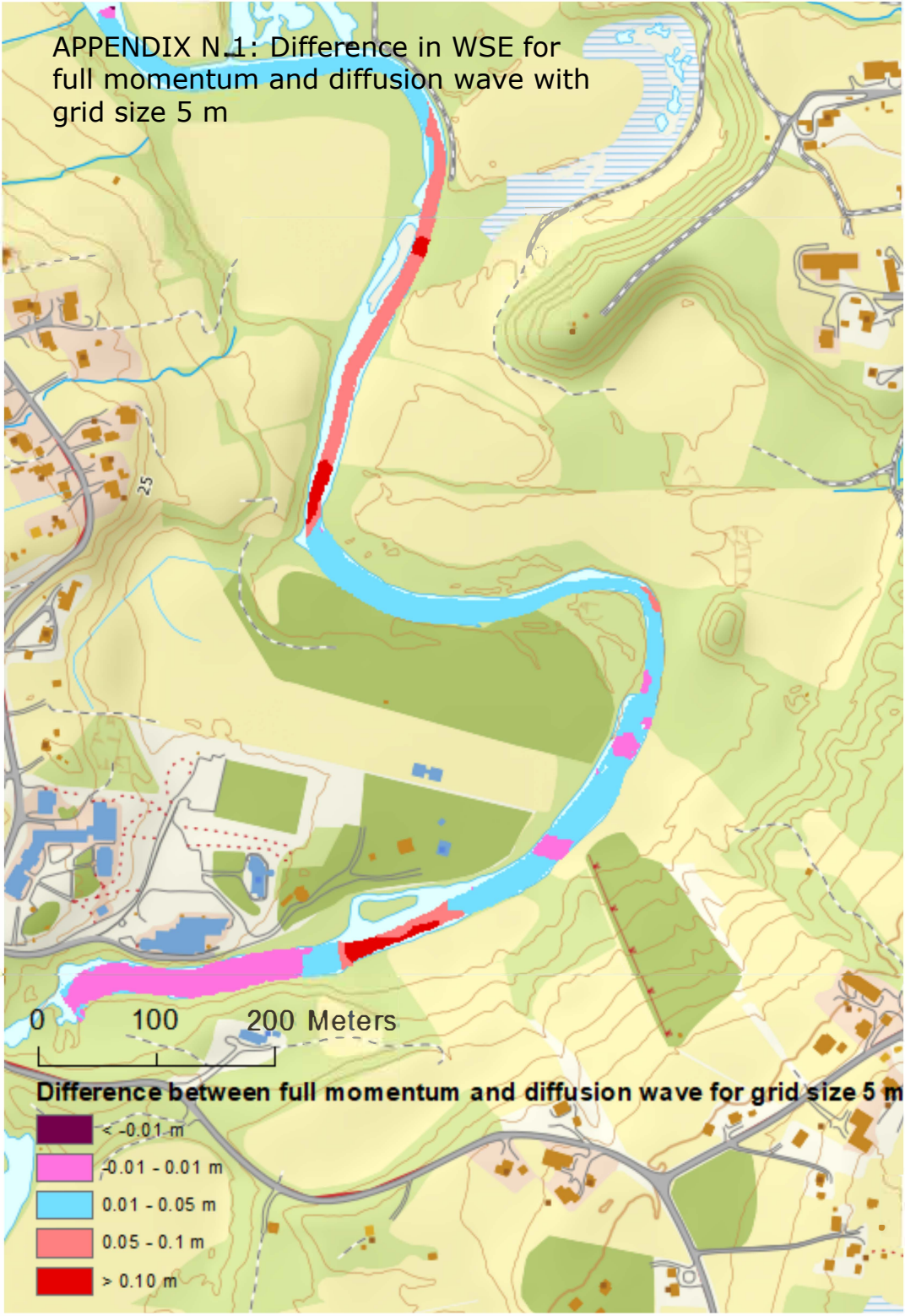
APPENDIX M.1: Difference in WSE for
theta=1 and theta=0.6



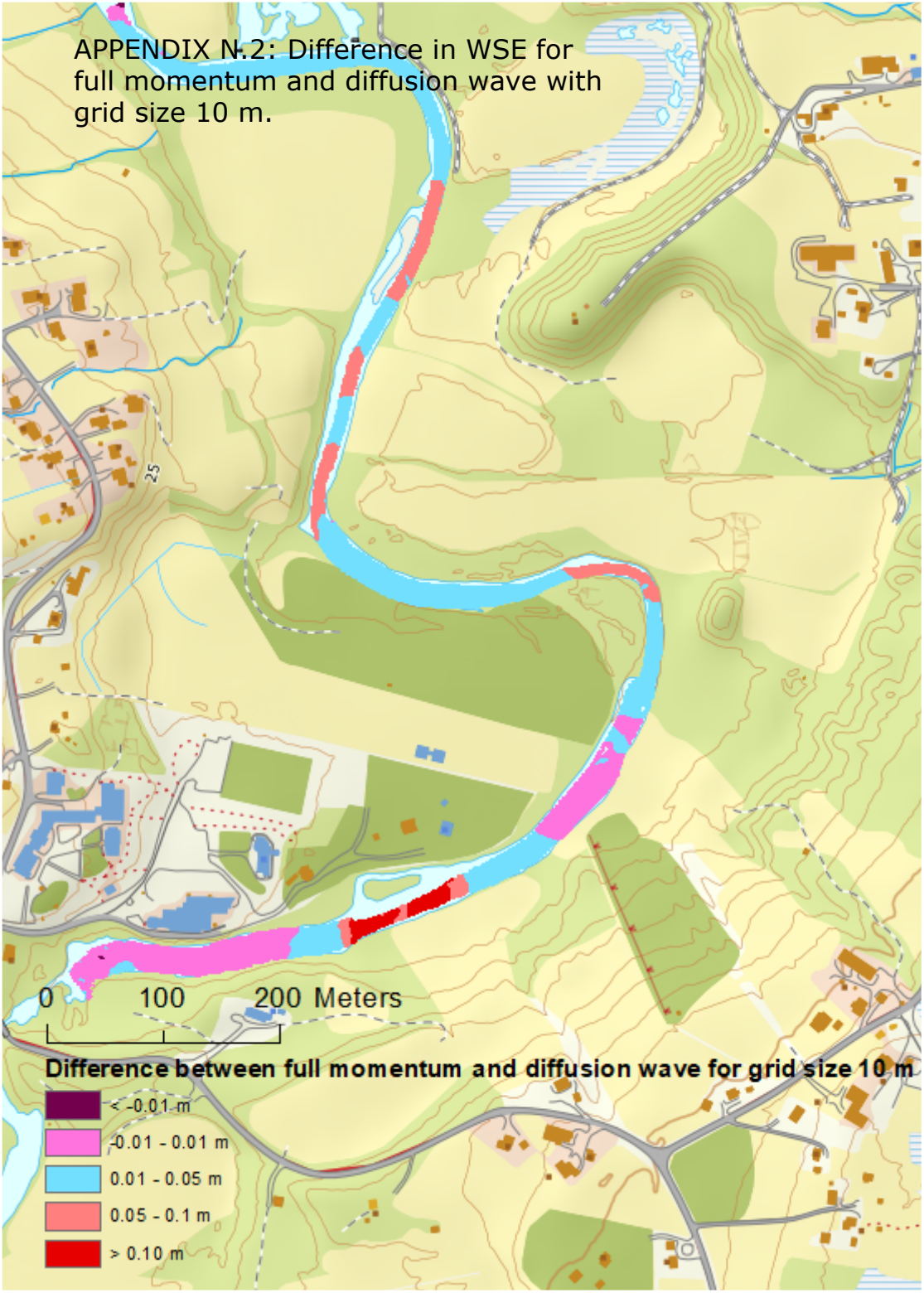
APPENDIX M.2: Difference in WSE for
theta = 0.8 and theta = 0,6



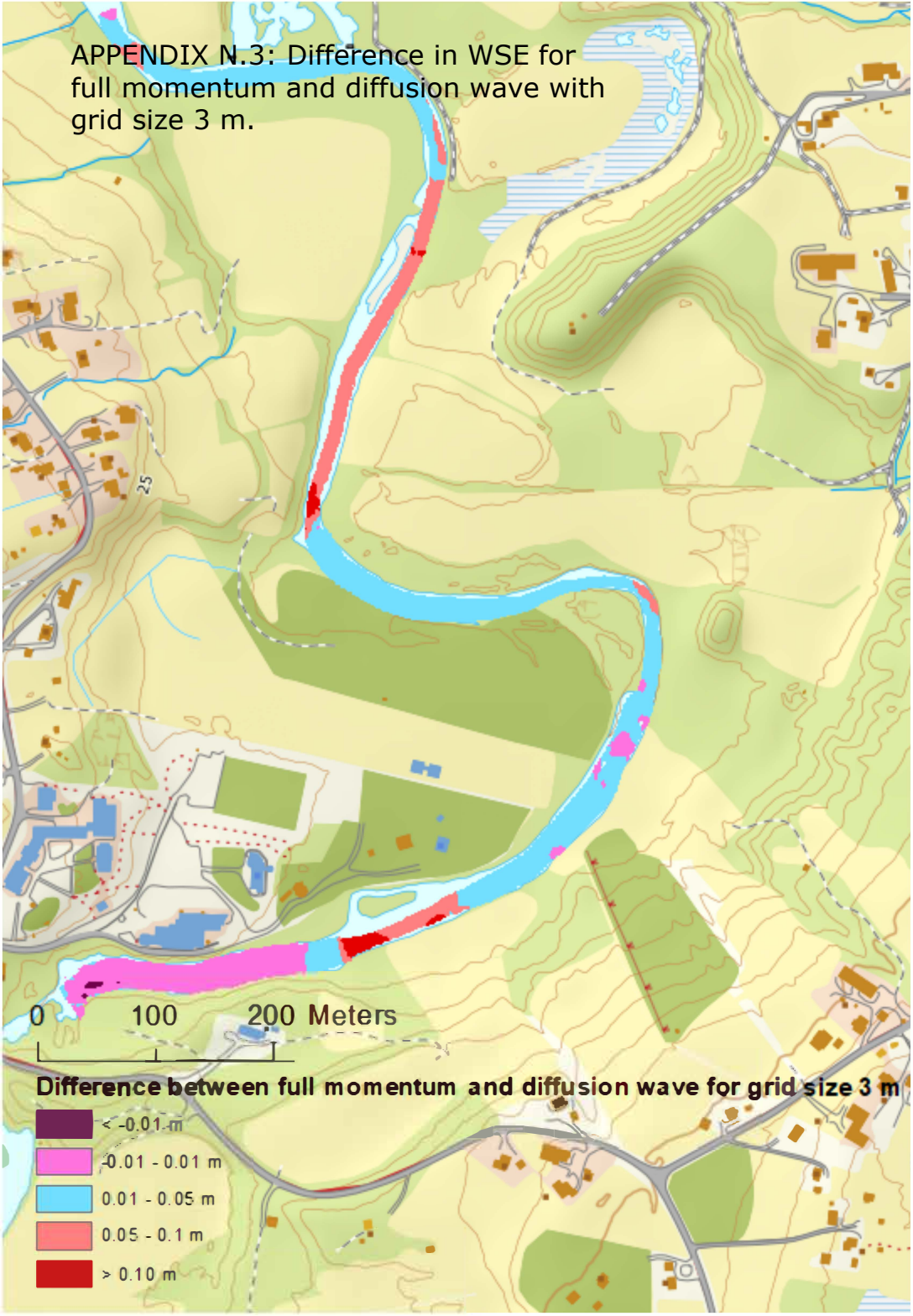
APPENDIX N.1: Difference in WSE for full momentum and diffusion wave with grid size 5 m



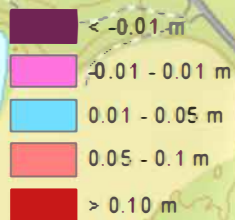
APPENDIX N.2: Difference in WSE for full momentum and diffusion wave with grid size 10 m.



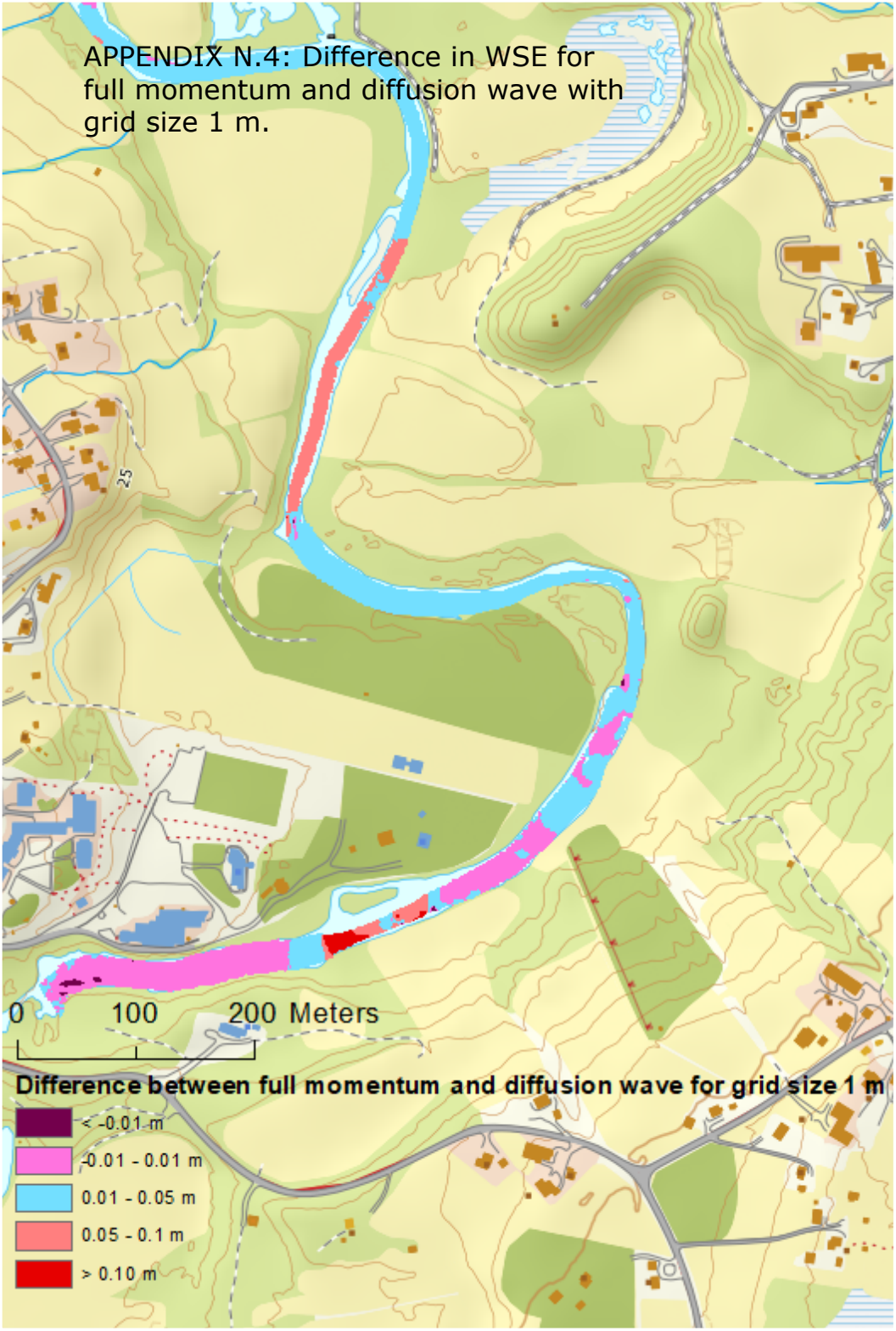
APPENDIX N.3: Difference in WSE for full momentum and diffusion wave with grid size 3 m.



Difference between full momentum and diffusion wave for grid size 3 m



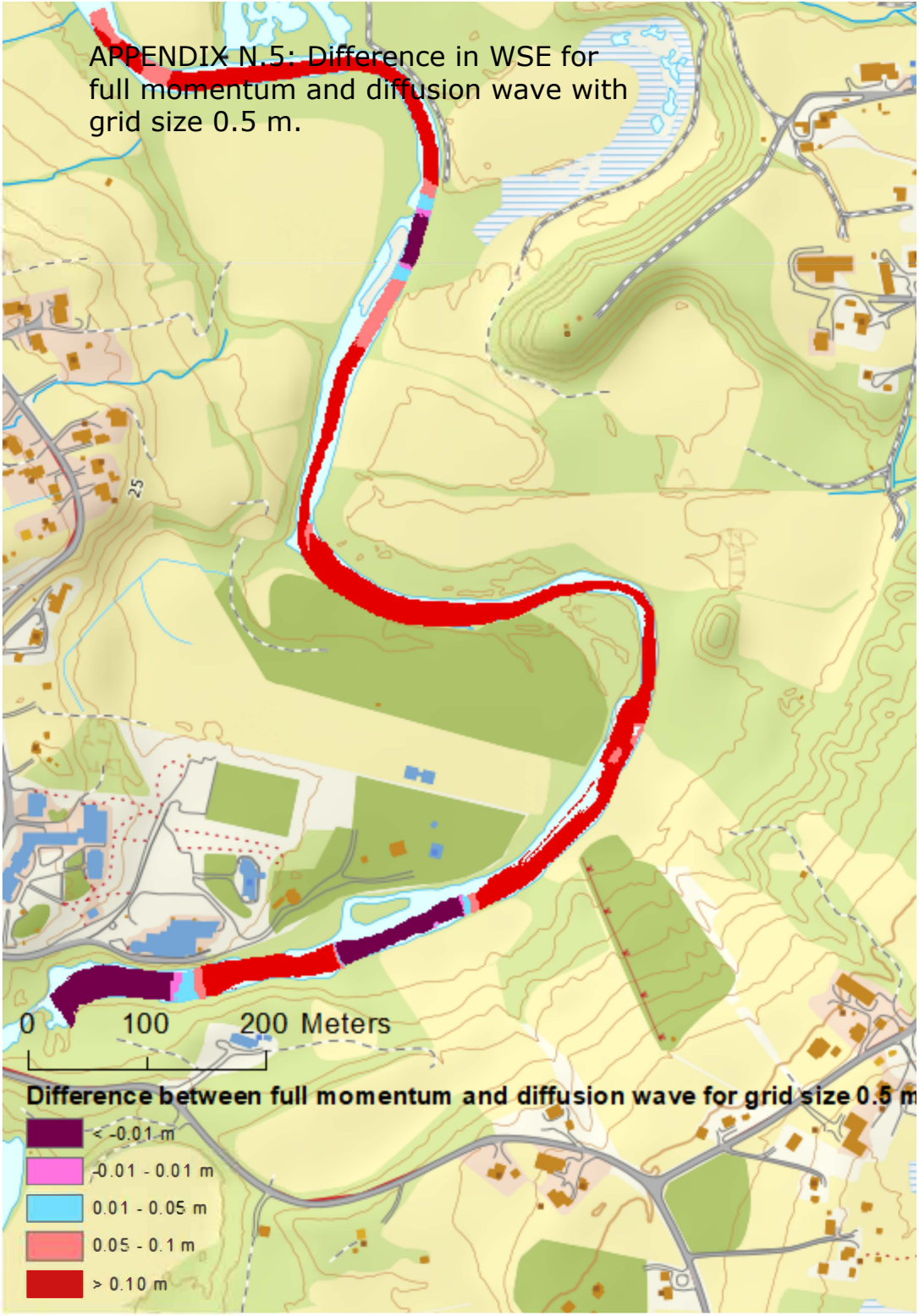
APPENDIX N.4: Difference in WSE for full momentum and diffusion wave with grid size 1 m.



Difference between full momentum and diffusion wave for grid size 1 m

- < -0.01 m
- $-0.01 - 0.01$ m
- $0.01 - 0.05$ m
- $0.05 - 0.1$ m
- > 0.10 m

APPENDIX N.5: Difference in WSE for full momentum and diffusion wave with grid size 0.5 m.



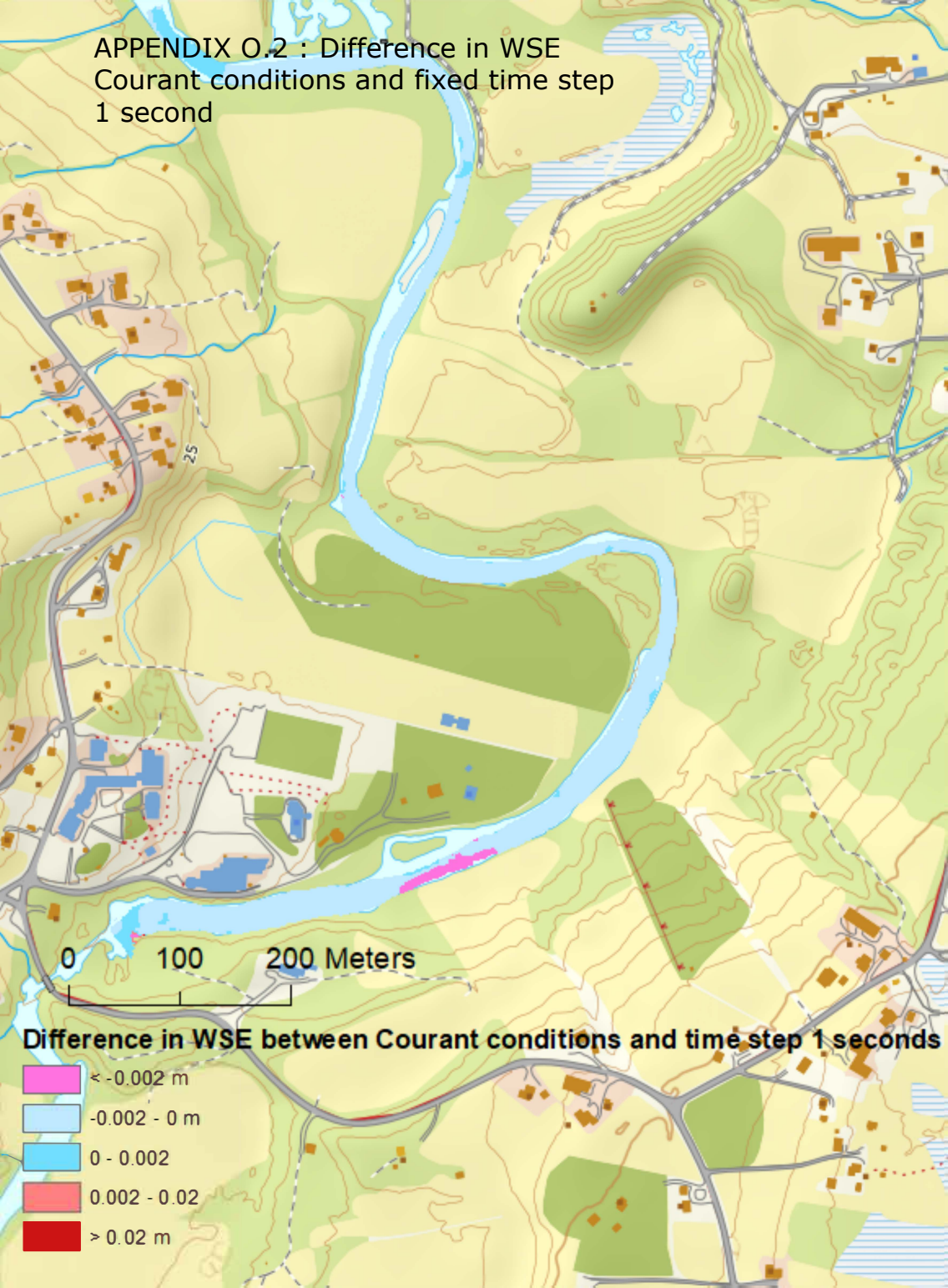
APPENDIX N.5: Difference in WSE for full momentum and diffusion wave with grid size 0.5 m. Different legend



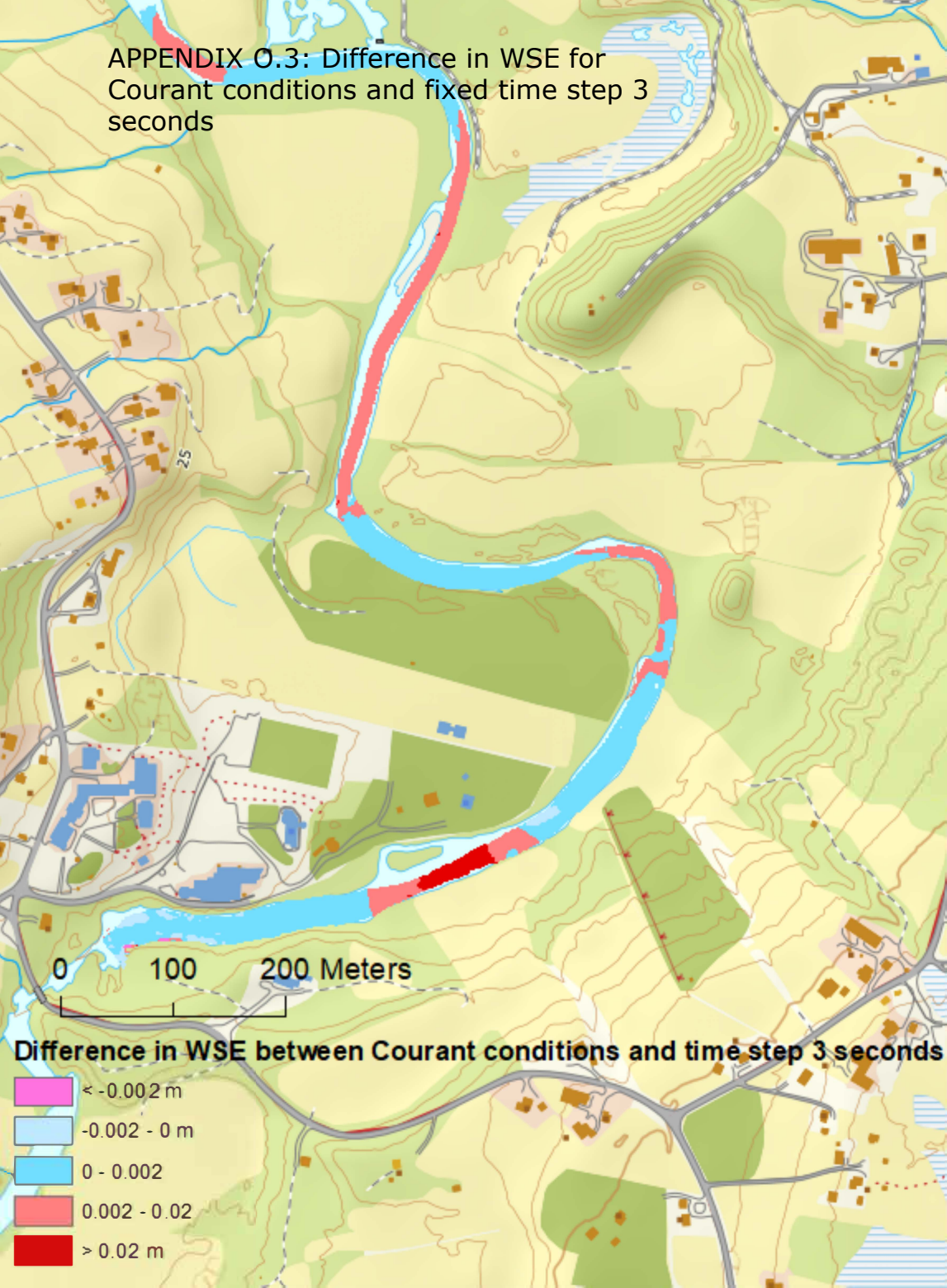
APPENDIX O.1: Difference in WSE for Courant Conditions and fixed time step 0.1 s



APPENDIX O.2 : Difference in WSE
Courant conditions and fixed time step
1 second



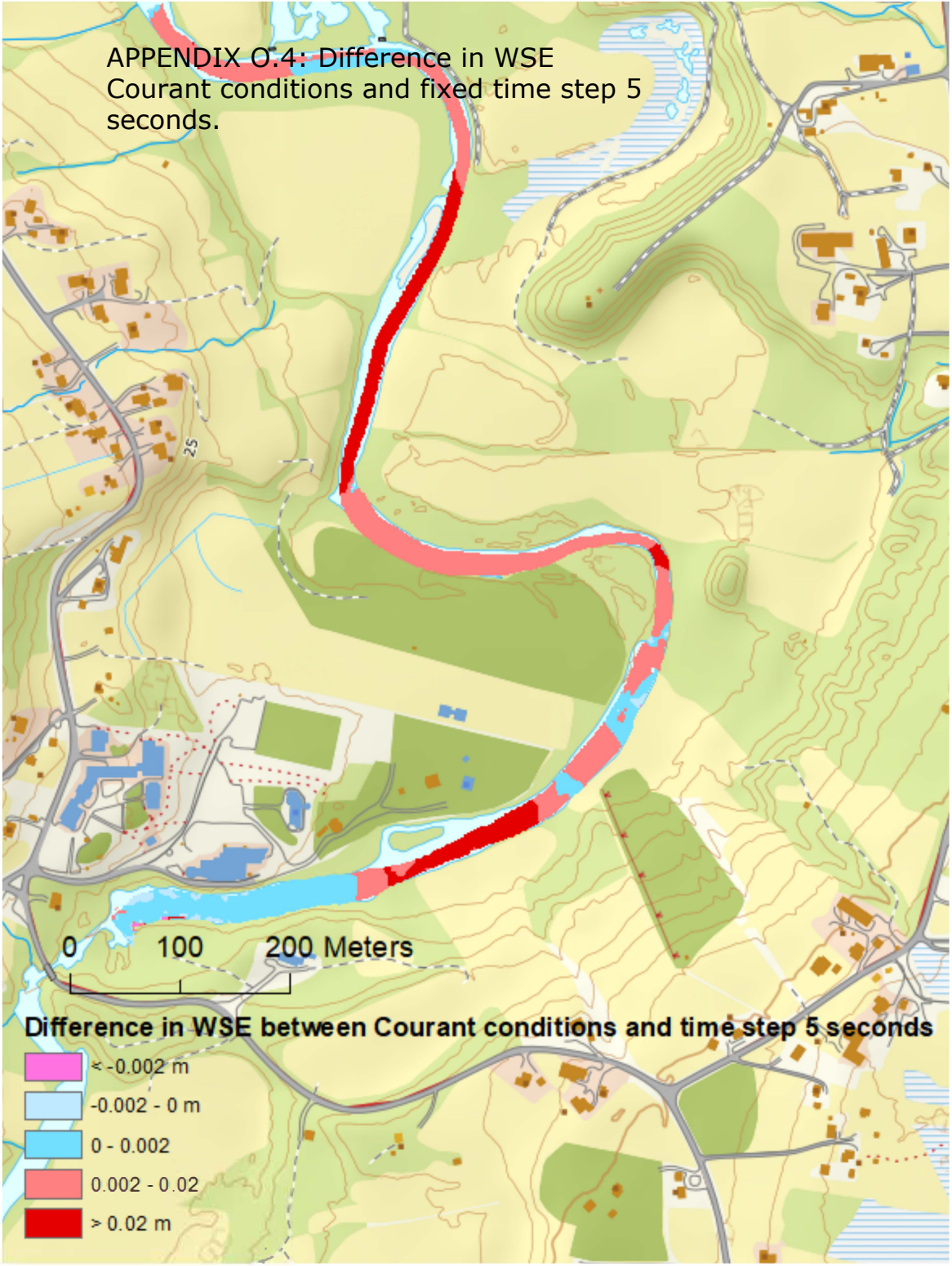
APPENDIX O.3: Difference in WSE for Courant conditions and fixed time step 3 seconds



Difference in WSE between Courant conditions and time step 3 seconds

- <math>< -0.002\text{ m}</math>
- $-0.002 - 0\text{ m}$
- $0 - 0.002$
- $0.002 - 0.02$
- $> 0.02\text{ m}$

APPENDIX O.4: Difference in WSE
Courant conditions and fixed time step 5
seconds.



APPENDIX O.5: Simulation crash, fixed time step 10 seconds

Unsteady Flow Analysis

File Options Help

Plan : 2.1. Sensitivity analysis_fixed_time6 Short ID: 2.1_Sensitivity analysis_fix

Geometry File : 2.Total_area_calibration_3m_1
 Unsteady Flow File : 2.Calibration_Q6.33

Programs to Run

- Geometry Preprocessor
- Unsteady Flow Simulation
- Sediment
- Post Processor
- Floodplain Mapping

Simulation Time Window

Starting Date: 01MAR2019 Starting Time: 0000
 Ending Date: 01MAR2019 Ending Time: 0600

Computation Settings

Computation Interval: 10 Second Hydrograph Output Interval: 5 Minute
 Mapping Output Interval: 5 Minute Detailed Output Interval: 5 Minute

DSS Output Filename: C:\Users\jodaar\Documents\01.Masteroppgrave_Eletern_deskto

Compute

HEC-RAS Computations

Write Geometry Information
 Layer: COMPLETE

Geometry Processor
 River: Reach: RS: Node Type: Storage Area
 IB Curve:

Unsteady Flow Simulation
 Simulation: 0.5361 01MAR
 Time: 0.5361 01MAR
 Unsteady Flow Computations

Computation Messages

```

01MAR2019 00:27:20 flow_area
01MAR2019 00:27:30 flow_area
01MAR2019 00:27:40 flow_area
01MAR2019 00:27:50 flow_area
01MAR2019 00:28:00 flow_area
01MAR2019 00:28:10 flow_area
01MAR2019 00:28:20 flow_area
01MAR2019 00:28:30 flow_area
01MAR2019 00:28:40 flow_area
01MAR2019 00:28:50 flow_area
01MAR2019 00:29:00 flow_area
01MAR2019 00:29:10 flow_area
01MAR2019 00:29:20 flow_area
01MAR2019 00:29:30 flow_area
01MAR2019 00:29:40 flow_area
01MAR2019 00:29:50 flow_area
01MAR2019 00:30:00 flow_area
01MAR2019 00:30:10 flow_area
01MAR2019 00:30:20 flow_area
01MAR2019 00:30:30 flow_area
01MAR2019 00:30:40 flow_area
01MAR2019 00:30:50 flow_area
01MAR2019 00:31:00 flow_area
01MAR2019 00:31:10 flow_area
01MAR2019 00:31:20 flow_area
01MAR2019 00:31:30 flow_area
01MAR2019 00:31:40 flow_area
01MAR2019 00:31:50 flow_area
01MAR2019 00:32:00 flow_area
01MAR2019 00:32:10 flow_area
                    
```

Cell # 24 25 26 27 28 29 30 31 32

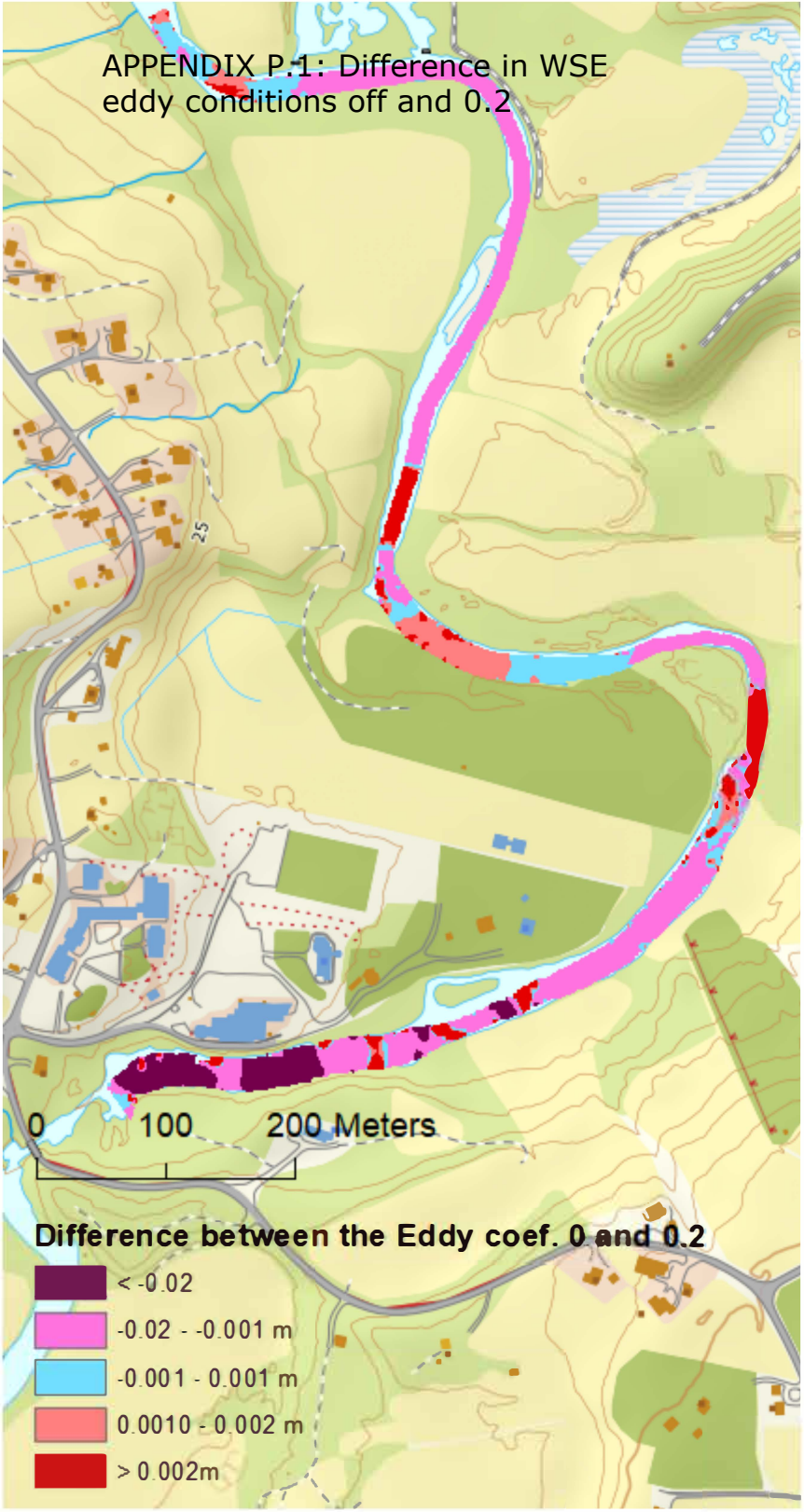
19.46 16.6110 2

Unsteady Flow Solver has stopped working

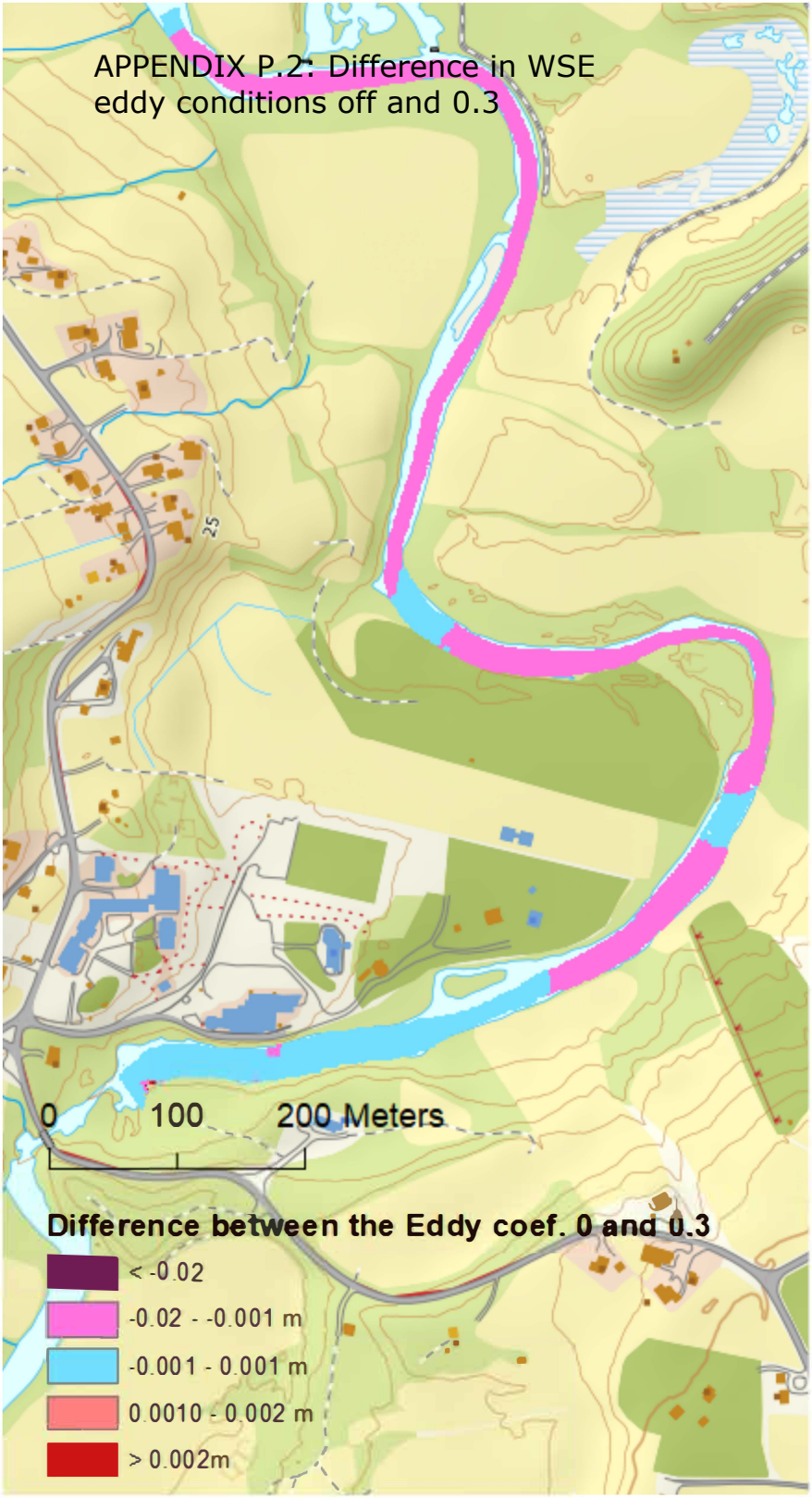
A problem caused the program to stop working correctly. Please close the program.

→ Close the program

APPENDIX P.1: Difference in WSE
eddy conditions off and 0.2



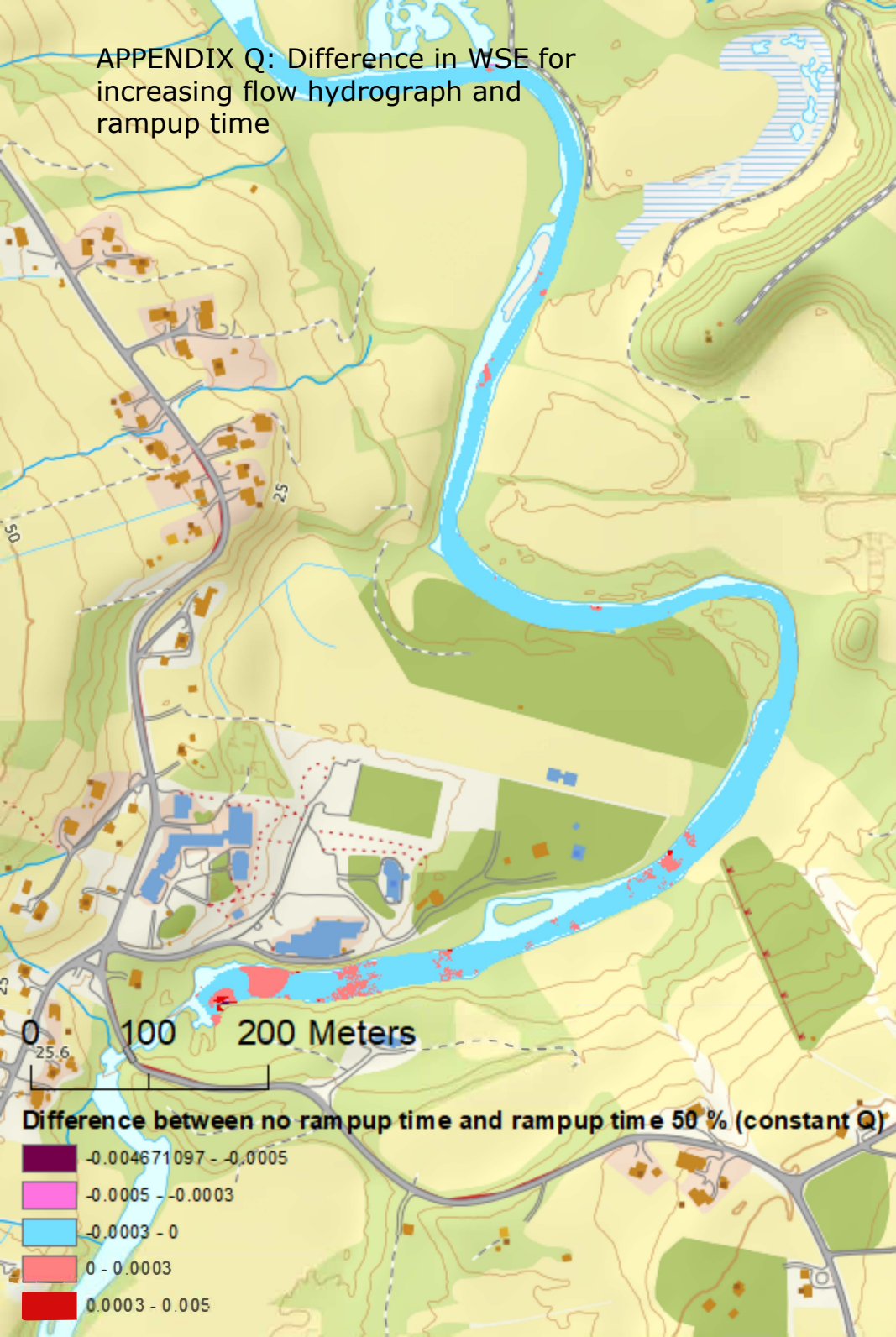
APPENDIX P.2: Difference in WSE
eddy conditions off and 0.3



APPENDIX P.3: Difference in WSE eddy conditions off and 5



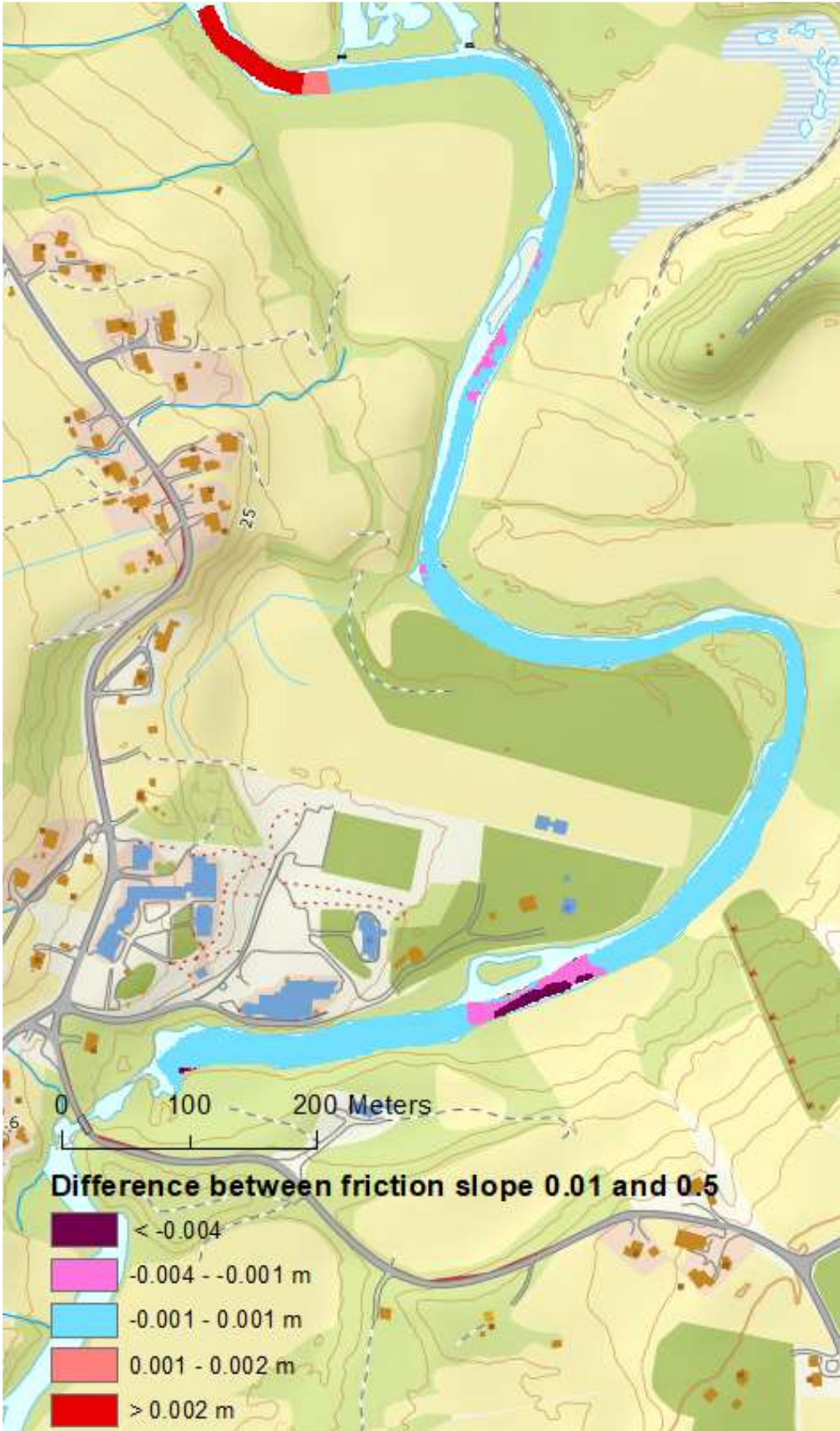
APPENDIX Q: Difference in WSE for increasing flow hydrograph and rampup time



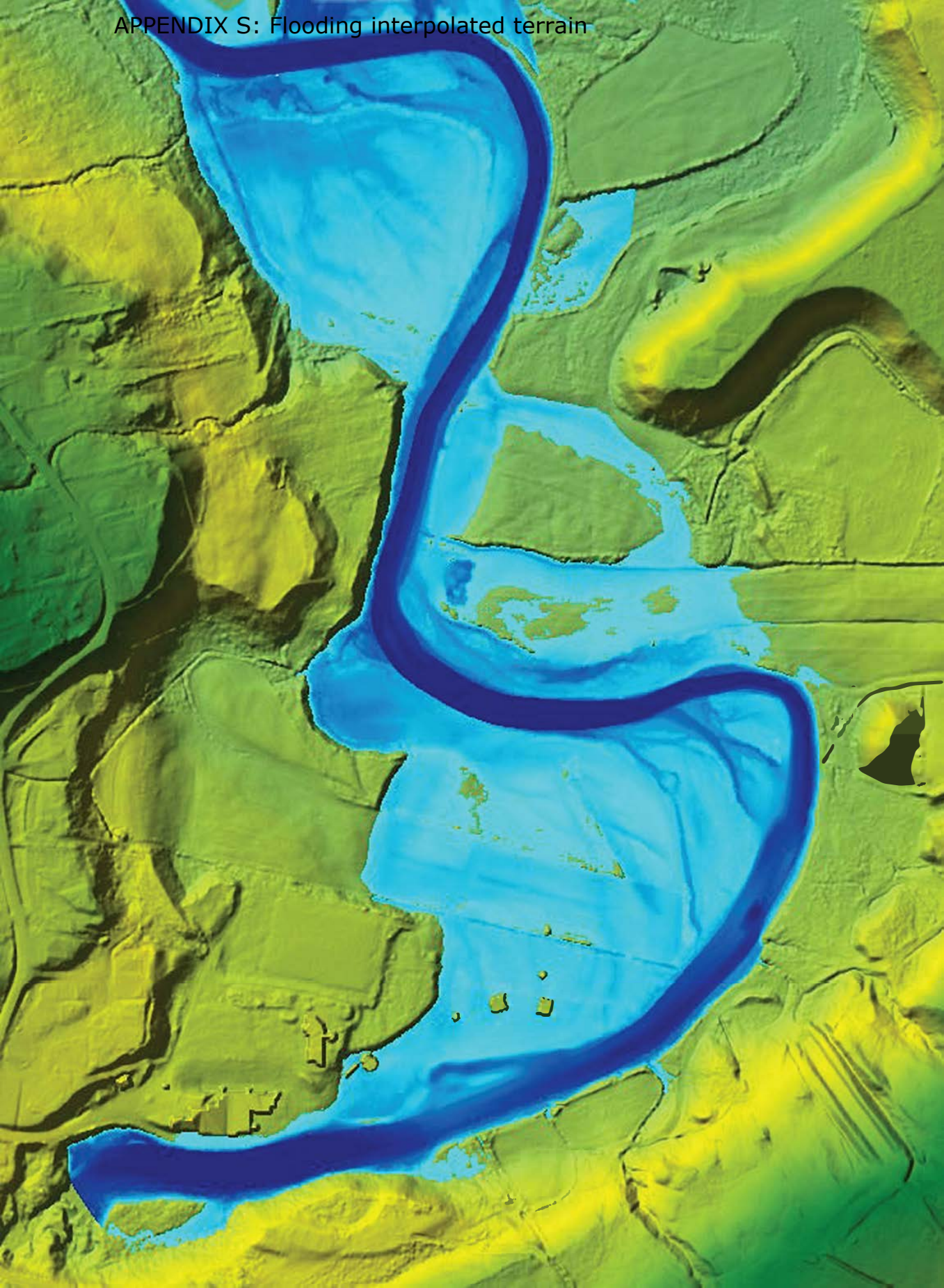
APPENDIX R.1: Difference in WSE for friction slope 0.01 and 0.05



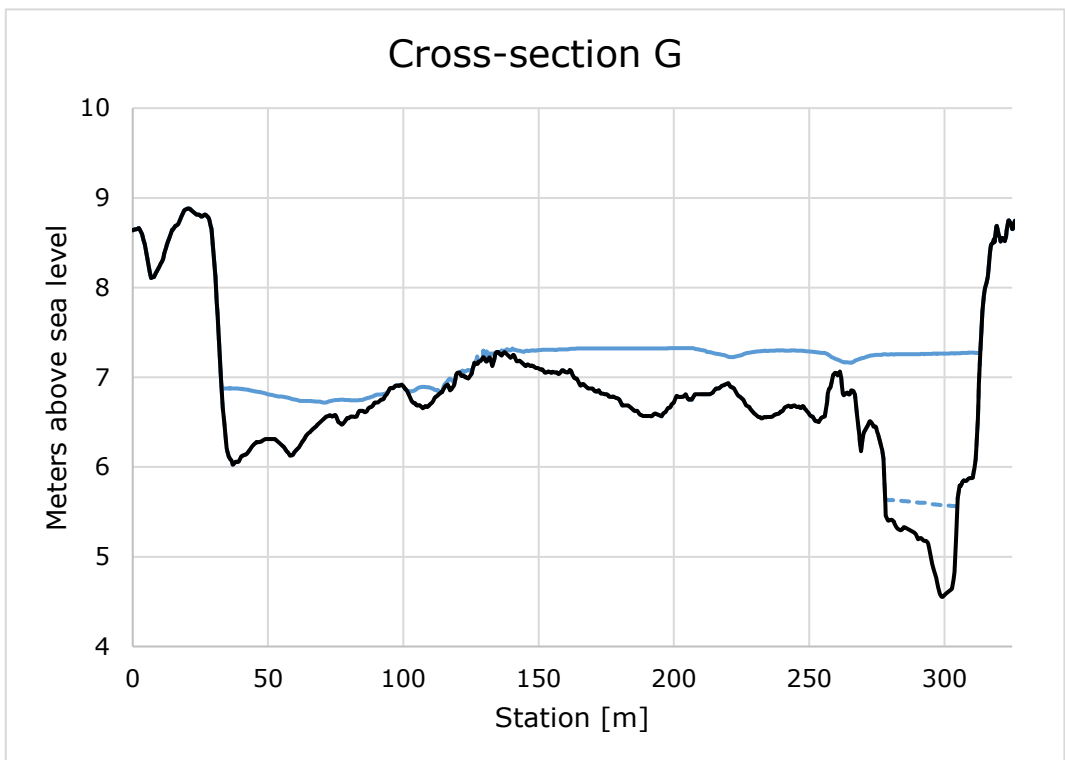
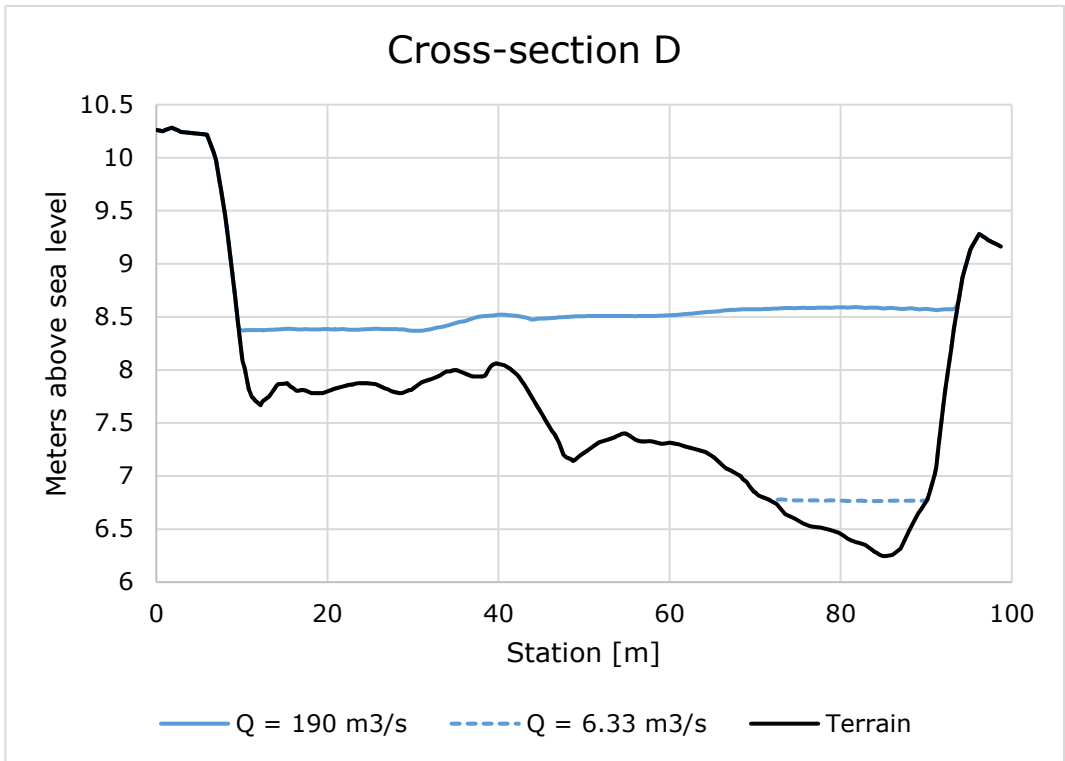
APPENDIX R.2: Difference in WSE for friction slope 0.01 and 0.5



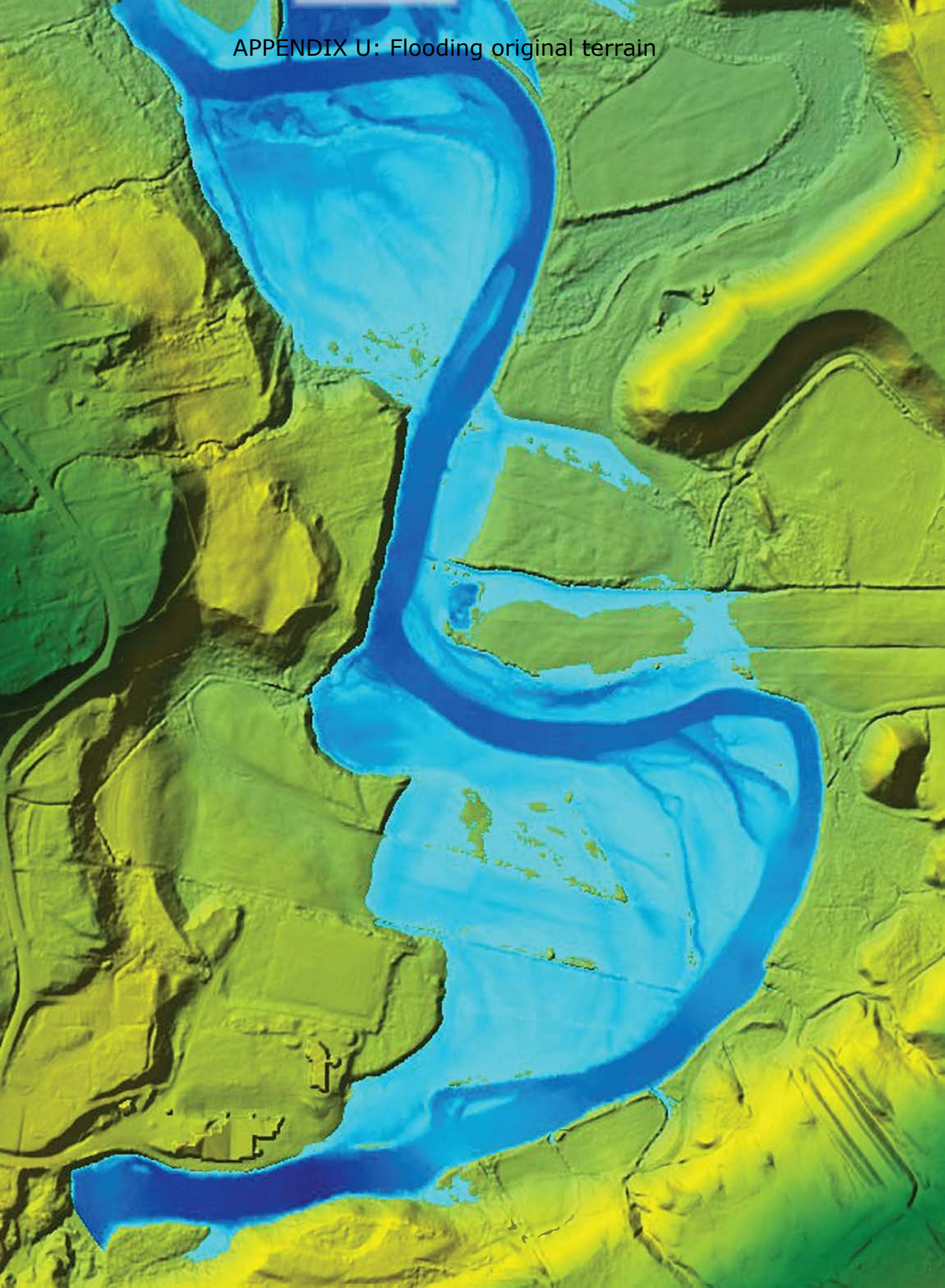
APPENDIX S: Flooding interpolated terrain



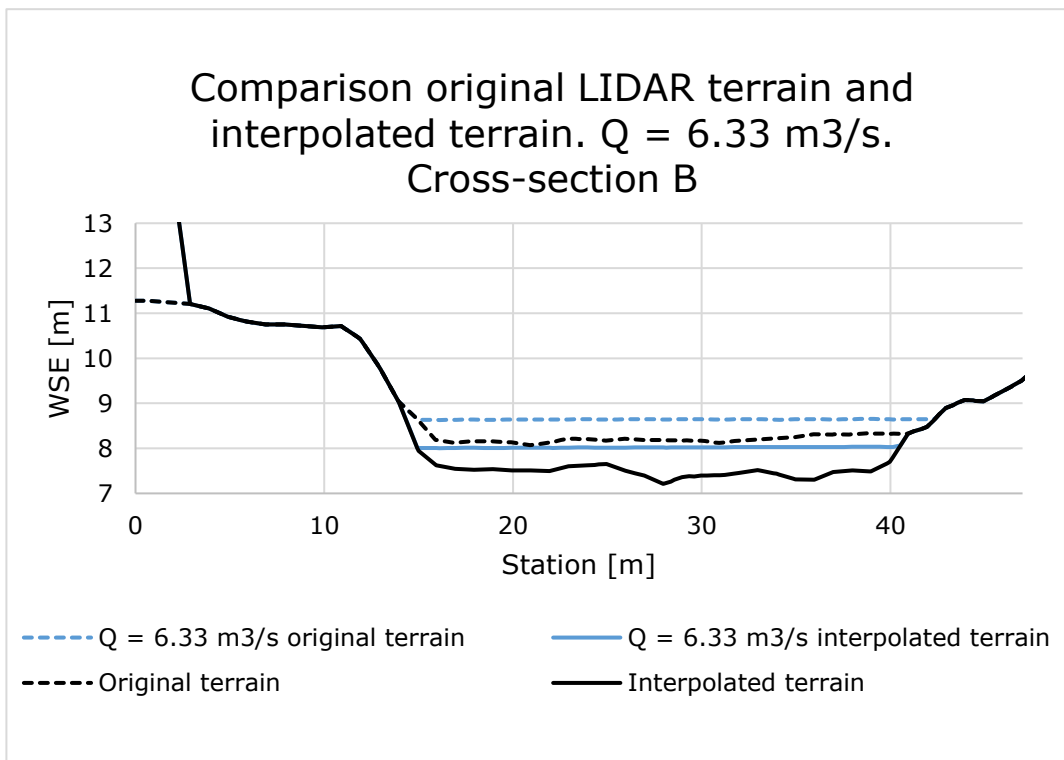
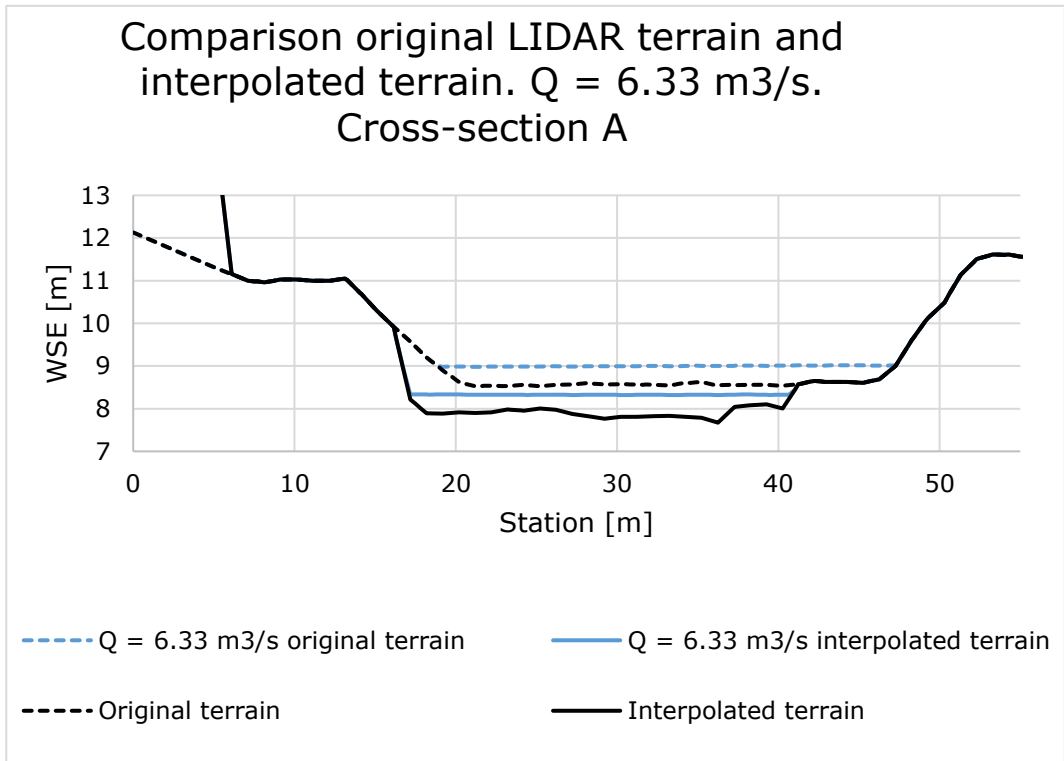
APPENDIX T: Cross-section D and G - flood simulation



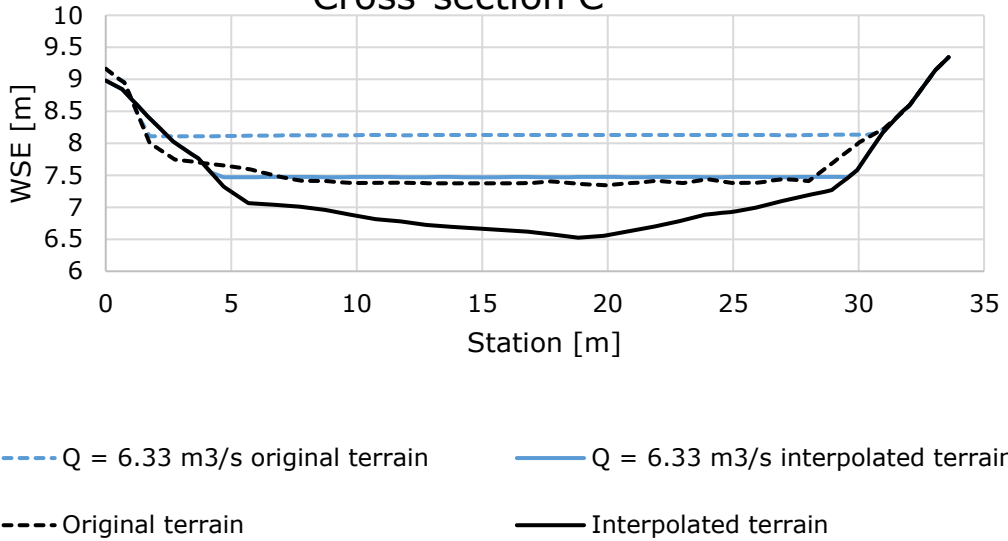
APPENDIX U: Flooding original terrain



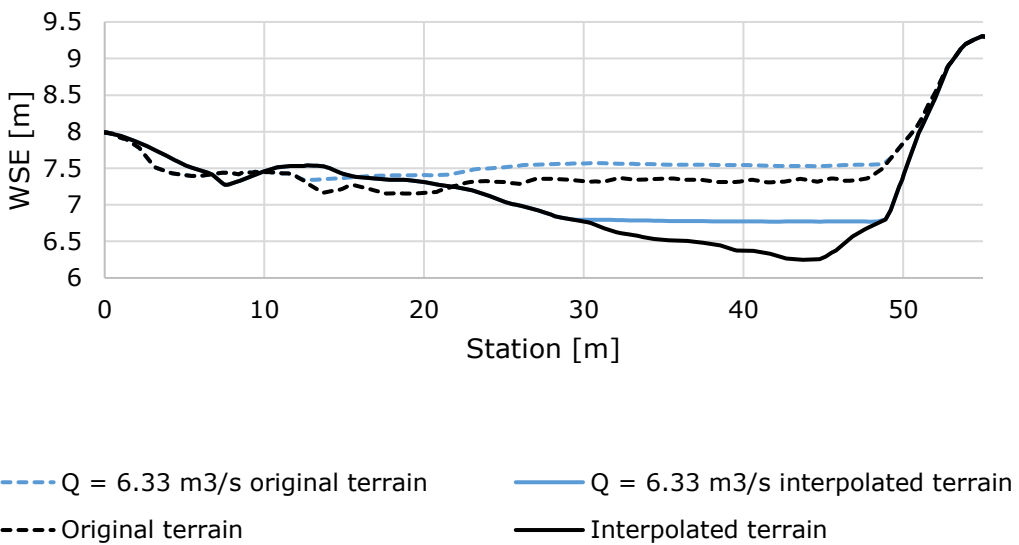
APPENDIX V: Comparison original LIDAR terrain and interpolated terrain. 6.33 m³/s



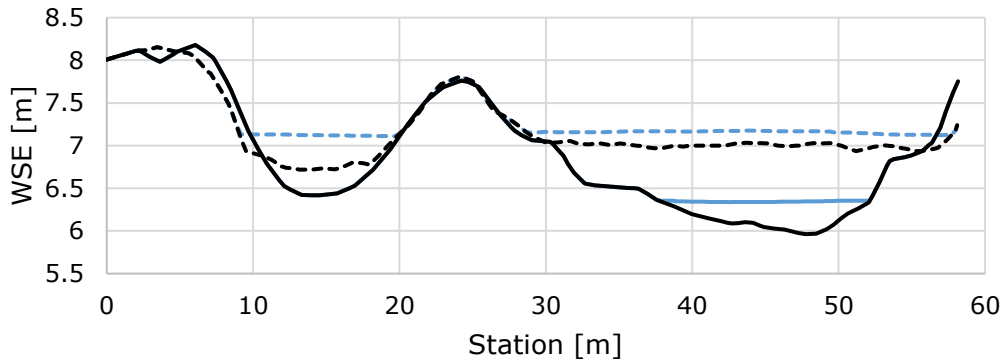
Comparison original LIDAR terrain and interpolated terrain. $Q = 6.33 \text{ m}^3/\text{s}$.
Cross-section C



Comparison original LIDAR terrain and interpolated terrain. $Q = 6.33 \text{ m}^3/\text{s}$.
Cross-section D

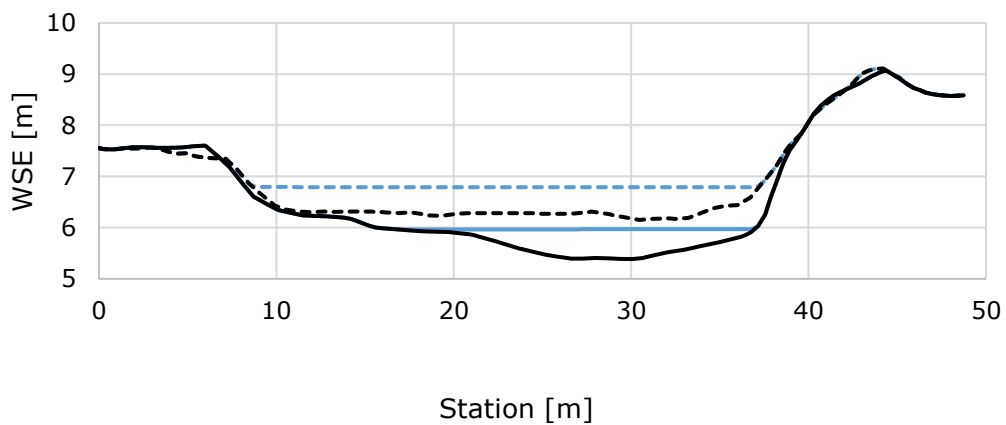


Original LIDAR terrain and interpolated terrain. $Q = 6.33 \text{ m}^3/\text{s}$.
Cross-section E



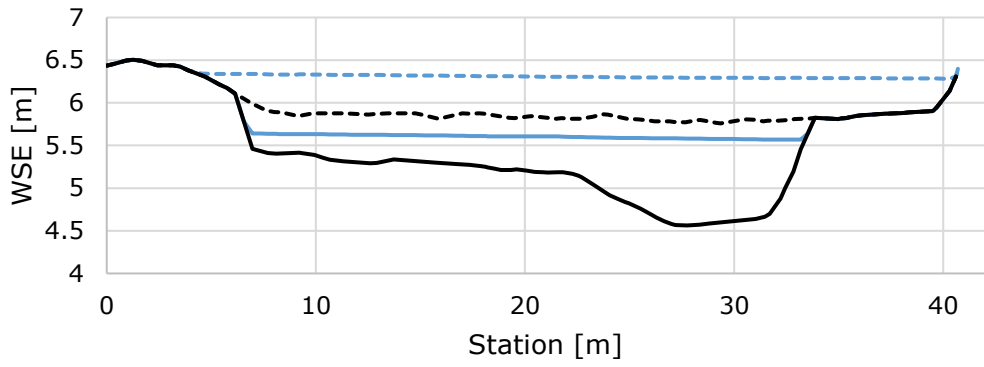
----- $Q = 6.33 \text{ m}^3/\text{s}$ original terrain ———— $Q = 6.33 \text{ m}^3/\text{s}$ interpolated terrain
----- Original terrain ———— Interpolated terrain

Original LIDAR terrain and interpolated terrain. $Q = 6.33 \text{ m}^3/\text{s}$.
Cross-section F

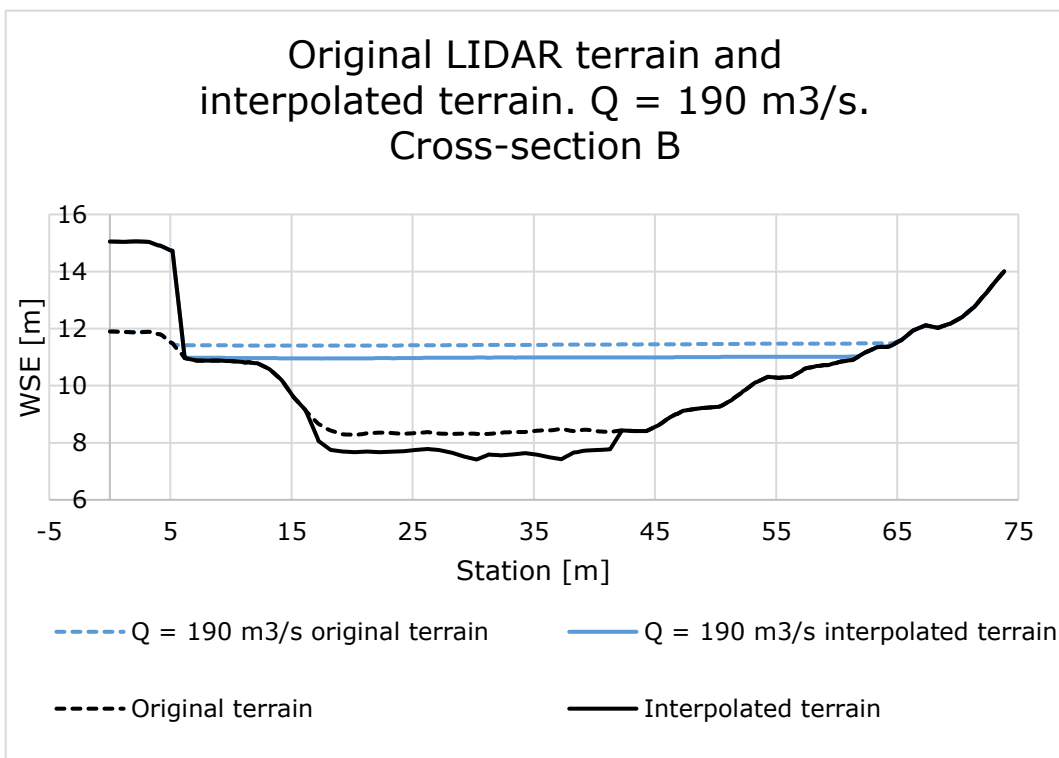
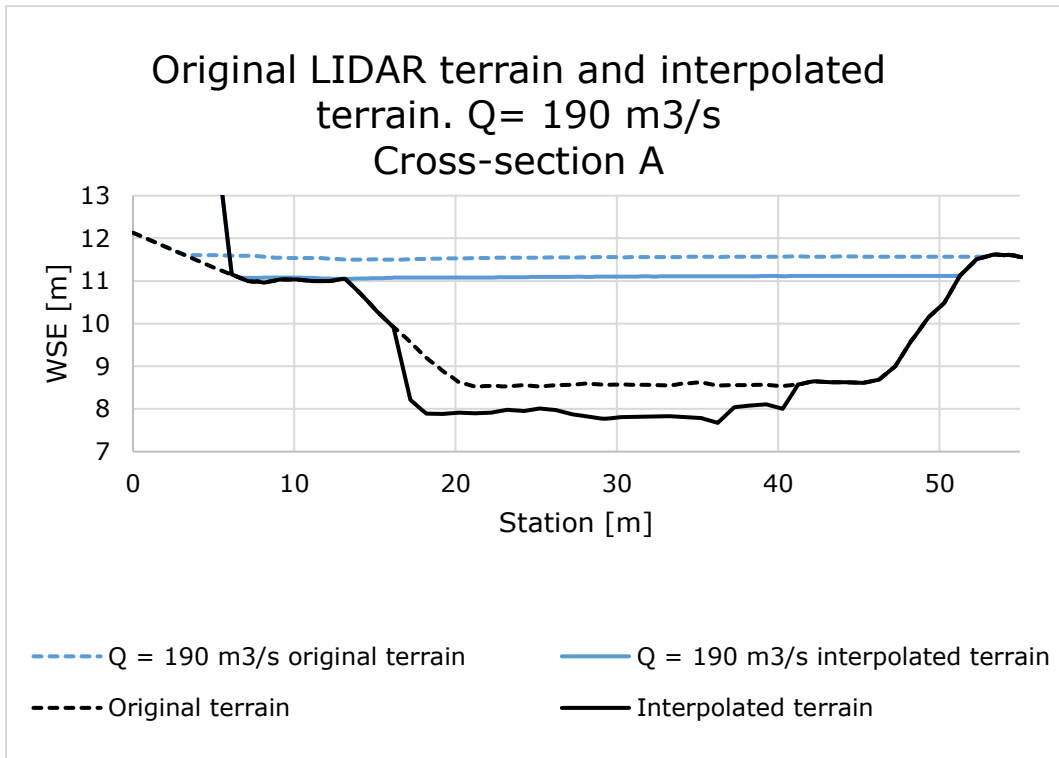


----- $Q = 6.33 \text{ m}^3/\text{s}$ original terrain ———— $Q = 6.33 \text{ m}^3/\text{s}$ interpolated terrain
----- Original terrain ———— Interpolated terrain

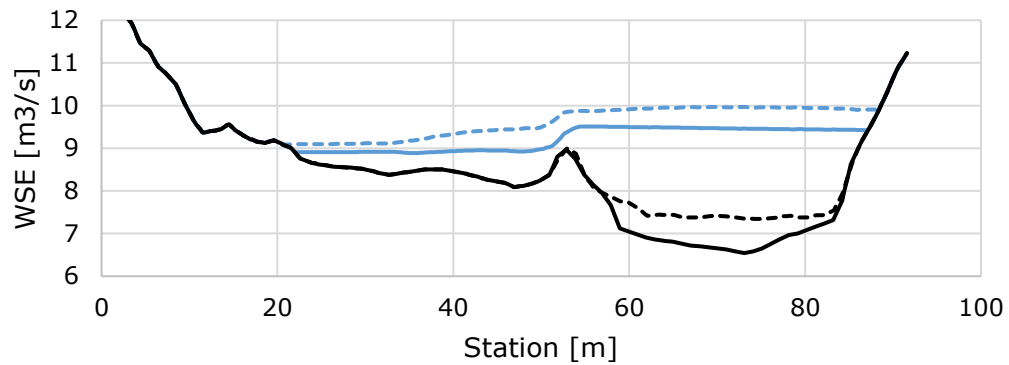
Original LIDAR terrain and interpolated terrain. $Q = 6.33 \text{ m}^3/\text{s}$.
Cross-section G



- Q = 6.33 m³/s original terrain
- Q = 6.33 m³/s interpolated terrain
- Original terrain
- Interpolated terrain

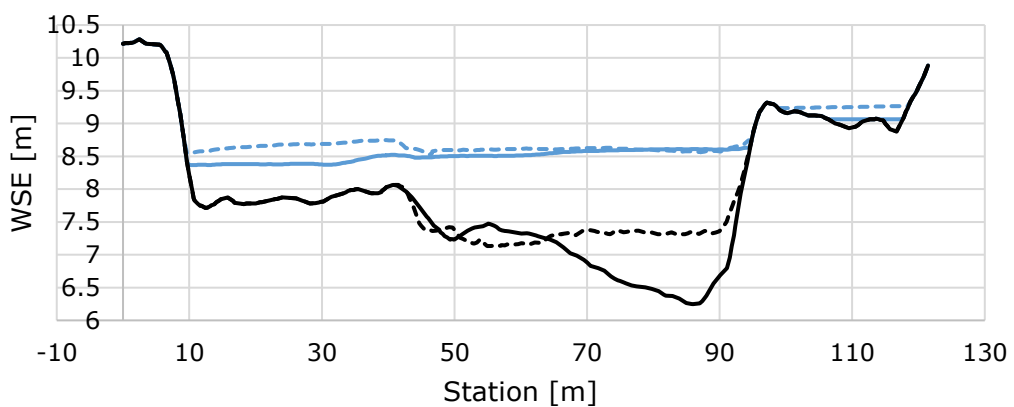


Original LIDAR terrain and interpolated terrain. $Q = 190 \text{ m}^3/\text{s}$
Cross-section C



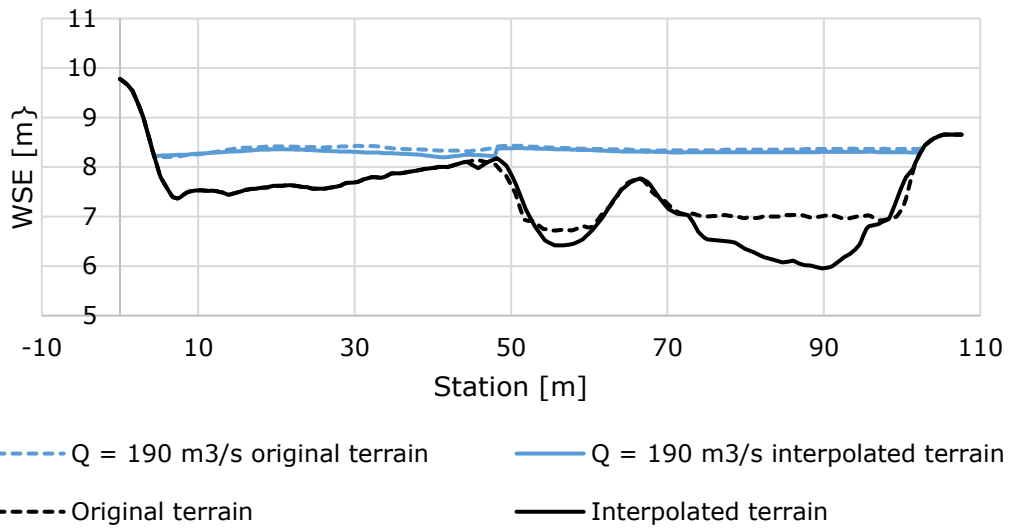
--- $Q = 190 \text{ m}^3/\text{s}$ original terrain — $Q = 190 \text{ m}^3/\text{s}$ interpolated terrain
- - - Original terrain — Interpolated terrain

Original LIDAR terrain and interpolated terrain. $Q = 190 \text{ m}^3/\text{s}$.
Cross-section D

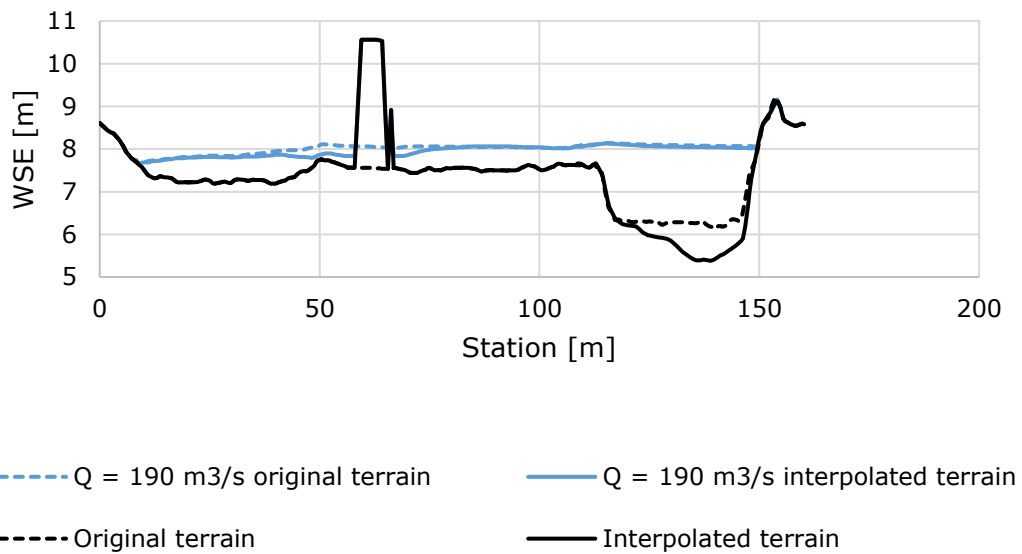


--- $Q = 190 \text{ m}^3/\text{s}$ original terrain — $Q = 190 \text{ m}^3/\text{s}$ interpolated terrain
- - - Original terrain — Interpolated terrain

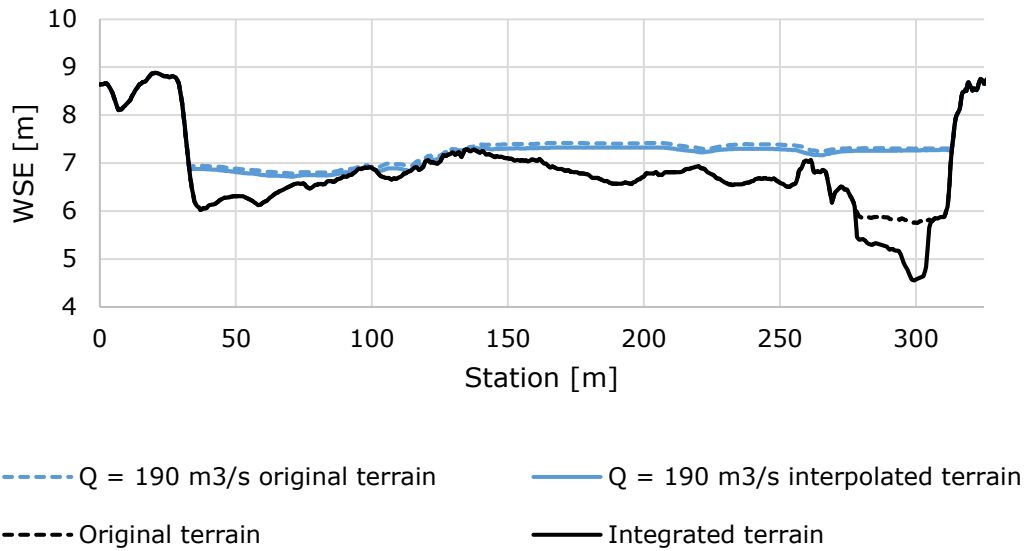
Original LIDAR terrain and interpolated terrain. $Q = 190 \text{ m}^3/\text{s}$.
Cross-section E



Original LIDAR terrain and interpolated terrain. $Q = 190 \text{ m}^3/\text{s}$.
Cross-section F

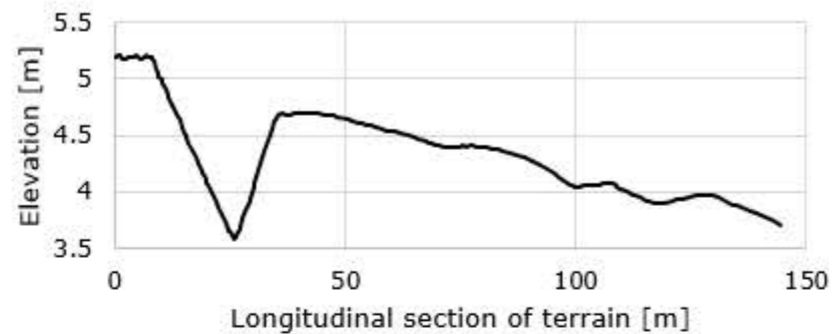


Original LIDAR terrain and
interpolated terrain. $Q = 190 \text{ m}^3/\text{s}$.
Cross-section G

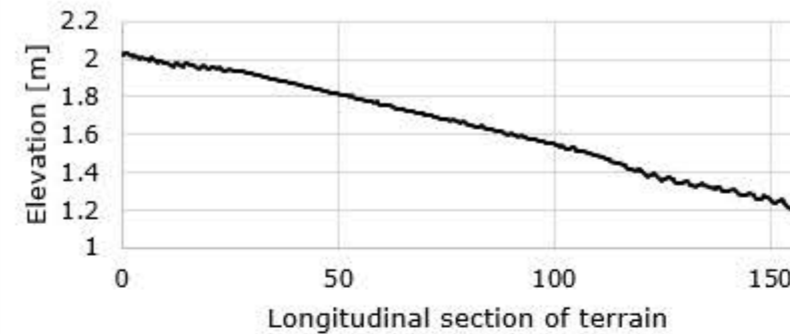


APPENDIX X: Variation in terrain

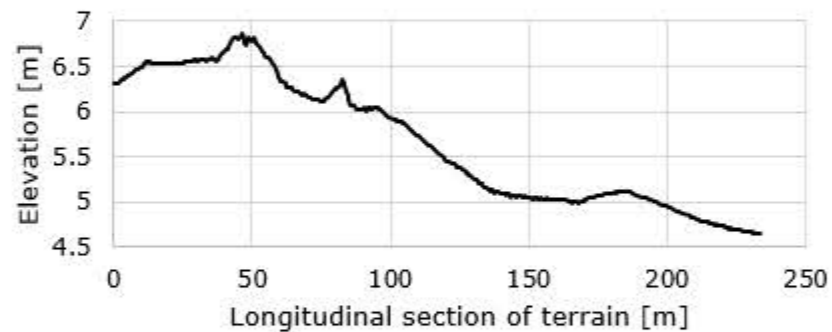
Elevation area C



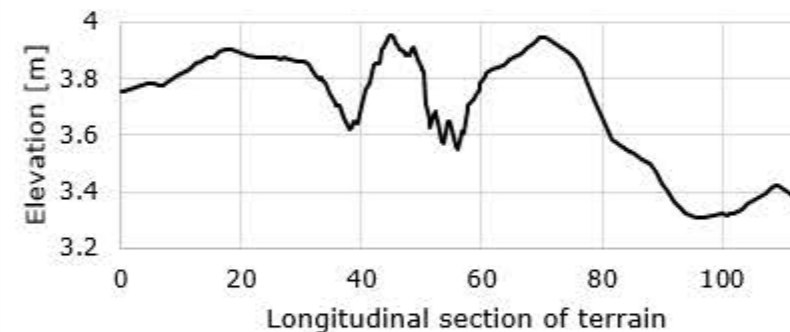
Elevation area E



Elevation area B



Elevation area D



Elevation area A

